Oxford Brookes University
Faculty of Health and Life Sciences
Department of Biological and Medical Sciences

Searching for structural determinants of agonist selectivity in nicotinic acetylcholine receptors

Teresa Mínguez Viñas

A thesis submitted in partial fulfilment of the requirement of Oxford Brookes University for the degree of Doctor of Philosophy

PhD Thesis

March 2020

“Reserve your right to think, for even to think wrongly is better than not to think at all.”

— Hypatia of Alexandria

INDEX

PUBLICATIONS **9**

CONFERENCE ATTENDANCE **9**

LIST OF FIGURES **11**

LIST OF TABLES **13**

LIST OF ABBREVIATIONS **15**

ABSTRACT **17**

CHAPTER 1. INTRODUCTION **19**

1.1. Brief history of nicotine and nicotinic acetylcholine receptors **21**

1.2. nAChRs classification **23**

1.3. nAChRs structure **23**
- 1.3.1. nAChR subunits 25
- 1.3.2. The ECD 26
  - 1.3.2.a. The agonist binding site 27
  - 1.3.2.b. Allosteric sites at the ECD 28
- 1.3.3. The TMD 28
  - 1.3.3.a. The ion pore 29
  - 1.3.3.b. Allosteric binding sites at the TMD 31
- 1.3.4. The ICD 31

1.4. Activation of nAChRs **32**
- 1.4.1. Transitions between states 32
- 1.4.2. Agonist recognition 33
- 1.4.3. Molecular mechanisms of signal transduction 35
- 1.4.4. Molecular mechanisms of desensitization 36

1.5. Pharmacology of nAChRs **37**
- 1.5.1. Agonists 38
- 1.5.2. Antagonists 40
- 1.5.3. Allosteric modulators 42

1.6. nAChRs distribution in the brain **44**

1.7. Neuronal nAChRs in brain pathologies **46**
- 1.7.1. Depression 46
- 1.7.2. Alzheimer’s disease 47
- 1.7.3. Parkinson’s disease 49

1.7.4. Schizophrenia 49
1.7.5. Pain........ 50
1.7.6. Autosomal dominant nocturnal frontal lobe epilepsy 51
1.7.7. Nicotine addiction........ 52

1.8. Aim of the thesis........ 55

CHAPTER 2. MATERIALS AND METHODS 57

2.1. Reagents 59

2.2. Animals........ 59

2.3. Molecular Biology........ 59
2.3.1. Single Point Mutations........ 60

2.4. *Xenopus laevis* oocytes preparation........ 62

2.5. Microinjection of cDNA and cRNA........ 62

2.6. Electrophysiological recordings 63
2.6.1. Manual two electrode voltage-clamp system 63
2.6.2. Automated two electrode voltage-clamp system........ 64
2.6.3. Concentration-response curves for agonists........ 64
2.6.4. Inhibitory concentration-response curves for low efficacy partial agonist........ 65

2.7. Double-mutant cycle analysis for long range coupling........ 66

2.8. Statistical analysis........ 68

2.9. Studies carried out in collaboration with external research groups 68
2.9.1. Computational biology........ 68
2.9.1.a. Comparative Modelling and Molecular Docking........ 68
2.9.1.b. Molecular Dynamic simulations 69
2.9.2. Radioligand binding assays 69
2.9.2.a. Saturation binding assays........ 70
2.9.2.b. Competition binding assays 70
2.9.2.c. Binding assays statistics........ 71

CHAPTER 3. PHARMACOLOGICAL CHARACTERIZATION OF C(10) CYT DERIVATIVES 73

3.1. Introduction 75

3.2. Results 79
3.2.1. Radioligand binding studies 80
3.2.2. Functional assays 81
3.2.2.a. C(10) Cyt derivatives as antagonists of nAChRs........ 85

3.3. Discussion........ 89

CHAPTER 4. MOLECULAR DETERMINANTS OF THE NACHR SUBTYPE SELECTIVITY OF C(10) CYT DERIVATIVES 93

4.1. Introduction 95

4.2. Results 97
4.2.1. Searching for agonist discriminatory elements using molecular docking 97
4.2.2. MD simulations identify an arginine residue as a critical element of agonist selectivity 100
4.2.3. G174D increases agonist potency in α7 nAChR. 103
4.2.4. G174D and R101 establish de novo electrostatic interactions 105
4.2.5. α4D185-β2R106 electrostatic interaction regulates cell surface expression of α4β2 nAChR 108

4.3. Discussion 111

CHAPTER 5. ROLE OF R101 IN α7 NACHRS 115

5.1. Introduction 117

5.2. Results 119
5.2.1. α7R101 mutations affect agonist potency and onset of current decay 119
5.2.2. α7R107A changes the dynamics of coupling elements in the agonist site 122
5.2.3. α7R107 is coupled to receptor gating 124
5.2.4. α7R101 dominates the electrostatic landscape near loop C 126

5.3. Discussion 127

CHAPTER 6. FINAL DISCUSSION 129

ACKNOWLEDGEMENTS 135

BIBLIOGRAPHY 137

PUBLICATIONS

- **Minguez T**, Oliveira ASF, Shoemark DK, Nielsen BE, Bouzat C, Sessions RB, Mulholland AJ, Wonnacott S, Gallagher T, Bermudez I. A novel determinant of agonist selectivity in nAChRs: a conserved residue with non-conserved function. (In preparation for PNAS submission)

- Rego-Campello H, Del Villar S, Honraedt A, **Minguez T**, Oliveira ASF, Ranaghan KE, Shoemark DK, Bermudez I, Gotti C, Sessions RB, Mulholland AJ, Wonnacott S, Gallagher T (2018). Unlocking Nicotinic Selectivity via Direct C-H Functionalization of (−)-Cytisine. *Chem*, 4(7), 1710–1725.

- Nielsen BE, **Minguez T**, Bermudez I, Bouzat C (2018). Molecular function of the novel α7β2 nicotinic receptor. *Cell Mol Life Sci*, 75(13): 2457-2471.

- Alcaino C, Musgaard M, **Minguez T**, Mazzaferro S, Faundez M, Iturriaga-Vasquez P, Biggin PC, Bermudez I (2017). Role of the cys loop and transmembrane domain in the allosteric modulation of α4β2 nicotinic acetylcholine receptors. *J BiolChem*, 292(2): 551-562.

CONFERENCE ATTENDANCE

- Chilean Pharmacological Society´s annual meeting (Puerto Varas, Nov 2018). Workshop presentation.

- Society for Neuroscience annual meeting (Chicago, Oct 2019). Poster presentation.

- British Pharmacological Society’s annual meeting (Edinburgh, Dec 2019). Poster presentation.

- 16th annual Chistmas meeting (Instituto Neurociencias Alicante, Dec 2019). 30 min oral presentation.

LIST OF FIGURES

CHAPTER 1. INTRODUCTION

Figure 1.1 Overall structure and fold of nAChRs 24
Figure 1.2 Assembly of neuronal nAChRs 26
Figure 1.3 Agonist binding site of nAChRs 27
Figure 1.4 The ion pore of nAChRs 30
Figure 1.5 "Catch and hold" activation model 33
Figure 1.6 Nic binding interactions at the AChBP agonist binding site 34
Figure 1.7 Conformational changes during receptor activation 35
Figure 1.8 Distribution of nAChRs in human brain 46
Figure 1.9 The mesolimbic reward system in the brain 52

CHAPTER 2. MATERIALS AND METHODS

Figure 2.1 Diagram of three steps for polymerase chain reaction (PCR) 61
Figure 2.2 Diagram of two electrodes voltage-clamping in *Xenopus laevis* oocytes 63
Figure 2.3 The elucidating long-range functional coupling of allosteric receptors 67

CHAPTER 3. PHARMACOLOGICAL CHARACTERIZATION OF C(10) CYT DERIVATIVES

Figure 3.1 Ir-catalyzed borylation of the C(10) within the pyridine ring of Cyt 77
Figure 3.2 Functional effects of C(10) Cyt derivatives on nAChR subtypes 83
Figure 3.3 Agonist effects of C(10) Cyt derivatives at α7 nAChR subtype 84
Figure 3.4 Cyt inhibits the ACh-evoked responses of nAChRs subtypes 86
Figure 3.5 Competitive antagonist activity of C(10) Cyt derivatives at α4β2 and α7 nAChR subtypes 88

CHAPTER 4. MOLECULAR DETERMINANTS OF THE NACHR SUBTYPE SELECTIVITY OF C(10) CYT DERIVATIVES

Figure 4.1 Cyt binding interactions at the α4β2 nAChR agonist binding site 96
Figure 4.2 Binding site orientations of BS40 in α4β2 and α7 nAChRs highlighting the structural differences among them 98
Figure 4.3 Dynamical behaviour of the agonists in α4β2 and α7 nAChRs 101

Figure 4.4 A conserved arginine in β3-strand in nAChR shows subtype-specific dynamical behaviour 102
Figure 4.5 Changes in BS40 binding orientation in α7 nAChR 102
Figure 4.6 Functional effects on the mutant α7G174D on receptor activation 104
Figure 4.7 Functional effects of changes in distance between the charged moieties at the position 174 in loop B and 101 in β3-strand of α7 nAChR 107
Figure 4.8 Functional effects of disrupting the α4D185-β2R106 interaction in $(\alpha4)_2(\beta2)_3$ nAChR 109

CHAPTER 5. ROLE OF R101 IN α7 NACHRS

Figure 5.1 Functional effects of substituting R101 in α7 nAChR on receptor activation... 121
Figure 5.2 α7 WT and α7R101A average structures of MD simulations of the first binding pocket for Ach, Cyt and BS40 123
Figure 5.3 Interactions between R101 and loop C in α7 nAChR and the effects of α7R101A mutation 124
Figure 5.4. α7R101 is functionally couple to L9' in the ion channel 125
Figure 5.5 Electrostatic maps for α7 WT and mutant α7R101A and α4β2 WT and α4β2R107A nAChRs 126

LIST OF TABLES

CHAPTER 1. INTRODUCTION

Table 1.1 Subunits diversity in the nAChR family 25
Table 1.2 Examples of agonists for nAChRs 39
Table 1.3 Examples of competitive and non-competitive antagonists for nAChRs 41
Table 1.4 Examples of allosteric modulators for nAChRs 43

CHAPTER 2. MATERIALS AND METHODS

Table 2.1 The α7 and α4β2 primers for single point mutations ……………........................ 61

CHAPTER 3. PHARMACOLOGICAL CHARACTERIZATION OF C(10) CYT DERIVATIVES

Table 3.1 C(10) Cyt derivatives along with their chemical structures 79
Table 3.2 Binding affinities (K_i) of C(10) Cyt derivatives for α4β2, α3β4 and α7 nAChR subtypes 81
Table 3.3 Comparison of agonist activity of ACh, Nic, Var, (–)-Cyt and (10) Cyt derivatives at nAChR subtypes 82
Table 3.4 Comparison of antagonist activity of (–)-Cyt and C(10) Cyt derivatives at nAChR subtypes 87

CHAPTER 4. MOLECULAR DETERMINANTS OF THE NACHR SUBTYPE SELECTIVITY OF C(10) CYT DERIVATIVES

Table 4.1 Agonist sensitivity to activation of α7 WT and mutant nAChRs 99
Table 4.2 Glycine to aspartate exchange in loop B increases agonist potency and binding affinity in α7 nAChR 105
Table 4.3 Effects of mutating 101 and 174 positions at α7 nAChR on agonist sensitivity.. 106
Table 4.4 Effects of ablactating the α4D185-β2R106 interaction on the receptor function and agonist binding of α4β2 WT and mutants 109

CHAPTER 5. ROLE OF R101 IN α7 NACHRS

Table 5.1 Functional effects of substituting R101 in α7 nAChR on receptor activation … 120
Table 5.2 Functional effects of substituting R101 in α7 nAChR on onset of current decay.. 122

LIST OF ABBREVIATIONS

ACh	Acetylcholine
AChBP	Acetylcholine binding protein
AChE	Acetylcholinesterase
AD	Alzheimer’s disease
ADNFLE	Autosomal dominant nocturnal frontal lobe epilepsy
Aβ	Amyloid-β
ANOVA	Analysis of variance
α-Bgt	α-Bungarotoxin
βEST	17β-estradiol
$\mathbf{B_{max}}$	Concentration of specific binding sites for the radioligand
BS40	(–)-10-Methylcytisine hydrochloride
C-terminal	Carboxy-terminal
cDNA	Complementary deoxyribose nucleic acid
CI	Confidence interval
CNS	Central nervous system
CRC	Concentration response curve
cDNA	Complementary deoxyribonucleic acid
cRNA	Complementary ribonucleic acid
Cryo-EM	Cryogenic electron microscopy
Cyt	(-)-Cytisine
DA	Dopamine
dNTP	Deoxyribonucleotide triphosphate
dFBr	Desformylflustrabromide
DHβE	Dihydro-β-erythroidine
DMSO	Dimethylsulphoxide
$\mathbf{EC_{50}}$	Concentration producing half maximal effect
ECD	Extracellular domain
ELFCAR	Elucidating long-range functional coupling of allosteric receptors
ELIC	*Ewinia* ligand-gated ion channels
Epi	(±)-Epibatidine
$\mathbf{GABA_{A\text{-}C}}$	ɣ-aminobutyric acid type A-C receptor
GLIC	*Gloeobacter* ligand-gated ion channels
GlyR	Glycine receptor
HEPES	N-2-hydroxyethylpiperazine-N’-2-ethansulphonic acid
ICD	Intracellular domain
$\mathbf{IC_{50}}$	Concentration producing half maximal inhibition
$\boldsymbol{K_D}$	Affinity constant in saturation binding assays
$\boldsymbol{K_i}$	Dissociation constant in competition binding assays
N-terminal	Amino-terminal
NAcc	Nucleus accumbens
nAChR	Nicotinic acetylcholine receptor

nH	Hill coefficient
NAM	Negative allosteric modulator
Nic	(-)-Nicotine
NTR	Nicotine Replacement Therapy
MA	Membrane associated α-helix of M4
MD	Molecular dynamics
MX	Short post-M3 loop
PAM	Positive allosteric modulator
PBS	Phosphate-buffered saline
PD	Parkinson’s disease
PCR	Polymerase chain reaction
PNS	Peripheral nervous system
pLGIC	Pentameric ligand-gated ion channel
SEM	Standard error of the mean
TMD	Transmembrane domain
Var	Varenicline
VTA	Ventral tegmental area
ZAC	Zinc-activated receptor
5-HT$_3$	5-Hydroxytryptamine type 3

ABSTRACT

The α4β2 and α7 receptors are the most abundant nicotinic acetylcholine receptors (nAChRs) in the brain, where they contribute to cognition, reward, nociception and mood. They are also implicated in depression, schizophrenia, cognitive deficit and in addiction to nicotine (Nic). Activation of these receptors by partial agonists is considered as a valid strategy to intervene therapeutically in the aforementioned dysfunctions. For clinical scenarios such as Nic addiction receptor subtype-specificity may increase clinical efficacy by decreasing off-target effects. Designing subtype-specific agonists is however problematic, mainly because of the highly conserved nature of the agonist binding site in the nAChR family. This thesis focuses on identifying elements in nAChR subtypes to aid the design of novel smoking cessation drugs. Functional and radioligand binding assays showed that novel C(10) cytisine (Cyt) derivatives maintain the potency and efficacy of the smoking cessation drug Cyt at α4β2 nAChR but had no significant activity at α7 subtype. Molecular docking in combination with functional assays showed that differences in residues in the complementary side of the agonist site do not account for the selectivity of the C(10) Cyt derivatives. However, molecular dynamics simulations revealed a conserved arginine residue (R101) in β3-strand that impairs agonist binding in α7 nAChR. In α4β2, the arginine residue (R106) establishes an inter-subunit electrostatic interaction with an aspartate residue (D185) in loop B, an interaction that is needed for functional expression. In α7, the aspartate residue is exchanged for glycine (G174), which makes the side chain of R101 highly mobile, allowing it to orientate towards the agonist binding site, which ultimately weakens agonist binding. In accord, stabilising R101 by introducing mutation G174D increases the potency of Cyt and its C(10) derivatives at α7 nAChR. Functional assays of R101 mutants suggested that this arginine affects agonist-activation and the onset of decay of agonist responses. R101 also couples to a channel mutation (L9’T) that influences gating. The mobility of the side chain of R101 sets the electrostatic landscape of the regions reached by the side chain. This effect may underlie the effects of R101 on α7 nAChR and raise the possibility that R101 may be a good target to increase receptor subtype-specificity.

CHAPTER 1. INTRODUCTION

1.1. Brief history of nicotine and nicotinic acetylcholine receptors

Nicotiana spp., better known as tobacco plants, were discovered by the native people of Mesoamerica and South America thousands of years ago. The fact that the first cultivation of tobacco plants has been estimated to have started around 5000-3000 BC points out the importance given to this plant by the native Mesoamerican and South American people (Tushingham *et al.*, 2018). In sharp contrast to its current recreational use, tobacco was considered as a sacred plant that was used in rituals and ceremonies by indigenous communities in the Peruvian/Ecuadorean Andes (Gately, 2001). Tobacco was also used as an insecticide and its smoke was blown over the crops. Nevertheless, the most important use of tobacco was as a medicinal plant. Tobacco leaves in powdered form were applied externally for catarrhs or for ring worms, fungal diseases of the skin, wounds, ulcers, bruises, sores or mouth lesions (Charlton, 2004). After the arrival of the Spanish Conquistadores to America at the end of the 15th century, the tobacco plant was introduced into Europe. In 1560 the French ambassador to Lisbon, Jean Nicot, brought *Nicotiana tabacum* to the French court giving his name to the plant (Dani and Balfour, 2011). The pleasurable effects of tobacco smoking soon made the plant spread worldwide and its "medicinal" properties stimulated scientific investigation.

In 1828, the tobacco alkaloid nicotine (Nic) was first isolated from the leaves of the tobacco plant (Charlton, 2004). Three decades later, Claude Bernard reported for the first time the effects of Nic at the neuromuscular junction (Hurst *et al.*, *2013*). At the beginning of the 19th century, John Newport Langley suggested the existence of nicotinic acetylcholine receptors (nAChRs) for the first time. Langley named them as "receptive substances" that combine with Nic to receive and transmit motor stimuli (Langley, 1905). Almost 70 years later, the first nAChR was biochemically isolated from the *Torpedo* electric organ (Changeux *et al.*, 1970). This breakthrough paved the way for subsequent scientific studies that have significantly increased our knowledge of nAChRs and their homologues in the pentameric ligand gated ion channels (pLGIC) family (Changeux, 2012).

The industrial revolution fundamentally changed the use of tobacco leaves by introducing cigarettes, which rapidly became a global mass consumable. This remained so until the 1950s, when researches showed for the first time that tobacco smoking increases the risk of lung cancer and cardiovascular diseases (Dani and Balfour, 2011). Nic was later identified as the cause of this addiction due to its ability to activate the reward system in the brain through binding nAChRs present in this system (Corrigal *et al.*, 1994).

Despite its detrimental effects on health, the activation of nAChRs by Nic has also unquestionable benefits. Preclinical and clinical studies have shown that Nic has analgesic (Hamman and Martin, 1992), short-term antidepressant (Picciotto *et al.,* 2002), cognitive-enhancing (Leiser *et al.*, 2009) and neuroprotective (Quik *et al.*, 2008) effects. These properties have led to the validation of brain nAChRs as important targets for therapeutic intervention in a wide range of brain disorders, including chronic pain, depression, Alzheimer's and Parkinson's diseases and schizophrenia (Taly *et al.*, 2009). Indeed, since the late 1980's most pharmaceutical companies, big and small, have developed nAChR drug discovery programs. However, despite intense research efforts during this period, only one novel nicotinic compound has been successfully approved for clinical use: varenicline (Var) (Hurst *et al.*, *2013*). This compound was approved for aiding smoking cessation treatments in 2006. A key reason for these unsatisfactory results is that most nicotinic ligands display some degree of overlapping nAChR subtype activity or cross-reactivity with other pLGICs (e.g., 5-HT$_3$ receptors), which may underlie the autonomic side effects and/or off-target brain effects that have been reported for nAChR drugs (e.g., Yang *et al.*, 2017). An example is Var itself. Var users may experience side effects such as nausea, sleep problems, constipation, gas or vomiting (Chantix® official site). Var has also been reported to cause thoughts of suicide and erratic behaviour by a post-launch study in 2007 (MHRA, 2007), although subsequent meta-analysis studies were not able to find evidence of psychiatric side effects (Thomas *et al.*, 2015). It is likely that the off-target effects of Var are due to its ability to activate a variety of neuronal nAChRs, including α4β2, α7 and α3β4 nAChRs (Rego-Campello *et al.*, 2018) as well as 5-HT$_3$ receptors (Lummis *et al.*, 2011). The ability of Var to interact with a multiplicity of nAChR subtypes and 5-HT$_3$ receptors stems from the high level of conservation of the agonist binding site in the family -and indeed among all members of the Cys loop ligand-gated ion channel family. The design of subtype specific nAChR ligands in this scenario is not an easy task. Therefore, a better understanding of nAChR structure, especially of structural differences between nAChR subtypes, is essential to decrease off-target effects in drug-based therapies. This thesis focuses on the identification of structural elements that may contribute to define the selectivity of C(10) derivatives of cytisine (Cyt) for α4β2 nAChR over α7 subtype. Cyt, like Var, activates neuronal nAChRs, with varying potency and efficacy, depending on the receptor subtype and can be used as a cheap alternative to Var in smoking cessation therapies (Rego-Campello *et al.*, 2018).

1.2. nAChRs classification

The nAChRs are pentameric ligand-gated ion channels that belong to the superfamily of the pLGICs. The pLGIC family includes prokaryotic proteins as well as vertebrates, the latter comprising the Cys loop family of neurotransmitter-gated ion channels. The Cys loop family includes the nAChR family, the γ-aminobutyric acid ($GABA_A$ and $GABA_C$), glycine (Gly), serotonin ($5\text{-}HT_3$) and zinc-activated (ZAC) receptors (Thompson *et al.*, 2010). Cys loop receptors present, unlike their prokaryotic homologues ELIC and GLIC, a signature loop at the N-terminal formed by a pair of disulphide-bonded cysteines (Cys) separated by 13 conserved amino acids (Pless and Lynagh, 2014), which gives the name to the superfamily. Each of these receptors is selective for anions or cations and thus classified as inhibitory and excitatory receptors. nAChRs are excitatory receptors selective for the cations Na^+, K^+ and, depending on subtype, Ca^{2+} ions.

The nAChR family comprises the skeletal muscle receptors, which mediate skeletal muscle contraction at the neuromuscular junction, and neuronal receptors, which are involved in both fast synaptic transmission and presynaptic modulation of neurotransmitter release at the peripheral (PNS) and central nervous system (CNS). Neuronal nAChRs have also been detected in non-neuronal cells such as macrophages, bronchial epithelial cells, endothelial cells of blood vessel cells and skin keratinocytes (Millar and Gotti, 2009; Wonnacott, 2015). Thus, a more apt classification for nAChRs should be dividing them into muscle and non-muscle nAChRs.

1.3. nAChRs structure

Insight into nAChR structure has expanded rapidly in recent years with the resolution of a number of atomic structures, including the water soluble homologues (ACh binding proteins, AChBP) of the nAChR agonist-binding domain (Brejc *et al.*, 2001; Celie *et al.*, 2004; Dellisanti *et al.*, 2007; Hansen *et al.*, 2005; Li *et al.*, 2011), the *Torpedo* nAChR (Unwin, 2005), the prokaryotic pentameric ligand-gated ion channels (pLGICs), *Erwinia* ligand gated ion channel (ELIC) (Hilf and Dutzler, 2008) and *Gloebacter* ligand-gated ion channel

(GLIC) (Bocquet *et al*., 2009; Hilf and Dutzler, 2009), the *Caenorhabditis elegans* glutamate-activated chloride channel (GluCl) (Hibbs and Gouaux, 2011), the human $GABA_A$ receptor (Miller and Aricescu, 2014), mouse $5\text{-}HT_{3\text{-}A}$ receptor (Hassaine *et al*., 2014), the human $(\alpha4)_2(\beta2)_3$ nAChR (Morales-Perez *et al*., 2016), $(\alpha4)_3(\beta2)_2$ (Walsh *et al*., 2018) and α3β4 (Gharpure *et al.,* 2019) nAChRs. These studies firmly established the structural architecture of the pLGIC superfamily, in which all members adopt a similar quaternary structure formed from five subunits (**Fig. 1.1**). Each subunit consists of a large hydrophilic amino-terminal extracellular domain (ECD) that houses the agonist binding site, a transmembrane domain (TMD) formed by four hydrophobic segments (M1-M4), an ion channel whose walls are lined by M2 helices and an external C-terminus of variable length (**Fig. 1.1**) (Cecchini and Changeux, 2015). Cys loop receptors possess an intracellular domain (ICD) of 70 to 150 amino acids that is important for their trafficking and clustering in the plasma membrane (Thompson *et al*., 2010) (**Fig. 1.1**). In nAChRs and $5\text{-}HT_3$ receptors, the ICD plays an important role in cation permeability (Thompson *et al*., 2010; Cechinni and Changeux, 2014).

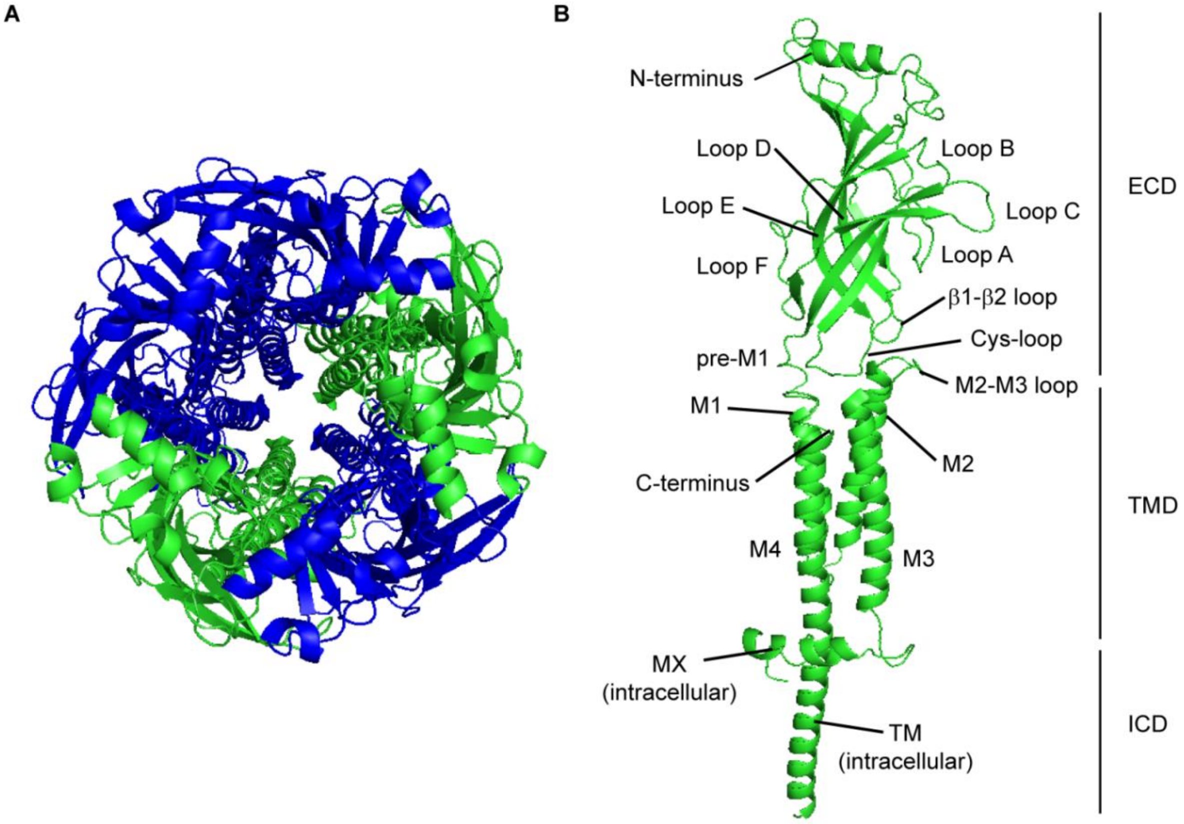

Figure 1.1. Overall structure and fold of nAChRs. A) Top view of the nAChR as viewed from the extracellular side. B) Lateral view showing ECD, TMD and ICD of an α subunit. Generated from the published structure 6pv7.pdb (Gharpure *et al*., 2019) using PyMol (http://www.pymol.org).

1.3.1. nAChR subunits

To date, seventeen different nAChR subunit types have been identified in vertebrates. They are divided into four subfamilies (I–IV) based on similarities in protein sequence (**Table 1.1**). The nAChR subunits are highly conserved and each single subunit has more than 80% amino acid identity across vertebrate species. Unlike non-α nAChR subunits (e.g., β, δ, γ and ε subunits), all α subunits with the exception of α5, possess a flexible loop in the ECD that is flanked by two conserved aromatic residues (TyrC1 and TyrC2) and contains a cysteine-bridge on its tip. This loop, termed loop C, is a key agonist-binding signal transduction element making the presence of α subunits a requirement for functionality (Albuquerque *et al.*, 2009).

The subunits of the nAChR family combine in pentameric ensembles to form diverse receptor subtypes. However, the subunit combinations permitted are restricted; groups I to III form receptors present in the nervous system and other non-muscle cells but group IV only contributes to the muscle nAChR (**Table 1.1**) (Corringer *et al.*, 2000). Type I to III subunits form diverse receptor subtypes, all of which differ in their agonist sensitivity, channel kinetics, Ca^{2+} permeability, assembly, interactions with chaperones, trafficking and cell localization (Corringer *et al.*, 2000; Alburquerque *et al.*, 2009; Wonnacott, 2014). α subunits such as the α7 and α9 can form homomeric receptors (i.e., α7 and α9 nAChRs). The α8 subunit also form homomeric nAChRs but it has been only found in avian species (Lohmann *et al.*, 2000). α7 and α9 subunits can also combine with other subunits to form heteromeric ensembles. Thus, α7 subunits combine with β2 subunits to form α7β2 receptors (Khiroug *et al.*, 2002) and the α9 subunit interacts with α10 subunits to form the cochlear nAChR α9α10 receptors (Elgoyhen *et al.*, 2001).

Table 1.1. Subunits diversity in the nAChR family.

Neuronal-type			**Muscle-type**
I	**II**	**III**	**IV**
α9, α10	α7, α8	α2-α6 and β2-β4	α1, β1, δ, ε and γ

Heteromeric receptors comprise α subunits and β2 or β4 subunits organised as two pairwise combinations of α with β; an arrangement that provides two operational agonist binding sites. The fifth position can be occupied by any subunit member of group III, giving rise to receptors such as $(\alpha4)_3(\beta2)_2$, $(\alpha4)_2(\beta2)_3$ or $(\alpha4)_2(\beta2)_2\alpha5$. The subunit in the fifth position has a variety of functions, depending on its nature. For example, in the $(\alpha4)_3(\beta2)_2$ contributes to a third agonist site and in the $(\alpha4)_2(\beta2)_2\alpha5$ subtype defines the overall Ca^{2+} permeability and desensitization kinetics of the receptor (for a review see Wonnacott, 2014) (**Fig. 1.2**). Heteromeric nAChR like the α4β2 subtype can present two alternate stoichiometries, the $(\alpha4)_2(\beta2)_3$ and the $(\alpha4)_3(\beta2)_2$ stoichiometries. These alternate forms display different pharmacological profiles and biophysical properties (Moroni *et al.*, 2006; 2008; Tapia *et al.*, 2007; Harpsøe *et al.*, 2011; Mazzaferro *et al.*, 2011; Fucile, 2004) and trafficking and cell localization (Colombo *et al.*, 2013). The functional differences between these receptor forms are defined by the subunit in the fifth position (Moroni *et al.*, 2006; Harpsøe *et al.*, 2011; Fucile, 2004; Mazzaferro *et al.*, 2011; 2014; 2017).

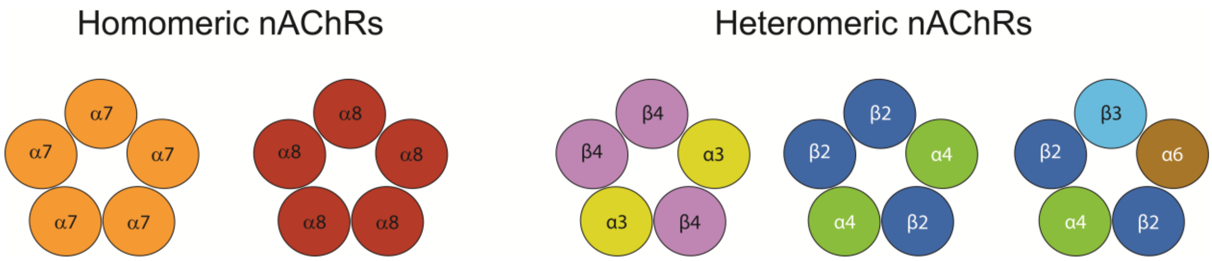

Figure 1.2. Assembly of neuronal nAChRs. Diagram showing some examples of heteromeric and homomeric neuronal nAChRs.

1.3.2. The ECD

The ECD of nAChR subunits, and indeed of all Cys loop proteins, is composed of six inner β-strands (β1-β6) and four outer strands (β7-β10) forming a β-sandwich core stabilized by inner hydrophobic residues (**Fig. 1.1**). The ECD is covalently linked to the TMD through the N-terminal of β10 strand and the C-terminal of TM1. The β-strands are also connected to one another by loops that vary in length and structure. Some of these loops like the Cys-loop (β6-β7 linker), the β1-β2 loop, the β8-β9 (F) loop, loop A, loop B and loop C play critical roles in agonist binding and coupling agonist binding to the opening of the ion channel (Corringer *et al.*, 2012).

1.3.2.a. The agonist binding site

Biochemical and electrophysiological studies (Mishina *et al*., 1985; Tomaselli *et al*., 1991; Akk *et al*., 1999; Kao *et al*., 1984; Galzi *et al*., 1990), together with the crystal structures of either AChBP or nAChR bound to agonists or antagonists (Brejc *et al*., 2001; Unwin 2005; Morales-Perez *et al*., 2016; Walsh *et al*., 2018; Gharpure *et al*., 2019), located the agonist binding site between the ECD of an α-subunit and an adjacent subunit. These elements of the agonist binding site are referred as principal or (+) side and complementary or (-) side, respectively. The agonist binding site is mainly formed by six non-contiguous regions historically designated as loops A to F. Loops A, B and C are localized on the principal side, whereas loops D, E, and F are localized on the complementary side. Loops D and E are actually residues of β–strands; they were considered as loops before the atomistic structures for this family of proteins became available (Pless and Lynagh, 2014). In general, loops from the principal side of the binding site are highly conserved and associated with ligand affinity, whereas loops from the complementary region are more variable and assumed to contribute to ligand subtype selectivity (Marotta *et al*., 2014). Five aromatic residues from these loops have been identified to establish binding interaction with agonists. These residues, named by the loop on which they reside, are TyrA, TrpB, TyrC1, TyrC2 and TrpD and define the aromatic box (Cecchini and Changeux, 2015) (**Fig. 1.3**).

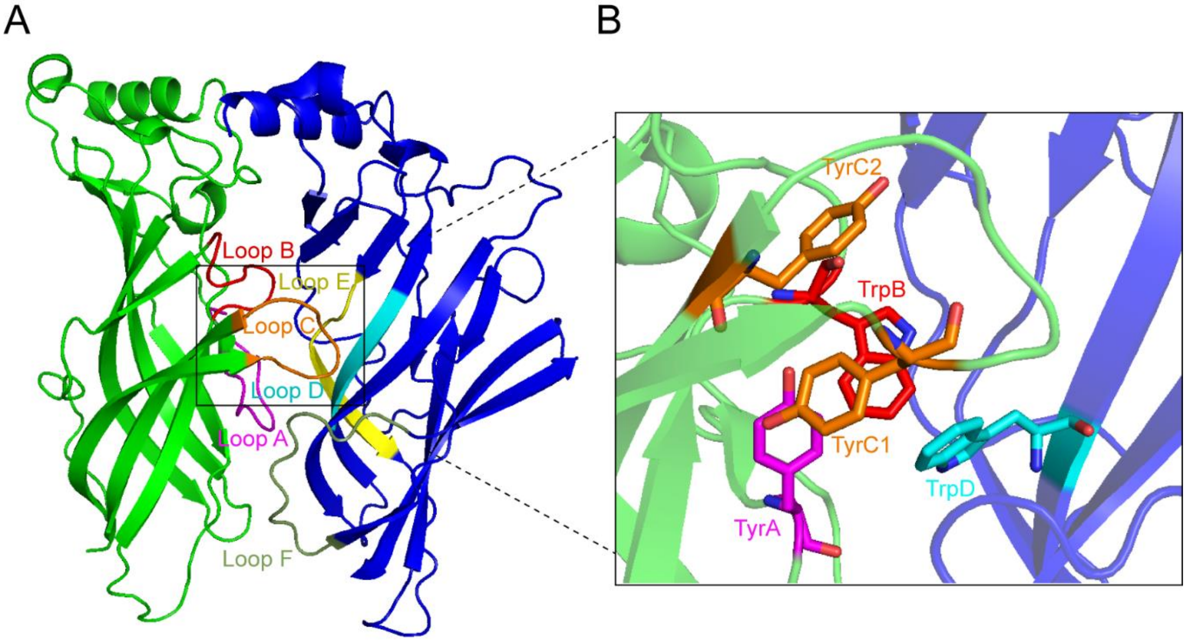

Figure 1.3. Agonist binding site of nAChRs. **A)** Conserved loops in the principal (+) side (A, B and C) and in the complementary (-) side (E, D and F). **B)** Conserved aromatic residues (TyrA, TrpB, TyrC1, TyrC2 and TrpD) at the agonist biding site of nAChRs. Generated from the published structure 5kxi.pdb (Morales-Perez *et al*., 2016) using PyMol (http://www.pymol.org).

Efficacious activation of any nAChR occurs when an agonist occupies at least two agonist binding sites; binding to a single site fails to induce the overall conformational change needed for receptor gating (Wang *et al.*, 2015). In homomeric receptors with five putative agonist binding sites, full receptor activation is achieved by the occupancy of 3 non-consecutive sites (Wang *et al.*, 2015; Rayes *et al.*, 2009), but higher occupancy promotes desensitization (Rayes *et al.*, 2009). In contrast, full activation is achieved in heteromeric nAChRs with occupation of only two agonists sites (e.g., muscle or $(\alpha4)_2(\beta2)_3$ nAChRs). Some heteromeric nAChR such as $(\alpha4)_3(\beta2)_2$ present three agonist binding sites and, although occupation of two sites is sufficient for efficacious receptor activation, occupation of the three sites increases the amplitude of the maximal current (Harpsøe *et al.*, 2011; Mazzaferro *et al.*, 2011; 2014).

1.3.2.b. Allosteric sites at the ECD

In addition to the agonist binding sites, the ECD of nAChRs also presents binding sites for a variety of allosteric ligands. Most neuronal nAChRs present an allosteric binding site for Ca^{2+} located close to the TMD at the subunit interfaces that host the agonist binding sites (Galzi *et al.*, 1996). The α4/α4 interface of $(\alpha4)_3(\beta2)_2$ stoichiometry also hosts allosteric sites for the potentiators Zn^{2+} (Moroni *et al.*, 2008) and NS 9283 (Timmermann *et al.*, 2012). Also, morantel, an α3β2 potentiator binds at the β(+)/α(-) interface of the ECD of this receptor subtype (Seo *et al.*, 2009). The β(+)/α(-) interface in α4β2 nAChR also contains the inhibitory binding site for Zn^{2+} (Moroni *et al.*, 2008).

1.3.3. The TMD

The composition of the TMD was initially predicted by hydropathy plots (Schofiel *et al.*, 1987) and later confirmed by the 4 Å model of the *Torpedo* nAChR (Unwin, 2005) and subsequently refined by the insights provided by the resolved X-ray structures of Cys loop proteins (e.g. Miller and Aricescu, 2014; Morales-Perez *et al.*, 2016) . The TMD comprises four membrane-spanning α-helices in each subunit of the pentamer (**Fig. 1.4A-B**). They are symmetrically arranged forming an inner ring of M2 helices, an intermediate ring of M1 and M3 that shields the inner ring, and an outer ring of M4 (Morales-Perez *et al.*, 2016). The M4 helices are located on the periphery of each subunit and are highly exposed to the lipid bilayer with which they interact extensively (Henault *et al.,* 2015). These four α-helices are structurally connected by functionally important loops. The M1 is connected to the β10 strand of the ECD and also to the M2 through an intracellular linker. The long intracellular linker between M3 and M4 varies in length depending on the subunit subtype and contains several phosphorylation sites (Hunganir and Greengard, 1990). On the contrary, the M2-M3 linker is extracellular and a well-established element of the gating process (Campos-Caro *et al.*, 1996; Lee and Sine, 2005). The C-terminal part of every subunit is also exposed to the extracellular space.

1.3.3.a. The ion pore

Before the resolution of full-length crystal structures of nAChRs, early affinity-labelling experiments using ion channel-blockers (Giraudat *et al.*, 1986; Hucho *et al.,* 1986) showed that the ion pore was a cavity that transverses the plasma membrane and that the walls of the pore were made by the M2 α-helices of each subunit contributing to the pentameric complex. The lining of the pore consists of concentric rings of hydrophobic residues that are numbered by their position from the bottom (-1’) to the ECD (20’) as shown in **Fig. 1.4C**. Generally, the 20’ ring consists of polar residues followed by two rings of hydrophobic residues at positions 16’ and 13’ (leucine and valine, respectively). A highly conserved leucine residue is present at position 9’ (L9’). The last three rings are formed by polar residues. Negatively-charged glutamate residues at -1’ position, namely the selectivity filter, provide a favourable electrostatic environment for the coordination of the cations (Gielen and Corringer, 2018).

The ion pore diameter changes depending on the functional state of the receptor. Crystal structures in resting or close states (Miyazawa *et al.*, 2003; Unwin, 2005) show a 6 Å constriction at the level of 9’ and 13’ rings sufficient to block the ion flow and which is not present in open states structures (Du *et al.*, 2015). This strongly suggests that this hydrophobic girdle is the main gate. Desensitized structures (Morales-Perez *et al.*, 2016; Gharpure *et al.*, 2019) present the narrowest point at the -1 ring of the pore (**Fig. 1.4**).

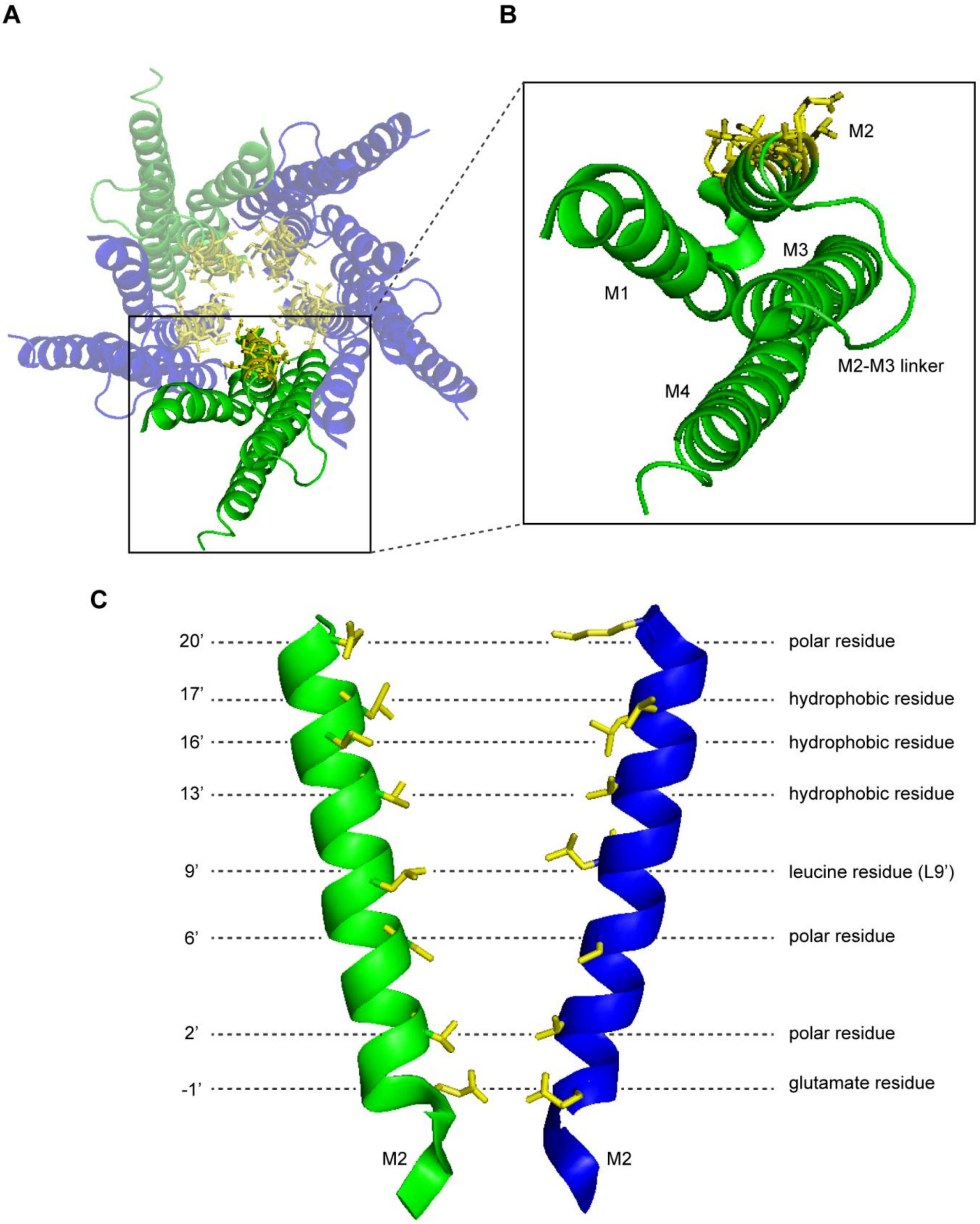
A
B
M2
M3
M1
M2-M3 linker
M4
C
20’
17’
16’
13’
9’
6’
2’
-1’
polar residue
hydrophobic residue
hydrophobic residue
hydrophobic residue
leucine residue (L9’)
polar residue
polar residue
glutamate residue
M2
M2

Figure 1.4. The ion pore of nAChRs. **A)** Top view of TMD showing as sticks the residues at the M2 helice lining of the ion pore. **B)** The four α-helices (M1-M4) from the ECD of a single subunit. **C)** Positions of ordered residues in the ion pore and corresponding residue types in a desensitized receptor. Generated from the published structure 5kxi.pdb (Morales-Perez *et al.*, 2016) using PyMol (http://www.pymol.org).

1.3.3.b. Allosteric binding sites at the TMD

The TMD of the nAChRs and, indeed of all pLGICs (Taly *et al.*, 2014) contain binding sites for various allosteric modulators. The intersubunit cavity located in the upper part of the TMD has been determined as a common allosteric site. α7 allosteric modulators such as invermectin, LY 2087101 or PNU 120596 bind at this site (Corringer *et al.*, 2012; Pandya and Yakel, 2013). The cavity between M3 and M4 helices of the α4 subunit presents an allosteric site for the α4β2 potentiator desformylflustrabromine (dFBr) (Alcaino *et al.*, 2017). Other allosteric sites are located between two subunits at the TMD. For example, the general anesthetic etomidate binds at a cavity in the TMD between the γ/α interface of the *Torpedo* nAChR (Hamouda *et al.*, 2013). The M2-M3 loop also has been identified to host an allosteric site for the α7 selective allosteric modulator NS1738.

1.3.4. The ICD

The recently published cryo-EM structure of the α3β4 nAChR (Gharpure *et al.,* 2019) shows for the first time, in a high-resolution, the ICD. Atomistic structures for Cys loop receptors prior to the work of Gharpure *et al.* (2019) were obtained for receptor constructs lacking the ICD domain to mimic their prokaryotic counterparts. Gharpure and his team reconstituted the receptor into a functionally supportive lipidic environment avoiding its loss as happened in previous structures (Morales-Perez *et al.*, 2016; Walsh *et al.*, 2018). The ICD consists of a short post-M3 loop (MX) and a membrane-associated helix of M4 (MA) (**Fig. 1.1**), separated by a flexible and very variable portion. MA and MX play important roles in cellular trafficking, gating process and ion conductance (Bouzat *et al.*, 1994; Hales *et al.*, 2006; St John, 2009).

The MA is an extension of the M4 helix that penetrates into the cytosol and forms a conical intracellular vestibule at the bottom of the ion pore. The vestibule lining is composed by polar residues and presents an “hydrophobic plug” at the bottom of the structure (Gharpure *et al.*, 2019). Conserved electropositive residues at this region are projected into the lateral portals and force the ions flow in this direction. The MX lies parallel to the plane of the membrane and may be stabilized through interactions with MA helix. Despite this orientation it does not appear to fully block the ion permeation (Gharpure *et al.*, 2019). However, in the 5-HT$_{3A}$ structure the MX seems to be pulled away from the lateral portals (Basak *et al.*, 2018).

1.4. Activation of nAChRs

The activation of nAChRs (and indeed of all Cys loop receptor activation) is essentially an allosteric process that couples the binding of agonist to the agonist site in the ECD to the gating of the ion channel located approximately 50 Å away in the TMD (Albuquerque *et al.*, 2009).

Upon prolonged agonist binding, the channel enters into a desensitized state that does not allow ion permeation (Albuquerque *et al.*, 2009). After desensitization, receptor transitions to the resting state in order to be again available for agonist activation. This recovery involves first agonist dissociation from the desensitized state followed by conformational changes toward the resting state which, depending on the receptor subtype, can be a slow or rapid trasition.

1.4.1. Transitions between states

In order to explain the transitions between these states, different mechanistic models have been proposed. The first one corresponds to Del Castillo and Katz (1957), who distinguished the agonist binding and the gating as two different processes, being the first a pre-requisite for the second. In this three steps model, a full agonist has infinite affinity for the open state whereas a partial agonist has a lower one. The Monod-Wyman-Changeux (MWC) model (Monod *et al.,* 1965) proposed that unliganded spontaneous openings can occur although the probability of this occurring is extremely low. This model can explain some gain-of-function mutations where this probability increases. When single-channel methods were developed, it became possible to estimate the binding affinities for the two agonist binding sites (Colquhoun and Sakmann, 1985).

The MWC model presented some limitations as it only predicts one shut state in absence of agonist and another shut state in saturating agonist concentrations that could not fit all the experimental data. Mutation studies using free energy relationships (Grosman *et al*., 2000) suggested that receptor activation occurs as a progressive stepwise wave of conformational changes from the agonist binding site to the ion pore. Lape *et al.* (2008) proposed three intermediate pre-active states called “flipped” states with a higher affinity for the agonist than the resting state. The “flip” model assumes that all the subunits flip simultaneously even if only one agonist binding site is occupied. To explain differences between full and partial agonists they proposed that partial agonists are inefficient at eliciting the change between shut and “flipped” states compared to full agonists. In contrast to the “flip” model, Mukhtasimova *et al.* (2009) proposed that subunits can “flip” (or “prime”) independently and thus, they predicted two pre-active states for each agonist binding site. A “catch and hold” model (Purohit *et al.*, 2014; Nayak and Auerbach, 2017) was also proposed. According to Plested (2014), in this model there is first a low affinity pre-active state (“catch”) followed by another high affinity pre-active state (“hold”), which can be seen as a “flip” into a globally high affinity conformation (**Fig. 1.5**). Clearly, these views are not per se contradictory but rather they seem to be simply different forms, largely guided by the experimental approaches used by the researchers, of describing the same phenomenon -that upon agonist activation the receptor undergo conformational changes that tip the complex to gating and that the key transitions that differentiate full agonists from partial agonists are the transitions that occur just before activation. A key task in the field is to capture those conformational stages.

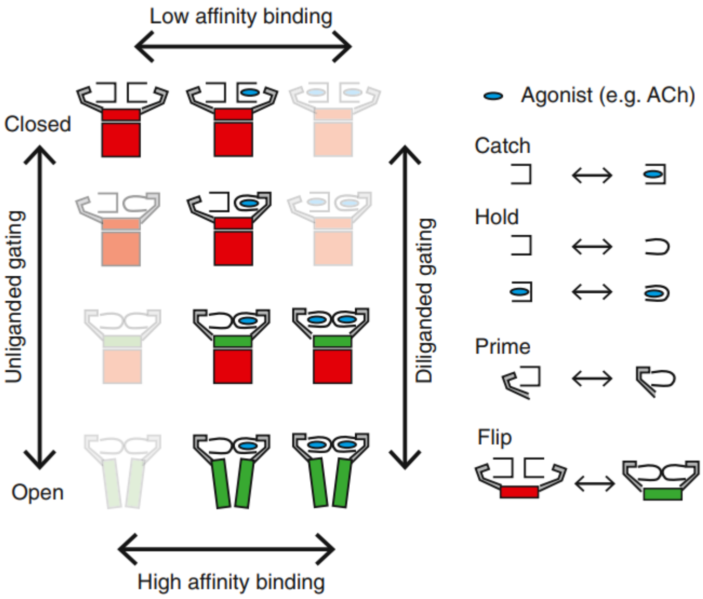

Figure 1.5. “Catch and hold” activation model. Schematic diagram of the transitions between different receptor states during receptor activation. Reproduced from Plested, 2014.

1.4.2. Agonist recognition

Based on the structures of AChBP or nAChR-bound to Nic (Celie *et al.*, 2004; Morales-Perez *et al.*, 2016), three main interactions are evident. i) Cation-π interactions between the Nic N^+H group of agonists and the TrpB and/or TyrC1. The cation-π is a critical stabilizing interaction between the electron-rich π system of an aromatic ring and an adjacent cation. ii) A hydrogen bond between the positively charged N^+H group and the negatively charged backbone CO of TrpB that cannot be substituted using conventional site-directed mutagenesis. iii) A water-bridged hydrogen bond between backbone carbonyls from loop E and the Nic pyridine nitrogen (**Fig. 1.6**). These interactions have also been seen for other agonists, including Cyt.

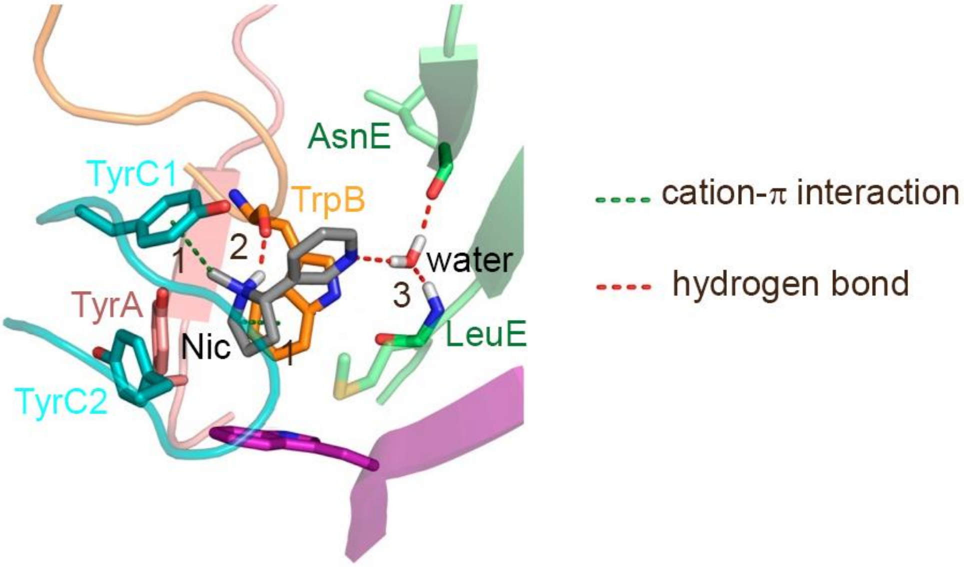

Figure 1.6. Nic binding interactions at the AChBP agonist binding site. The main interactions with Nic are numbered by 1) cation-π interactions through TrpB and TyrC1 2) hydrogen bond through TrpB and 3) water-bridged hydrogen bonds through residues at loop E. Adapted from Van Arnam and Dougherty, 2014.

Although the aromatic box is conserved across the nAChR family, the above interactions may vary among the subtypes, providing a basis for agonist subtype selectivity (see review by Pless and Ahern, 2013). The cation-π interaction is essential for ligand recognition and stabilization in nAChRs. In most nAChRs, this interaction is established with TrpB (Xiu *et al.*, 2009; Puskar *et al.*, 2011; Van Arnam and Dougherty, 2014) but in some subtypes such as the α7 receptor this interaction occurs via TyrA and/or TyrC2 (Puskar *et al.*, 2011). Despite not being involved in the cation-π interaction, TrpB is absolutely required for agonist recognition in α7 and universal for all the nAChRs. Regarding the hydrogen bond between TrpB and the N^+H group of Nic, this interaction is not present in all nAChRs. In α4β2 for example, the hydrogen bond with TrpB is present for most of the agonist except for ACh which present a strong cation-π interaction. For others like the α7 or the muscle receptor, the interaction appears to be weak or absent (Van Arnam and Dougherty, 2014). At the complementary side, loop E residues can form water-bridged hydrogen bonds in nAChRs. However, this interaction appears to be weak or absent for some subtypes such as the α7 nAChR (Van Arnam and Dougherty, 2014).

1.4.3. Molecular mechanisms of signal transduction

Some nAChR homologues such as GLIC (Prevost *et al.*, 2012; Sauget *et al.*, 2014), GluCl (Hibbs and Gouaux, 2011; Althoff *et al.*, 2014) and GlyR (Du *et al.*, 2015; Huang *et al.*, 2015) have been captured in the open, close and desensitized conformational states. Superimposition of the crystal structures in open and close states allowed to identify the overall rearrangements associated with channel gating. The "blooming" and "twisting" mechanism was proposed in order to explain a common phenomenon that crystal structure analysis and molecular dynamic simulations noted (Althoff *et al.*, 2014). During receptor activation, the ECD of the receptor goes from an expanded state (blooming) to a contracted state ("unbloomed") stabilized by agonist binding, and the entire receptor rotates (twisting) (**Fig. 1.7**). Simulations suggest that receptor twisting prevents the spontaneous re-organization of the TMD helices in the active state, thus "locking" the channel in the open form. To reach the contracted and twisted state, receptor transitions proceed through a progressive stepwise wave of conformational changes that starts from the agonist binding site, propagates to the ECD/TMD interface, moves down to the TMD helices and ultimately opens the ion pore (Calimet *et al.*, 2013; Sauguet *et al.*, 2014).

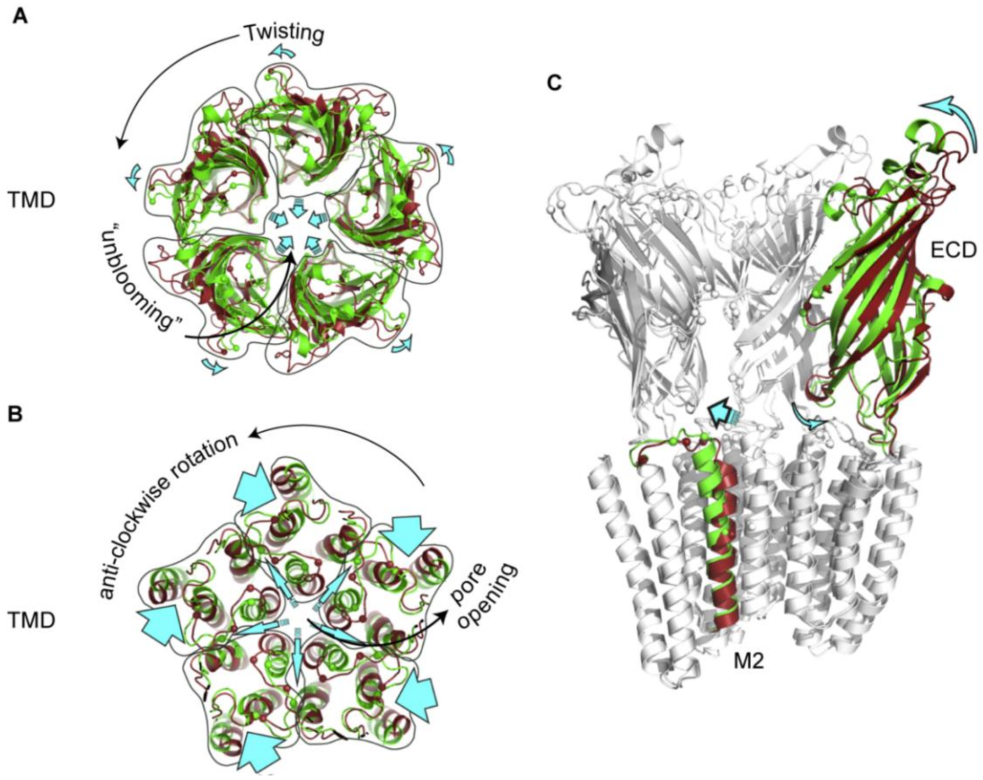

Figure 1.7. Conformational changes during receptor activation. Structural differences between resting and active states of **A)** the ECD, **B)** the TMD and **C)** the overall receptor. Generated by superposition of the published GLIC structures solved in active- (pH 4) and resting-like (pH 7) states. Adapted from Nemecz *et al.,* 2016.

First, loop C move towards receptor core “capping” the agonist within the binding site (Nemecz *et al.*, 2016). It has been proposed that the extent of capping is related to the nature of the ligand: antagonists induce an extended conformation, whereas full agonists induce full contraction of loop C and partial agonists, an internmediate contraction (Brams *et al.*, 2011). Auerbach and his team (Purohit *et al.*, 2014), however, proposed loop C contraction as a part of the “catch” state for partial agonists and “hold” state for full agonists.

Structural rearrangements were also observed in loop F. However, there is a lack of consensus among authors on the role of loop F. Some have suggested this loop is a key element in channel gating (Zhang *et al.*, 2009; Thompson *et al.*, 2006) whereas others concluded that loop F plays a role in ligand accommodation but not in receptor activation (Khatri *et al.,* 2009; Pless and Lynch, 2009). A recent study using molecular dynamics simulations on α4β2 nAChR bound to agonist (Oliveira *et al.*, 2019) proposes that loop F participates in the signal propagation that goes from loop C to loop F and then to the M2-M3 linker. The signal is then propagated to the ECD/TMD interface.

Communication between the ECD and TMD is mediated primarily by the covalent link between β10 and M1, as well as by non-covalent connections between the β1/β2 and Cys-loop of the ECD and the M2-M3 loop of the TMD (Lee and Sine, 2005; Jha *et al.*, 2007). Finally, the channel opening results from a quaternary twist of the protein where the ECD rotates clockwise and the TMD in the opposite direction. The anti-clockwise rotation of the TMD pulls the M2 helix away from the channel axis, thus enlarging the pore size for channel opening (Nemecz *et al.*, 2016) (**Fig. 1.7**).

1.4.4. Molecular mechanisms of desensitization

Continuous or repeated exposure to an agonist causes the receptor transit from active to desensitized state. The desensitized state consists of a non-conducting conformation where the agonist is still bound (Katz and Thesleff, 1957). The ion pore is closed limiting ion flow; in spite of the receptor having the highest affinity for the agonist.

Early experimental studies studied desensitization kinetics and distinct fast and slow desensitization states. Desensitization has been therefore classically considered as a two-component phenomenon (Giniatullin *et al.*, 2005). Transition towards the desensitized state results in a collapse of the lower part of the M2. Crystal structures solved in desensitized states (Morales-Perez *et al.*, 2016; Gharpure *et al.*, 2019) showed a hydrophobic constriction at the -1 ring of the ion pore. In addition, desensitization also involves rearrangements of the upper part of the TMD reaching the ECD-TMD interface (Bouzat *et al.*, 2008; Gielen and Corringer, 2018).

The mechanism of desensitization is not fully understood but it has been suggested to play an important role in preventing receptor over-activation in pathological conditions (Jones and Westbrook, 1996) and likely defines the signalling functions of nAChRs in the brain (Giniatullin *et al.*, 2005). Hence, modulation of desensitisation is a valid target for drug discovery, particularly those targeting α7 nAChR (see **section 1.5.3** of this chapter). Impaired desensitization has been associated with several diseases. For example, autosomal dominant nocturnal frontal lobe epilepsy (ADNFLE) can be produced by mutations in nAChR subunit genes that cause faster desensitization kinetics (Bertrand *et al.*, 1998).

1.5. Pharmacology of nAChRs

As for other functional proteins, nAChR ligands are classified according to their functional effects. First, ligands that bind the agonist binding site and produce full or partial receptor activation are classified as agonists. Second, compounds that bind the agonist site without inducing activation are termed competitive antagonists. And third, there are allosteric modulators, which bind at sites away from the agonist binding site. These compounds have no effects on their own but in the presence of agonists they enhance or decrease the responses elicited by the agonists, depending on whether they are positive allosteric modulators (PAMs) or negative allosteric modulators (NAMs) (Wonnacott, 2014). The overall functional effects of nAChR ligands are largely determined by the nature of the nAChR subtype. For example, Cyt is a full agonist at α7 nAChR but behaves as a poorly efficacious agonist at the α4β2 subtype. The efficacy of Cyt at $(\alpha4)_2(\beta2)_3$ nAChR is so low that this ligand is considered a competitive antagonist of this subtype (Rego-Campello *et al.*, 2018). Therefore, the ligand action is not an intrinsic property of the molecule but a consequence of the interaction with a particular nAChR subtype. It is those interactions that need to be identified to develop more selective ligands.

1.5.1. Agonists

nAChR agonists are structurally diverse but they all have a cationic nitrogen and hydrogen bond acceptors (**Table 1.2**). Typically, the cationic nitrogen binds through a cation-π interaction to TrpB and a hydrogen bond to the backbone carbonyl of the same residue. The hydrogen bond acceptor moiety (e.g., the pyridine nitrogen of Nic) makes hydrogen bonds to the backbone NH of LeuE of the complementary subunit of the agonist site (see section **1.4.2** of this chapter for exceptions to these interactions).

In general, nAChR agonists are able to activate most nAChRs, albeit with different affinity and efficacy (a measure of the ability of agonists to induce the same level of activation induced by maximal concentrations of ACh). For example, Nic or Cyt interact with all nAChRs but they do so with an affinity and efficacy defined by the nAChR subtype. Thus, Nic or Cyt activates α7 and muscle nAChRs with low potency but with full efficacy whereas at α4β2 nAChR, these agonists behave as partial agonists but with high potency (for a review see Wonnacott, 2014). Similarly, epibatidine (Epi), one of the most potent nAChR ligands so far identified, show marked differences in the affinity displayed at heteromeric and homomeric nAChRs (Xiao and Kellar, 2004) (**Table 1.2**). Some agonists are highly specific like PNU 282987 that appears to bind only the α7 subtype (Bodnar *et al*., 2005) and AT-1001 that displays agonist activity only at α3β4 nAChRs (Tuan *et al*., 2015; Xiao *et al*., 2006) (**Table 1.2**). There are also desensitising agonists. For example, NS6740 binds the agonist binding site of the α7 nAChR and induces desensitization without prior activation (Papke *et al*., 2015). Other types of ligands are the allosteric agonists that activate nAChRs by binding to sites different to the agonist site. A typical example is 4BP-TQS, which activates α7 nAChR by likely binding to an allosteric site within the TMD (Gill *et al.,* 2011). This compound however inhibits other nAChRs (**Table 1.2**). Another interesting feature of agonists is superagonism. Superagonists induce maximal responses that are greater than those induced by maximal currents of the endogenous agonist. An example of this type of agonist is TC-2559, a compound that at the $(\alpha4)_2(\beta2)_3$ nAChR subtype induces maximal responses that are four-fold greater than the responses stimulated by maximal concentrations of ACh (**Table 1.2**) (Moroni *et al*., 2006).

It is clear from the above discussion that despite some degree of selectivity, nAChR agonists display receptor subtype promiscuity. It is this promiscuity that likely underlies most of the off-target effects of nAChR ligands and leads to poor clinical outcomes. A key task of the nAChR field is, therefore, the identification of receptor subtype-specific structural elements that may aid the development of highly specific agonists. Considering that binding interactions with the aromatic box are highly conserved, this search may be more fructiferous if it is focused outside the aromatic box.

Table 1.2. Examples of agonists for the nAChRs. Classical, subtype-selective, silent and allosteric agonists are included together with their chemical structure and a brief comment about their action on nAChRs. Adapted from Wonnacott, 2014.

Agonist	Chemical structure	Description
Acetylcholine (ACh)	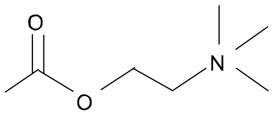	Endogenous non-selective nAChR agonist that also activates muscarinic receptors.
(-)-Nicotine (Nic)	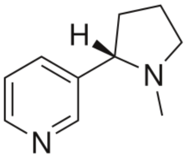	Tobacco alkaloid that activates all nAChR subtypes except α9. Binds preferentially α4β2 with high affinity.
(±)-Epibatidine (Epi)	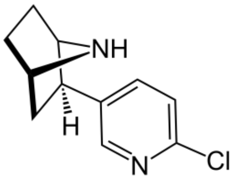	Very potent non-selective originally obtained from skin extracts of the Amazonian frog. Binds preferentially heteromeric receptors.
(±)-Anatoxin A	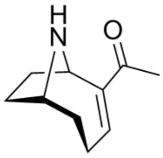	Potent non-selective agonist isolated from a blue green algae. Displays similar properties to ACh
(-)-Cytisine (Cyt)	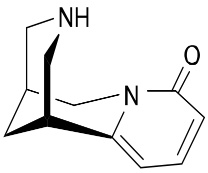	Non-selective alkaloid found in plants of the *Leguminosae* family. Partial agonist with high affinity for α4β2 nAChR but full agonist for α7 and α3β4 with low potency.
Varenicline (Var)	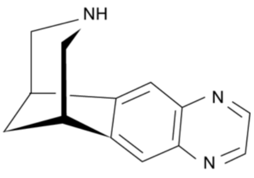	Comercialized as Chantix™ or Chantix™ as treatment for smoking cessation due to its high affinity for α4β2 nAChR. Non-selective agonist similar to Cyt.

Choline	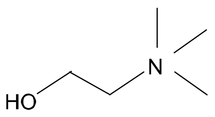	Substrate and hydrolysis product of ACh. Full agonist for α7 and weak partial agonist for α3β4 nAChR.
TC-2559	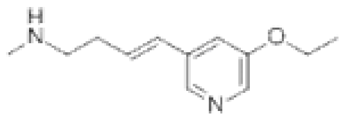	α4β2 selective agonist that acts on $(\alpha4)_2(\beta2)_3$ stoichiometry as a “superagonist” and on $(\alpha4)_3(\beta2)_2$ as a partial agonist.
Sazetidine A (Saz-A)	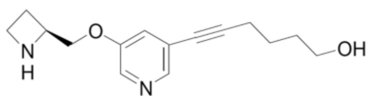	Also a selective agonist for $(\alpha4)_2(\beta2)_3$ stoichiometry and first potent desensitizing agent reported.
PNU 282987	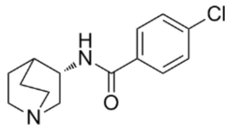	Potent α7 selective full agonist with weak activity on 5-HT_3 receptors.
AT-1001	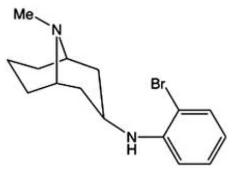	α3β4 selective partial agonist with a sub-nanomolar affinity.
NS-6740	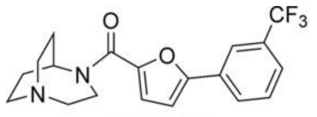	Silent agonist for α7 nAChR. Very weak partial agonist (< 2%) or strong desensitizer of α7 nAChR activity.
4BP-TQS	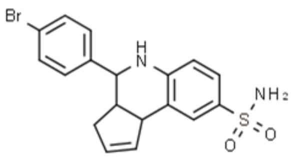	Allosteric agonist for α7 nAChR that behaves as antagonist on α3β4, α4β2 and muscle nAChRs.

1.5.2. Antagonists

The number of potent competitive nAChR antagonists is limited and the design of subtype-selective antagonists is as challenging as that of agonists. Competitive antagonists have been used as pharmacological tools in the identification, characterization and purification of nAChRs subtypes. α-Bungarotoxin (α-Bgt) is a pseudo-irreversible competitive antagonist found within the venom of a Taiwanese snake. Historically nAChRs were classified into α-Bgt-sensitive nAChRs (e.g., α7, α7β2 and the muscle nAChRs) or α-Bgt-insensitive (eg., α2-6β heteromeric nAChRs) (Gotti *et al.*, 2009). In contrast, dihydro-β-erythroidine (DHβE) is often used to detect β2-containing heteromeric nAChR (Harvey *et al.*, 1996).

Numerous toxins have been extracted from marine cone snails and have been named as α-conotoxins. They are peptides of 12-19 amino acids in length that act as highly selective competitive antagonists for different nAChR subtypes depending on the α-conotoxin. Vc1.1 is selective for α9α10 nAChR whereas MII is selective for α3β2 and α6-containing nAChRs (**Table 1.3**) (Azam and McIntosh, 2009).

There are nAChR inhibitors that are neither competitive nor NAMs. Non-competitive antagonists are typically channel blockers that may interact specifically with residues at the lining of the pore obstructing the ion flow. For example, mecamylamine is a non-selective nAChR ion blocker (Harvey *et al.*, 1996). Some antidepressants like bupropion, Ca^{2+} channel blockers or NMDA receptor antagonists can also behave as nAChR channel blockers. Indeed, bupropion is the only non-nicotine drug marketed for smoking cessation (Zyban®), whose principal pharmacological target is inhibition of dopamine and noradrenaline transporters (Wonnacott, 2014). However, bupropion has also been shown to act as a non-competitive inhibitor of human α3β4 ganglionic nAChRs (Fryer and Lukas, 1999) and inhibits α3β2, α4β2 and α7 nAChRs expressed in *Xenopus* oocytes (Slemmer *et al.*, 2000). Thus, bupropion smoking cessation properties may result from both its nAChR antagonism and its effects on dopamine and noradrenaline uptake systems. In addition, many agonists at high concentrations as well as any positively charged small molecule can potentially act as a channel blocker (Wonnacott, 2014).

Table 1.3. Examples of competitive and non-competitive antagonists for nAChRs. Their chemical structure and a brief description of their action on nAChRs are also included. Adapted from Wonnacott, 2014.

Antagonist	Chemical structure	Description
α-Bungarotoxin (α-Bgt)	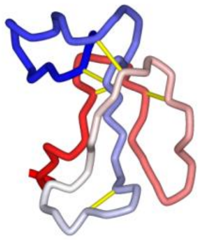	Peptide competitive antagonist found within the venom of a Taiwanese snake. Binds to nAChRs containing α7-α10 subunits and the muscle nAChR.
Dihydro-β-erythroidine (DHβE)	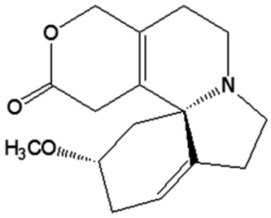	Alkaloid isolated from *Erythrina* seeds. Competitive antagonist of neuronal nAChRs showing high affinity for β2-containing nAChRs.

α-Conotoxin Vc1.1	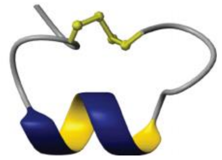	α-Conotoxin peptide effective on α9α10 but on other nAChRs as well (α3β4 and α6-containing nAChRs).
α-Conotoxin MII	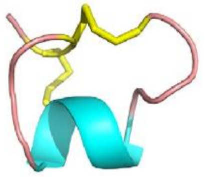	α-Conotoxin peptide that acts as a selective potent competitive antagonist for α3β2 and α6-containing nAChRs.
Mecamylamine	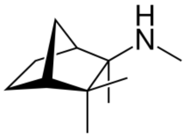	Channel blocker of neuronal nAChRs. Binds preferentially heteromeric nAChRs but it also inhibits α7 and muscle nAChRs.
d-tubocurarine	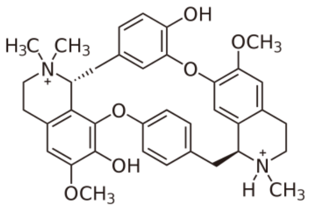 OH OCH3 H3C CH3 N+ O O OH OCH3 N+ H CH3	Muscle relaxant that acts as a channel blocker of muscle nAChR expressed at the neuromuscular junction.

1.5.3. Allosteric modulators

In addition to ligands acting at the agonist binding site and within the channel lumen, nAChRs are modulated by a variety of molecules acting at topographically distinct allosteric sites. Typically, these molecules have low intrinsic activity (though in a few cases act as agonists) but provide selective potentiation or inhibition of physiological activity without directly affecting the ongoing signalling processes of the neurotransmitter. The major modulatory sites (Taly *et al.*, 2009) are located within (i) the agonist site regions (Ca^{2+}, potentiating Zn^{2+}, NS9283), (ii) at sites homologous to the orthosteric site but present at non-agonist binding subunit interfaces (inhibitory Zn^{2+}) and (iii) within the TMD, which is the target of a wide variety of allosteric modulators including dFBr and Type I and II modulators of the α7 nAChR.

PAMs can either lower the energy barrier from resting to active states (type I PAMs) or raise the barrier from open to desensitized (type II PAMs). Both actions result in enhanced agonist-elicited response. **Table 1.4** summarises the best characterised nAChR modulators so far. Like in most Cys loop receptors, ions such as Ca^{2+} and Zn^{2+} allosterically enhance the responses of nAChRs. Although Ca^{2+} does not appear to be receptor subtype specific,

Zn^{2+} may potentiate or inhibit nAChR, depending on nAChR subtype. Thus, Zn^{2+} inhibits α7 and $(\alpha4)_2(\beta2)_3$ nAChRs but potentiates $(\alpha4)_3(\beta2)_2$ subtype (Hsiao *et al.*, 2001; Moroni *et al.*, 2008). In general, PAMs display more subtype discrimination than agonists, even though allosteric binding sites in the Cys loop family of ion channels are conserved (Cechinni and Changeux, 2014). An example of a prototypical type II PAM is PNU 120596 that enhances α7 receptor function but has no effects on other nAChRs. This compound extends the time course of agonist-evoked responses by preventing desensitization (Grønlien *et al.*, 2007) (**Table 1.4**). Also, NS 9283 is a potentiator for α4β2, α2β2 and α4β4 only when they assemble in the stoichiometry containing three α subunits and two β2 and, therefore with an α/α interface (Timmermann *et al.*, 2012).

In contrast to PAMs, NAMs increase the energy barrier from resting to active state and, thus decrease the amplitude of agonist-elicited responses. Progesterone is a typical α4β2 NAM but there are others such as oxantel also for α4β2 nAChR or HDMP for α7 nAChR (Mantione *et al.*, 2012; Abdrakhmanova *et al.*, 2010) (**Table 1.4**).

Table 1.4. Examples of allosteric modulators for nAChRs. Their chemical structure and a brief description of their action on nAChRs are also included. Adapted from Wonnacott, 2014.

Allosteric modulators	**Chemical structure**	**Description**
Desformylflustrabromine (dFBr)	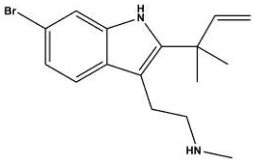	α4β2 selective PAM that also potentiates α2β2 nAChRs. At concentrations higher than 10 µM, it inhibits α4β2 by blocking the ion pore.
Ivermectin	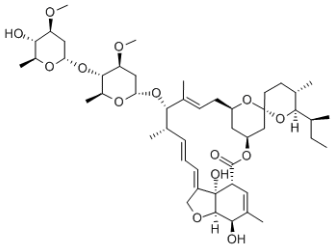	α7 selective type I PAM that also activates $GABA_A$ and GlyR.
PNU 120596	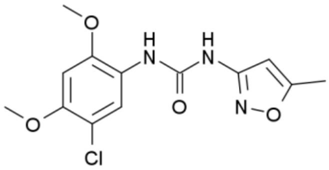	Prototypical type II PAM selective for α7 nAChR that extends agonist response duration by preventing desensitization.

NS9283	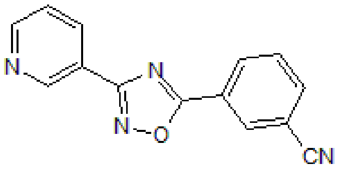	Potentiator for α4β2, α2β2 and α4β4 only when they display a stoichiometry containing three α subunits and two β2.
Divalent cations	Ca^{2+} Zn^{2+}	Ca^{2+} is able to potentiate most neuronal nAChR. Zn^{2+} potentiates α4β4 nAChRs and the $(\alpha4)_3(\beta2)_2$ stoichiometry whereas it inhibits the other α4β2 stoichiometry.
Progesterone	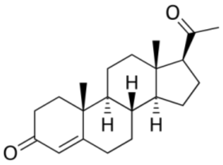	NAM for α4β2 nAChRs.
HDMP	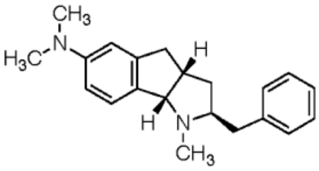	NAM for α4β2 nAChRs.
Oxantel	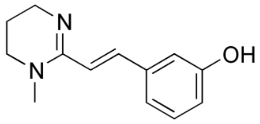	Potent NAM on α7 nAChR that also inhibits α4β2 and α3β4 nAChRs.

1.6. nAChRs distribution in the brain

Neuronal nAChRs are distributed in both central (CNS) and peripheral (PNS) nervous systems. Some subtypes also occur in non-neuronal tissues, including glial, immune and endothelial cells, where they respond to paracrine ACh or choline in the case of α7 nAChRs (Millar and Gotti, 2009; Wonnacott, 2014). In the brain, nAChRs are mostly located in presynaptic terminals from where they modulate the release of neurotransmitters such as dopamine (DA), glutamate, GABA, serotonin or noradrenaline or extrasynaptically (cell body, axons) from where they modulate neuronal excitability (see review by Millar and Gotti, 2009). nAChRs have been also found postsynaptically at cholinergic synapses in the nervous system (Turrini *et al*., 2001). Based on their preferential non-postsynaptic location, it is thought that neuronal nAChRs signal through volume transmission; however, recent studies suggest that these nAChRs drive phasic cholinergic signalling, at least in the forebrain (Sarter and Lustig, 2020).

Most cholinergic neurons in the brain are found in four regions but they project to almost all parts of the brain. These four regions are (i) the brainstem pedunculo-pontine and lateral dorsal tegmental nuclei, (ii) a subset of thalamic nuclei, (iii) the interneurons from striatum and (iv) the basal forebrain nuclei. The four collectively project to neocortex, hippocampus and amygdala (Ahmed *et al.*, 2019). This cholinergic system comprises metabotropic muscarinic receptors and nAChRs and is involved in a variety of physiological functions such as cognition (attention and executive function), learning and memory, mood, reward and sensory processing (Miwa *et al.*, 2011).

In contrast to muscle nAChRs, there is greater diversity among neuronal nAChRs as illustrated in **Fig. 1.8**. The heteromeric α4β2* (* indicates that another subunit such as the α5 or α6 may also be present) and the homomeric α7 nAChRs are the most abundant nAChRs in the mammalian brain, comprising more than 90% of the nAChRs (Albuquerque *et al.*, 2009; Gotti *et al.*, 2009). Like other brain nAChRs, these two subtypes modulate neurotransmitter release. This modulation is especially important in the hippocampus and basal forebrain where they have been associated with plasticity, learning and memory (Levin, 2013). The α7 nAChR is also expressed by non-neuronal immune cells as lymphocytes, macrophages and microglial cells and associated with inflammation (Hone and McIntosh, 2017).

The rest of the subunits appear to have a more restricted distribution in the brain (Gotti *et al.*, 2006a). The heteromeric α7β2 nAChR has been found in the basal forebrain (Moretti *et al.*, 2014) and cortex (Thomsen *et al.*, 2015) of human brains. The α3β4 nAChR is predominant in the autonomic ganglia but it can also be found in the brain and in non-neuronal cells (McCallum *et al.*, 2012; Wessler and Kirkpatrick, 2008). The α5 subunit is associated with approximately 15-40% of the α4β2* nAChRs (Brown *et al.*, 2007). The α6 and β3 subunits are commonly co-expressed and their distribution is restricted to dopaminergic neurones in the striatum and noradrenergic neurons in the visual pathway (Yang *et al.*, 2009; Wonnacott, 2014). The α9 and α10 subunits are not expressed in the brain but they form heteromeric receptors in mechanosensory hair cells from the cochlea where they contribute to auditory processing (Elgoyhen and Katz, 2012).

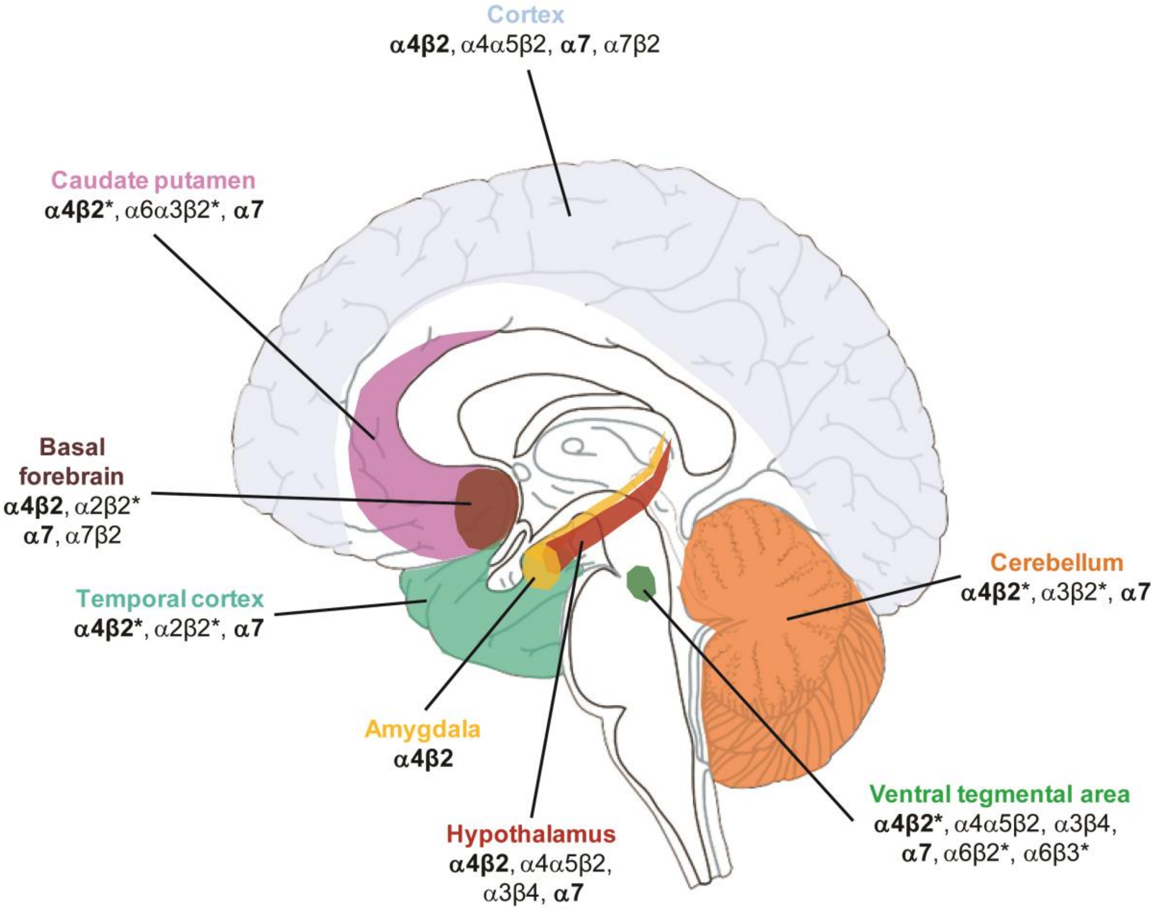
Cortex
α4β2, α4α5β2, α7, α7β2
Caudate putamen
α4β2*, α6α3β2*, α7
Basal forebrain
α4β2, α2β2*
α7, α7β2
Temporal cortex
α4β2*, α2β2*, α7
Amygdala
α4β2
Hypothalamus
α4β2, α4α5β2,
α3β4, α7
Cerebellum
α4β2*, α3β2*, α7
Ventral tegmental area
α4β2*, α4α5β2, α3β4,
α7, α6β2*, α6β3*

Figure 1.8. Distribution of nAChRs in human brain. Adapted from Zoli *et al.*, 2015.

1.7. Neuronal nAChRs in brain pathologies

nAChRs has been linked to a number of human diseases such as Parkinson's disease, Alzheimer's disease, schizophrenia and depression and, they also play an important role in Nic addiction (Steinlein and Bertrand, 2008). Below, the main brain diseases in which neuronal nAChRs have been implicated are briefly described.

1.7.1. Depression

Depression is one of the most common psychiatric illnesses in the world (McLaughlin, 2011). According to the World Health Organization (WHO), a quarter of Europe's population presents depressive or anxiety symptoms and about 7% of the population suffer from a major depression episode every year. The depressed mood is characterised by a loss of interest or pleasure and is often accompanied by other symptoms such as appetite or sleep disturbance, loss of energy, poor concentration or suicidal thoughts.

In 1972, Janowsky *et al*. proposed the cholinergic-adrenergic hypothesis of the depression which postulates that cholinergic hyperactivity contributes to this illness (Janowsky *et al*., 1972). Subsequent clinical and preclinical studies supported this view. A study using proton spectroscopy showed that patients with depression present higher levels of choline in the cerebrospinal fluid, indicating higher cholinergic signalling activity (Charles *et al*., 1994). A more recent imaging study also suggested higher levels of ACh in the brain (Saricicek *et al*., 2012). Moreover, inhibitors of acetylcholinesterase (AChE) seem to exacerbate the depression symptoms whereas inhibitors of nAChRs appear to increase measures of indicators of normal mood (Martinowich *et al*., 2012; George *et al*., 2008). Consistently, epidemiological studies suggest that depression is associated with higher smoking prevalence (Weinberger *et al*., 2016). The smoking rate among patients suffering major depression is around 46-60% compared to the 20% observed in the general population.

Nic has been shown to have antidepressant properties in both preclinical and clinical studies (Phillip *et al*., 2012). Complementing these studies, clinical studies have also shown that transdermal Nic can improve mood in depressed smokers and nonsmokers (Philip *et al*., 2012). The antidepressant effects of Nic are thought to be due to initial activation of nAChRs, followed by rapid desensitisation that leads to long term antagonism (Mineur *et al*., 2018). It is not yet known which nAChR subtype is involved in mood, although work by Marina Picciotto and her team suggests that several types may be involved (Mineur *et al*., 2018). In this study, Picciotto and colleagues (Mineur *et al*., 2018) explored the effect of α7 nAChR antagonists in animal models of depression and found that they ameliorated some symptoms. In addition to α7 antagonists, α4β2 antagonists such as DhβE or mecamylamine also display antidepressant-like effects in mice (Andreasen *et al*., 2009, Shytle *et al*., 2002). A neuronal nAChR antagonist, TC-5214 was tested as adjunct therapy for depression but it showed no efficacy in phase II clinical trials (Vieta *et al*., 2014). In general, inhibition of neuronal nAChR is beneficial in the treatment of depression and trials with new antagonist are on-going.

1.7.2. Alzheimer's disease

Alzheimer's disease (AD) is the most common neurodegenerative disease in the elderly and is characterized by memory and cognitive loss. The aberrant accumulation of amyloid-β

(Aβ) and the development of tau neurofibrillary tangles are biomarkers of this disease (Dineley *et al.*, 2015).

An extensive neuronal loss has been also observed in patients with AD, particularly at the basal forebrain causing a cholinergic deficit. This deficit is evident by the significant reduction in AChE and choline acetyltransferase activities (Dineley *et al.*, 2015). In agreement, the use of AChE inhibitors improves memory and other cognitive functions in AD (Giacobini, 2004). Postmortem studies showed a significant reduction of nAChRs in the brain of patients with AD (Guan *et al.*, 2000; Gotti *et al.*, 2006a).

Additionally, numerous studies have reported that Aβ interacts with nAChRs. In early AD, Aβ tends to accumulate in enriched regions for α7 nAChRs (Wang *et al.*, 2000) and both α7-containing nAChRs and Aβ seem to interact with high affinity (Grassi *et al.*, 2003; Liu Q *et al.*, 2012). However, this interaction is not well understood and studies have reported either activation or inhibition of the receptor by Aβ (Pettit *et al.*, 2001; Tozaki *et al.*, 2002). These differences may depend on the methodology used. In general, short incubation and lower concentrations of Aβ lead to receptor activation, while longer incubation periods and higher concentrations produce an inhibitory effect (Lombardo and Maskos, 2015). The α4β2 nAChR is inhibited by Aβ (Liu Q *et al.*, 2009) and its expression levels are significantly reduced in AD patients (Guan *et al.*, 2000).

Together, these findings support nAChRs as valid targets for AD therapies. Indeed, Nic and its metabolite cotinine seem to exhibit neuroprotective effects against Aβ neurotoxicity (Gao *et al.*, 2014). The already approved smoking cessation medication, Var, showed promising preclinical effects but it did not improve cognitive deficits in phase II clinical trial causing off-target effects (Kim *et al.*, 2014). As explained in **section 1.5.1**, Var activate α7 and α4β2 nAChRs but also the α3β4 subtype which can be the cause of failure. Also, encenicline is an α7 partial agonist that progressed to phase III trials but subsequently was withdrawn due to gastrointestinal toxicity (Mehta *et al.,* 2017). Despite a variety of full and partial agonists for α4β2 and α7 nAChRs have been tested, only the α7 selective partial agonist EVP6124 seems to improve cognition in patients with mild to moderate AD in clinical studies (Deardorff *et al.*, 2015). In general, α7 nAChR agonists and potentially PAMs remain a viable therapeutic strategy for the treatment of AD; however, selectivity and toxicity profiles should be improved (Yang *et al.*, 2017).

1.7.3. Parkinson's disease

Parkinson's disease (PD) is the second most common neurodegenerative disease characterized by a decline in dopaminergic neurons of the nigrostriatal pathway. Symptoms are tremor, postural imbalance, slowness of movement, and rigidity.

Nic facilitates DA release on nigrostriatal neurons (Morens *et al.*, 1995) where $\alpha4\beta2^*$ and $\alpha6$-containing nAChR are the most abundant nAChR subtypes (Grady *et al.*, 2007). Postmortem brains from patients with PD also showed a pronounced decrease in $\alpha6\beta2^*$ nAChR levels (Bordia *et al.*, 2007). A moderate decrease was also observed in $\alpha4$ subunits (Gotti *et al.*, 2006b) but not in $\alpha7$ subunits. Epidemiological studies have shown that smoking is inversely associated with PD, in which tobacco smokers present a lower risk of contracting the disease (Ritz and Rhodes, 2010).

Current therapies use levodopa (L-dopa), the precursor of DA to increase DA levels in this disease (Haddad *et al.*, 2017). However, the aforementined findings suggest that nAChR agonists or PAMs could be beneficial in PD. Nic administration has been reported as an adjunct therapy to minimize L-Dopa-induced dyskinesias, a troubling side effect of L-Dopa therapy (Quik and Wonnacott, 2011). Furthermore, Var has entered in a phase II trial and phase IV as treatments for postural imbalance and excessive daytime sleepiness, respectively (Charvin *et al.*, 2018).

1.7.4. Schizophrenia

Schizophrenia is a neurodevelopmental disorder that affects 1% of the world population. It is characterized by cognitive deficit and schizophrenic patients suffer hallucinations, delusions and paranoia.

There is a high occurrence of Nic smoking (80-90%) and vulnerability to Nic addiction among patients with schizophrenia compared to the general population (de Leon and Diaz, 2005). An explanation for this prevalence is that patients with schizophrenia use Nic as a form of self-medication to compensate for their cognitive deficit (Kumari and Postma, 2005). Indeed, the smoking cessation drug Var also seems to improve cognition deficit associated with schizophrenia (Rollema *et al.*, 2009a).

There is experimental evidence of an association between α7 nAChRs and schizophrenia. First, levels of α7 nAChR mRNA is decreased in the cortex and hippocampus of patients with schizophrenia (Mexal *et al.*, 2010) and α-Bgt binding is also decreased in the thalamus (Court *et al.*, 2002). Additionally, polymorphisms in the upstream regulatory region of the α7 subunit gene (CHRNA7) (Stephens *et al.*, 2009) as well as deletions in the α7 gene have been associated with schizophrenia and psychoses (Stefansson *et al.*, 2008). Moreover, a 2pb deletion polymorphism in the duplicated α7 gene (dupα7) is also significantly associated with schizophrenia (Wang *et al.*, 2014). Human CHRNA7 gene is partially duplicated and the gene product of this duplication (dupα7) lacks the signal peptide and part of the binding site but conserves the TMD (Gault *et al.*, 1998). Both dupα7 and α7 subunits can combine forming a functional receptor (Wang *et al.*, 2014) that may modulate synaptic transmission and cholinergic anti-inflammatory response (Maldifassi *et al.*, 2018).

Several compounds targeting α7 nAChRs entered clinical trials progressing to phases II and III. The first potential nicotinic drug for schizophrenia treatment was DMXB-A, a partial agonist for α7 nAChRs, which improved the negative symptoms in low doses but had no effect in longer treatments (Freedman *et al.*, 2008). However, lack of effectiveness in longer trials was also observed for other nAChR agonists and it has been associated with receptor desensitization produced by Nic from smoking or to the slow-release of the drug into the blood (Kem *et al.*, 2018). To avoid the desensitization problem, α7 PAMs were also tested in schizophrenia but they showed non-significant effects on cognition (Gee *et al.*, 2017). Var, a partial agonist for α4β2 nAChR and a full agonist for α7 nAChRs, improved cognition in patients with schizophrenia as adjunctive to treatment with antipsychotics (Shim *et al.*, 2012).

1.7.5. Pain

Pain is an unpleasant sensation that can be caused by tissue damage (nociceptive) or nerve damage (neuropathic). If the pain persists for longer than 3 months it is considered as chronic pain.

For many years, nAChRs have been explored as targets for pain management. Since Epi as well as Nic display analgesic effects, many studies focused on the potential role of α4β2 nAChR in nociception (Qian *et al.,* 1993; Hamman and Martin, 1992). Potent α4β2 full agonists such as ABT-594 also showed analgesic efficacy in animal models of pain (Banon *et al.*, 1998). However, in human studies these compounds caused analgesia at concentrations that also induced off-target effects (Rowbotham *et al.*, 2009). To reduce adverse effects, PAMs could be used but so far such potentiators have not been described (Lee *et al.*, 2011). While activation of α4β2 nAChRs may be required, it was suggested that activation of other receptors like the α3-containing nAChR would be necessary for a complete analgesic effect (Dineley *et al.*, 2015).

It has also been proposed that agonists or PAMs of the α7 nAChR subtype may be useful as an analgesic. This suggestion is based on the finding that α7 receptors contribute to the inflammatory response (AlSharari *et al.*, 2013; Jonge and Ulloa, 2007). Choline is a selective agonist for α7 nAChRs and showed analgesic effects (Wang *et al.*, 2005). However, most of α7 nAChR agonists failed to produce analgesia and thus, they are not a priority target for pain drug discovery programs. Despite the failure of α7 agonists as analgesics, allosteric modulators of this receptor subtype such as the type II PAM PNU 120596 or silent agonists like NS6740 have been evaluated and showed promising results in animal models of pain (Freitas *et al.*, 2013; Papke *et al.*, 2015).

In addition to α4β2 and α7 receptors, the potential use of α9α10 nAChRs for neuropathic pain treatment has been recently reviewed (Hone *et al.*, 2018). This receptor has been identified in dorsal root ganglia and associated to pain processing (Lips *et al.*, 2002). Selective antagonists and inhibitors for α9α10 nAChRs like RgIA4 or the α-conotoxin Vc1.1 prevent the development of chronic neuropathic pain (Satkunanathan *et al.*, 2005; Romero *et al.*, 2017).

1.7.6. Autosomal dominant nocturnal frontal lobe epilepsy

Autosomal dominant nocturnal frontal lobe epilepsy (ADNFLE) is a rare focal epilepsy with seizures typically arising from the frontal lobe during non-rapid eye movement (NREM) sleep. The seizures are often stereotyped and brief with durations between 5 seconds to 5 minutes. This rare type of epilepsy displays Mendelian inheritance and between 10-15% of the ADNFLE families present gain-of-function mutations in genes encoding α4 or β2 nAChR subunits (Eggert *et al.*, 2015). Typically, these mutations are located at the M2 or the adjacent M3 helices and can produce either an increase in desensitization kinetics

(Bertrand *et al*., 1998) or an increment of $(\alpha4)_3(\beta2)_2$ levels (Son *et al*., 2009). Interestingly, ADFNL patients that possess α4S284L mutation also show cognitive disorders such as autism or intellectual disability (Miyajima *et al*., 2013).

Carbamazapine is a first-choice anticonvulsant for treating ADNFLE. It is a non-competitive channel inhibitor for heteromeric neuronal nAChRs which reduces seizures in about 70% of the patients (Provini *et al*., 2000). However, patients presenting the S284L mutation in the CHRNA4 gene and approximately 30% of other ADNFLE patients are resistant to carbazapine. These individuals are treated with zonisamide, a voltage-dependent sodium channel and T-type calcium channel blocker, and other anticonvulsants such as acetazolamide and topiramate (Fukuyama *et al*., 2020).

1.7.7. Nicotine addiction

Tobacco use is the most important preventable cause of disease and death in industrialized countries. It is a risk factor for cardiovascular and respiratory diseases, including coronary heart disease and lung cancer. According to the World Health Organization, more than 7 million deaths are associated with tobacco use every year (WHO, 2017). The high rates of tobacco smoking are essentially due to the presence of Nic in tobacco. Like other drugs of abuse, Nic produces DA release in the nucleus accumbens (nAcc) when it binds nAChRs in the ventral tegmental area (VTA). This pathway is part of the mesolimbic reward system of the brain (Corrigal *et al*., 1994) (**Fig. 1.9**) and its activation initiates a physiological response that contributes to the reinforcing effects of Nic.

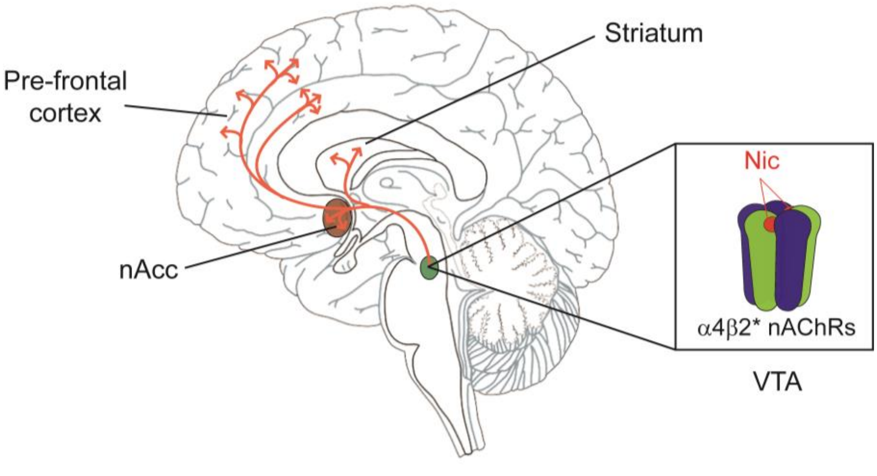

Figure 1.9. The mesolimbic reward system in the brain. The mesolimbic reward system of α4β2 nAChR in theVTA is stimulated by Nic causing the release of DA in the nAcc. Signals to the prefrontal cortex resulting in addictive behaviour (Corrigal *et al*., 1994).

The $(\alpha4)_2(\beta2)_3$ stoichiometry exhibits the highest affinity for Nic of all neuronal nAChRs representing more than the 90% of high-affinity Nic binding in the brain (Zoli, 1998) and, critically, α4 and β2 nAChR subunits are highly expressed in the mesolimbic dopaminergic pathway (Pons *et al*., 2008). Studies using transgenic knockout mice of β2 subunits show a loss in Nic self-administration behaviour, suggesting a central role of this subunit in Nic addiction (Picciotto *et al*., 1998). Re-expression of β2 subunit in these knockout mice rescues the addictive behaviour (Maskos *et al*., 2005). Similarly, α4 knockout mice do not self-administrate Nic and DA release at nAcc induced by this drug is not present in these mice (Pons *et al*., 2008). Also, when the gain-of-function α4L9'A mutation is present in mice they exhibit the same Nic-addiction behaviour than wild type but with a 50-fold lower concentration of Nic (Tapper *et al*., 2007). Chronic exposure to Nic upregulates α4β2 nAChRs, and this phenomenon may underlie the reinforcing properties of Nic. Upregulation of α4β2 nAChRs appears to occur through an increase in the assembly of $(\alpha4)_2(\beta2)_3$ nAChRs (Nelson *et al*., 2003; Moroni *et al*., 2006). Recently, a study carried out by Moretti *et al.* (2018) suggested that polymorphisms that reduce α4 subunit expression may increase α4β2 upregulation induced by Nic. Although Nic interacts with many nAChRs subtypes, activation of the mesolimbic α4- and β2-containing nAChRs is essential for the reinforcing effects of Nic.

In addition to α4 and β2 subunits, other subunits have been identified to play a role in Nic addiction. α6-containing nAChRs such as α6β2β3 and α4α6β2 are also expressed in the dopaminergic neuron cell bodies at the VTA and seem to modulate DA release (Liu L *et al*., 2012). α6 knockout mice exhibit decreased Nic self-administration (Mohamed *et al*., 2015). Moreover, genome-wide association studies (GWAS) have identified polymorphisms in the genes encoding for α3, α5 and β4 subunits associated with a high risk of tobacco dependence and/or lung cancer. The most thoroughly documented genetic variants are in the coding region of the α5 subunit gene (CHRNA5) like the D398N polymorphism that results in a decreased function of the subunit (Kuryatov *et al.,* 2011). In the brain, the α5 subunit combines with other subunits forming nAChRs such as $(\alpha4)_2(\beta2)_2\alpha5$ or $(\alpha3)_2(\beta4)_2\alpha5$. Fowler *et al*. (2011) showed that α5 knockout mice displayed an increased Nic self-administration behaviour due to the attenuation of negative effects of Nic. This finding suggests that α5-containing nAChRs limit Nic intake in rats.

The exact mechanism by which Nic causes addiction is not known but it is likely to involve receptor activation and/or desensitisation (Stoker and Markou, 2013). α4β2* nAChRs in the brain are most likely desensitized at the levels of Nic that smokers are exposed to daily (Benowitz, 2010). During smoking cessation, the decrease of Nic levels in the brain causes withdrawal symptoms such as anxiety, stress, irritability or depressed mood. Partial agonists for α4β2* nAChRs can both mimic some of the rewarding effects of Nic and act as antagonists relieving craving and withdrawal symptoms. In fact, currently approved drug treatments for smoking cessation include Var (approved by the US FDA) and Cyt (approved in East Europe) (Gonzales *et al.*, 2006), both potent partial agonists of the $(\alpha4)_2(\beta2)_3$ nAChR (Moroni *et al.*, 2006). However, these drugs are also full agonists at other nAChRs causing "off-target" effects. Activation of α7 nAChR by Var may be responsible for some adverse neuropsychiatric events observed (McClure *et al.*, 2009; Moore *et al.*, 2011) whereas the cardiovascular events may be attributable to the full activation of glanglionic α3β4 nAChR (Ware *et al.*, 2013). An ideal smoking cessation drug might be a partial agonist for α4β2 nAChR that desensitise/inhibit α3β4 nAChR (Lester and Dougherty, 2019) and do not activate α7 nAChR.

1.8. Aim of the thesis

The overall goal of this thesis was to characterise the nAChR selectivity of a novel group of C(10) Cyt derivatives. The specific objectives were:

a) To characterise the functional effects of C(10) Cyt derivatives on α4β2, α3β4 and α7 nAChRs.

b) To identify the structural determinants underlying the subtype selectivity of C(10) Cyt derivatives.

c) To determine the functional role of these structural elements in the function of α4β2 and α7 nAChRs.

CHAPTER 2. MATERIALS AND METHODS

2.1. Reagents

Standard laboratory chemicals were of Analar grade. Collagenase Type I (C-0130), ACh, Antibiotic/Antimycotic Solution x100 (10,000 units penicillin, 10 mg streptomycin and 25 μg amphotericin B per mL), and amikacin were purchased from Merck (Sigma-Aldrich, UK). Cyt was purchased from Tocris Chemicals (UK). C(10) Cyt derivatives were supplied by Professor Tim Gallagher (University of Bristol). (±)-[^{3}H]Epi with a specific activity of 56-60 Ci/mmol and [^{125}I]α-Bgt ([^{125}I]α-Bgt) with a specific activity of 200-213 Ci/mmol were purchased from Perkin Elmer (Boston MA) and non-radioactive Epi and α-Bgt from Sigma-Aldrich.

2.2. Animals

All animal care and experimental procedures were in accordance with the UK Home Office regulations and were approved by the Animal Use Committee of Oxford Brookes University and Oxford University Biomedical Services. Adult female *Xenopus laevis* toads were purchased from NASCO (US) or *Xenopus* One (US). *Xenopus* toads were housed in static tanks filled with dechlorinated water at a fixed temperature of 17°C. The animals were kept under regular 12 hours light/dark cycles. Animals were fed twice a week with amphibian food pellets. For oocyte harvesting, *Xenopus* toads were were first anaesthetised by immersion in 0.5 % tricaine until non-responsive to toe pinch prior to culling by decapitation. Ovarian lobes were then removed by surgical laparotomy and oocytes prepared for injection, as detailed prepared in **section 2.4** of this chapter. Non-injected oocytes were maintained at 4 ◦C for up to 4-5 days for further injections, if needed. Only one toad per week was sacrificed, thus the overall number of froga used in this study was approximately 120.

2.3. Molecular Biology

Standard molecular cloning techniques, including maintenance and growth of *Escherichia coli* bacterial strains and the use of digestion restriction enzymes were carried out following the procedures described by Sambrook *et al*., (1989). All the nAChR subunit complementary DNA (cDNA) used in this study were previously cloned in house and their nucleotide sequence is as follows: α7 UniProt code P36544, α4 UniProt code P43681, β2 UniProt code P17787, α3 UniProt P32997 and β4 Uniprot P30926. For mutants that displayed a reduced functional expression, complementary RNA (cRNA) was synthesized in order to facilitate their expression by the injected oocytes. First, SwaI was used to linearize the subunit containing plasmids. Full length, capped cRNA was transcribed from linearized plasmids in a reaction mixture (20 µL) using mMESSAGE mMACHINE® T7 Kit (Invitrogen/Ambion Inc., US) and following the manufacturer's instructions. cRNA for the nAChR subunits used in the current study were kept at -80ºC until injection.

2.3.1. Single Point Mutations

Point mutations were carried out following the protocol from the QuikChange^{TM}, site directed mutagenesis Kit (Stratagene, The Netherlands). Oligonucleotide primers for polymerase chain reactions (PCR) were purchased from Eurofins (UK). The protocol used is described below.

I. Oligonucleotides primers (30 to 35 long, Melting T° > 80°C) carrying the mutated nucleotides in the middle of the sequence (**Table 2.1**) were synthesised by Eurofins Europe.
II. The synthesised primers were diluted to a final concentration of 125 ng/µl.
III. *Pfu* DNA Polymerase Kit from Promega (UK) was used to perform the PCR. Reaction mix consisted of the following:

DNA template (50 ng/µl)	1 µl
Forward primer (125 ng/µl)	1 µl
Reverse primer (125 ng/µl)	1 µl
Pfu Buffer 10X	5 µl
dNTPs (2 mM)	5 µl
Dimethyl sulfoxide (DMSO)	3 µl
High Fidelity *Pfu* enzyme	1 µl
Nuclease free water	33 µl
Final volume	50 µl

The parameters for the PCR run were as described in **Fig. 2.1**.

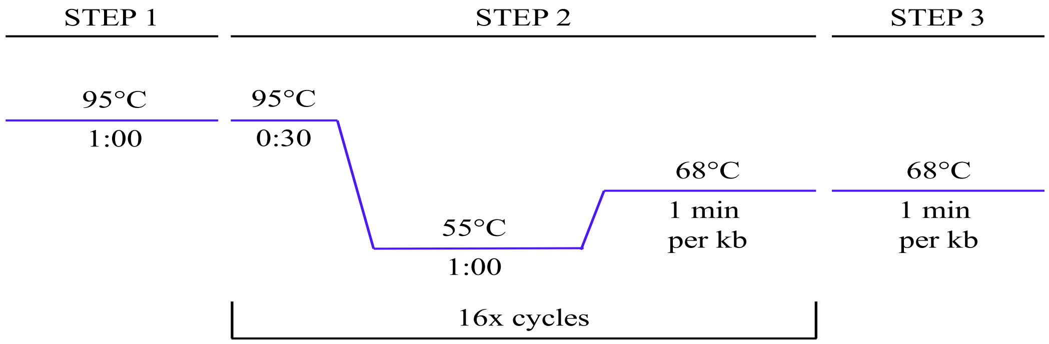

Figure 2.1. Diagram of three steps for polymerase chain reaction (PCR). Step 2 is repeated 16 times and comprises the main stages of the reaction: DNA denaturation (95°C), primer annealing (55°C) and primer extension (68°C).

IV. 1µl of the enzyme DpnI (Promega, UK) was added to the PCR mixture and incubated at 37 C° for one hour. DpnI degrades the methylated DNA. Since methylation is mediated by bacterial enzymes, it is only the template cDNA that is methylated. Thus, at the end of the incubation with DpnI, only the newly synthesised cDNA (the mutated cDNA) will remain.

V. 50 µl of XL10-Gold ultracompetent *E. coli* cells (Agilent, US) were transformed with 20 µl of the digestion product. After overnight incubation at 37°C, 3-5 colonies were picked and amplified by growing them in 10 ml of Terrific Broth medium (Sigma-Aldrich, US) with ampicillin (80µg/mL) at 37°C. The following day, the plasmid was isolated from the bacteria using a commercially available kit (SmartPure DNA purification kit; Eurogentec, Belgium), and fully sequenced to confirm the presence of the desired mutation and verify the sequence of the non-mutated regions.

Table 2.1. The α7 and α4β2 primers for single point mutations.

Mutation	Forward primers (5’ - 3’)	Reverse primers (3’ - 5’)
α7L60A	TTCAGCCTGAGCCTG**GCG**CAGATCATGGATGTG	CACATCCATGATCTG**CGC**CAGGCTCAGGCTGAA
α7L131V	TTCCACACCAACGTG**GTG**GTCAACAGCAGCGG	CCGCTGCTGTTGAC**CAC**CACGTTGGTGTGGAA
α7Q139F	AGCAGCGGACACTGC**TTC**TACCTGCCACCTGG	CCAGGTGGCAGGTA**GAA**GCAGTGTCCGCTGCT
α7T128S	GATGCCACCTTCCAC**AGC**AACGTGCTGGTCAAC	GTTGACCAGCACGTT**GCT**GTGGAAGGTGGCATC
α7S172T	AAGTTCGGAAGCTGG**ACC**TACGGCGGATGGTCC	GACCATCCGCCGTA**GGT**CCAGCTTCCGAACTT
α7G174D	TTCGGAAGCTGGTCCTAC**GAC**GGATGGTCCCTGG	CCAGGGACCATC**GTC**CGTAGGACCAGCTTCCGAA
α7G174A	TTCGGAAGCTGGTCCTAC**GCC**GGATGGTCCCTGG	CCAGGGACCATC**CGG**CGTAGGACCAGCTTCCGAA
α7G174R	TTCGGAAGCTGGTCCTAC**AGA**GGATGGTCCCTGG	CCAGGGACCATCC**TCT**GTAGGACCAGCTTCCGAA
α7G174E	TTCGGAAGCTGGTCCTAC**GAA**GGATGGTCCCTGG	CCAGGGACCATC**CTT**CGTAGGACCAGCTTCCGAA
α7R101A	TGGCGTGAAAACCGTC**GCC**TTCCCTGATGGACAG	CTGTCCATCAGGGAA**GGC**GACGGTTTTCACGCCA

α7R101K	TGGCGTGAAAACCGTC**AAG**TTCCCTGATGGACAG	CTGTCCATCAGGGAA**CTT**GACGGTTTTCACGCCA
α7R101D	TGGCGTGAAAACCGTC**GAT**TTCCCTGATGGACAG	CTGTCCATCAGGGAA**ATC**GACGGTTTTCACGCCA
α7E215A	TACGAGTGCTGCAAA**GCA**CCTTACCCTGATGTG	CACATCAGGGTAAGG**TGC**TTTGCAGCACTCGTA
α7L9’T	TGGGAATCACCGTG**CTG**ACCAGCCTGACCGTGTTC	GAACACGGTCAGGCTGGT**CAG**CACGGTGATTCCCA
α4D185G	TCCTGGACCTAC**GGC**AAGGCCAAGATCGAC	GTCGATCTTGGC**CTT**GCCGTAGGTCCAGGA
β2R106A	AACATGAAGAAAGTG**AGG**CTGCCTAGCAAGC	GCTTGCTAGGCAG**CCT**CACTTTCTTCATGTT

2.4. *Xenopus laevis* oocytes preparation

Harvested *Xenopus laevis* ovaries were stored in OR2 solution (82 mM NaCl, 2 mM KCl, 2 mM $MgCl_2$ and 5 mM Hepes adjusted to pH 7.6 with NaOH) until their preparation in the lab. Once there, ovaries were split into small groups of 5-6 oocytes and incubated for approximately 1 hour at r.t. in Type I collagenase (2 mg/ml) to remove the follicular layer that can cause interferences in electrophysiology studies. Only defolliculated oocytes at the stage V and VI of maturation were isolated. Oocytes were maintained at 17 C° in an incubator in a modified OR2 Ca^{2+} solution (82 mM NaCl, 2 mM KCl, 2 mM $CaCl_2$ and 5 mM Hepes supplemented with kanamycin 2 µg/ml, 1x Antibiotic Antimycotic Solution and 5% horse serum, pH 7.6 adjusted with NaOH).

2.5. Microinjection of cDNA and cRNA

Needles for microinjection were prepared from Drummond glass capillaries (Sartorius, UK), which were pulled in one stage using a Narishige PC-10 micropipette puller (Narishige, Japan). Prior to use the tip of a selected needle was broken using fine forceps to give a narrow tip length of approximately 3 mm with an external width ranging from 1.0 to 1.5 µm. The needle was back-filled with light mineral oil and loaded on to a Nanoject II microinjector (Drummond, US). Wild type and mutant receptors α7, α4β2 (subunits were mixed in ratios 10:1 and 1:10 to obtain the two stoichiometries $(\alpha4)_3(\beta2)_2$ and $(\alpha4)_2(\beta2)_3$, respectively), and α3β4 (in equal ratio 1:1) cDNAs were injected into the oocytes’ nucleus (23.0 nl at 0.1 ng/nL). cRNA of mutant nAChRs with a reduced functional expression were injected into the oocyte cytoplasm (50.6 nl at 0.1 ng/nl). Groups of approximately thirty injected oocytes were transferred to a petridish with modified OR2 Ca^{2+} solution and incubated at 17 C° for a maximum of 7 days. The OR2 Ca^{2+} solution was changed daily and oocytes that had degraded were removed in sterile conditions from the plate.

2.6. Electrophysiological recordings

The characterisation of the functional effects of the ligands or mutations was carried out using two electrode voltage-clamp recordings. Electrophysiological techniques are based on the electrical properties of the cell membrane. The differential distribution of ions across the membrane produces a transmembrane potential termed membrane potential (V_m). Activation of nAChRs by agonists allows the flow of ions across their intrinsic ion channel; this flow changes the V_m. In two electrode voltage-clamping there are two intracellular electrodes, one to monitor V_m and the other to inject a current to maintain it at a desired voltage (-60 mV). Thus, the currents produced with the ionic movement across the nAChRs are measured (**Fig. 2.2**).

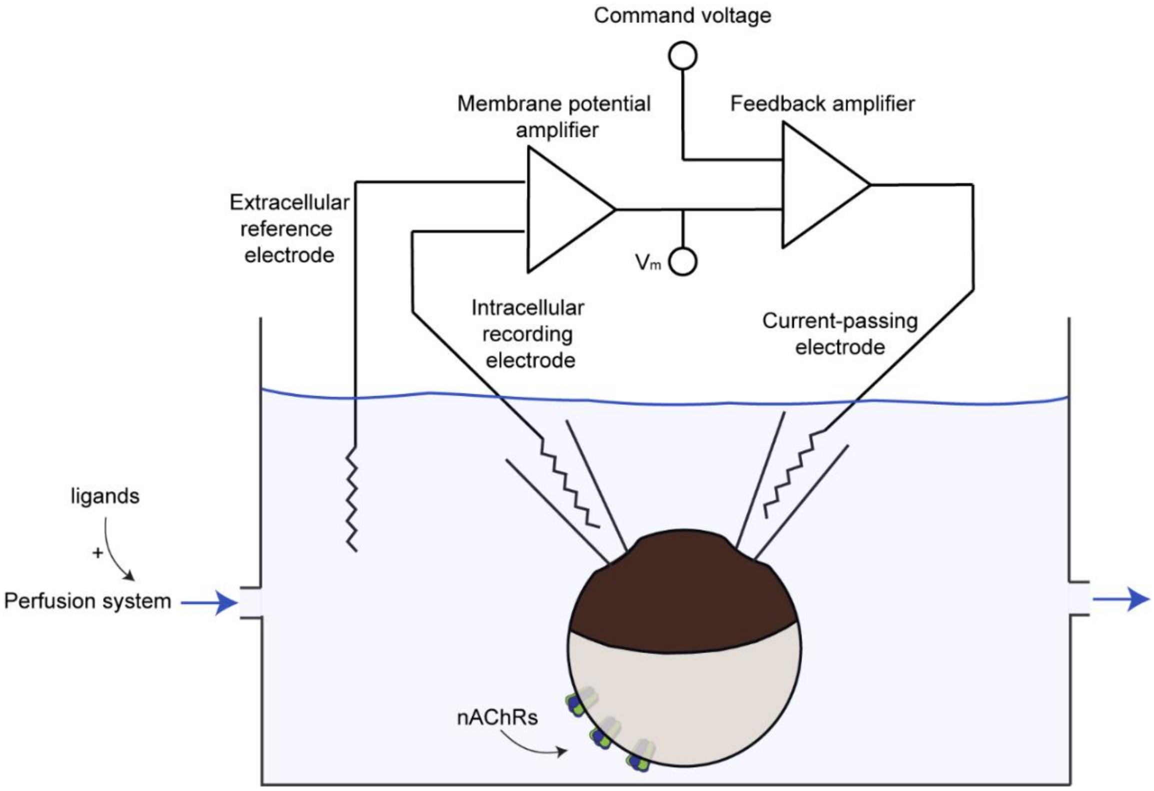
Command voltage
Membrane potential amplifier
Feedback amplifier
Extracellular reference electrode
V_m
Intracellular recording electrode
Current-passing electrode
ligands
+
Perfusion system
nAChRs

Figure 2.2. Diagram of two electrode voltage-clamp in *Xenopus laevis* oocytes.

2.6.1. Manual two electrode voltage-clamp system

Electrophysiological recordings were performed after 2-4 days post-injection in oocytes with integral membrane and no signs of degradation. The two electrode voltage-clamp electrophysiology was conducted in a faraday cage to reduce electrical noise. Within the cage, oocytes were placed in a 30 µl recording chamber (Digitimer Ltd, UK) and bathed with a Standard Oocytes Solution (hereafter named as SOS) (100 mM NaCl, 2 mM KCl, 1.8 mM $CaCl_2$ and 5 mM Hepes, pH 7.4 adjusted with NaOH). A gravity driven perfusion system was used for all the experiments at a rate of 10 ml/min. To add the tested ligands, solutions were switched through manually activated valves. All solutions were freshly made prior to recordings.

Oocytes were impaled by two electrodes connected to an Oocyte Clamp OC-725C (Warner Instruments, US) for standard voltage-clamp recordings. Briefly, electrodes were made from borosilicate capillary glass (Harvard Apparatus, GC 150 TF) using a vertical two stage electrode puller (Narishige PP-83) to give a top diameter of 1-2 µm. Prior to recordings electrodes were filled with 3 M KCl and only electrodes with a resistance between 0.2 and 2 MΩ were used for voltage clamping. The current signal was low-pass filtered at 1 kHz with a 4-pole Bessel filter in the Oocyte Clamp OC-725C, digitalized at 200 Hz using the iWork/118 analog to digital converter hardware (iWorx Systems Inc, US), and recorded digitally on a personal computer running Labscribe v3 software (iWorx Systems Inc, US).

2.6.2. Automated two electrode voltage-clamp system

HiClamp (Multichannel Systems, Germany) automated system was also used in order to validate the results from the experiments conducted using the manual system as well as to produce a larger n number. In the same way as manual recordings, automated electrophysiological recordings were performed after 2-4 days post-injection in oocytes with integral membrane and no signs of degradation. Oocytes were impaled by two electrodes made as in previous section that were connected to HiClamp. All recordings were performed at 18 °C and superfused with SOS (100 mM NaCl, 2 mM KCl, 1.8 mM $CaCl_2$ and 5 mM Hepes, pH 7.4 adjusted with NaOH) using the HiClamp peristaltic controlled multichannel system. Currents were recorded using an automated process equipped with the two electrode voltage-clamp configuration (Multi Channel Systems, Reutlingen, Germany).

2.6.3. Concentration-response curves for agonists

Concentration-response curves (CRC) for agonists were obtained by normalizing agonist-induced responses to the control responses induced by a near-maximum effective ACh concentration (100 µM for $(\alpha4)_2(\beta2)_3$ and 1 mM for α7, $(\alpha4)_3(\beta2)_2$ and α3β4). A minimum interval of 5 min for α4β2 and α3β4 receptors or 3 min for α7 receptors was allowed between agonist applications to ensure reproducible recordings. The CRC data were first fitted to the one-component Hill equation (**Eq. 1**).

$$\mathbf{I} = \frac{\mathbf{I_{max}}}{\mathbf{1+(EC_{50}/x)^{nH}}} \qquad \textbf{(Equation 1)}$$

where EC_{50} represents the concentration of agonist inducing 50% of the maximal response (I_{max}); x is the agonist concentration; and nH the Hill coefficient. EC_{50} value is a composite measurement of agonist binding and functional coupling. It is commonly used for functional comparisons; an increase corresponds to a loss-of-function whereas a decrease to a gain-of-function.

For C(10) Cyt derivatives with very low efficacy (maximal currents lower than 10% of the maximal currents elicited by 1 mM ACh), the EC_{50} could not be determined. In these cases, the relative efficacy of the ligand was estimated by using the **Eq. 2**.

$$\textbf{Relative efficacy} = \frac{\textbf{Compound } \mathbf{I_{max}}}{\textbf{ACh } \mathbf{I_{max}}} \qquad \textbf{(Equation 2)}$$

Were ACh I_{max} varies depending on nAChR subtype tested: 100 μM for $(\alpha4)_2(\beta2)_3$ and 1 mM for α7, α3β4 and $(\alpha4)_3(\beta2)_2$.

2.6.4. Inhibitory concentration-response curves for low efficacy partial agonist

To obtain a quantitative measure of the potency of Cyt derivatives with very low efficacy, the inhibitory potency was determined. Where agonist efficacy is very low, as for the C(10) Cyt derivatives described here, evaluation of the propensity of these ligands to act as competitive antagonists over a range of concentrations offers a more robust means of assessing their functional potency (Sharples *et al.*, 2000).

To obtain the CRC for the inhibitory effects of Cyt and its C(10) derivatives on the two stoichiometries of the α4β2 and α7 nAChRs, the compounds (1 nM to 1 mM) were co-applied with ACh EC_{80}: 30 μM for $(\alpha4)_2(\beta2)_3$ nAChR; 300 μM for $(\alpha4)_3(\beta2)_2$ and α7 nAChRs. The peak of the current responses obtained in this manner were then normalised to the peak of the responses elicited by ACh EC_{80} alone. The normalised data were then fit by non-linear regression to the Hill equation, as described for the agonist effects of the compounds. For comparative purposes, inhibitory constants were estimated using the Cheng and Prusoff equation (**Eq. 3**).

$$\mathbf{K_i = \frac{IC_{50}}{1+\frac{[x]}{K_a}}} \qquad \textbf{(Equation 3)}$$

where IC_{50} is the relative inhibitory potency of the compound tested; K_a is the apparent functional affinity; x is the concentration of ACh used to test the effects of the compounds.

K_a was estimated from the concentration response data by fitting the data to the equilibrium two-site receptor occupation equation (**Eq. 4**).

I = Imax[cA/(1 +cA]2 **(Equation 4)**

where cA represents the concentration of ACh divided by its K_a.

2.7. Double-mutant cycle analysis for long range coupling

The double-mutant cycle analysis is used to determine functional coupling between two residues in functional proteins (Hidalgo and MacKinnon, 1995; Faiman and Horovitz, 1996; Venkatachalan and Czajkowski, 2008). Typically, the analysis involves wild-type receptor (AB), two single mutants (A’B and AB’) and the corresponding double mutant receptor (A’B’). If the change in free energy associated with a structural or functional property of the receptor upon a double mutation differs from the sum of changes in free energy due to the single mutations, then the residues at the two positions are coupled. Such coupling reflects either direct or indirect interactions between these residues. The coupling parameter (Ω), which in the studies reported here is determined by determining changes in the parameter EC_{50}, is calculated using the equation shown in **Eq. 5**. If the two perturbations are independent of one another, Ω should be ~ 1. On the other hand, if Ω deviates significantly from 1, an interaction between the perturbed sites is established. Typically, a value of Ω > 2 is considered as significant coupling.

$$\Omega = \frac{\mathbf{EC_{50}(AB) * EC_{50}(A'B')}}{\mathbf{EC_{50}(A'B) * EC_{50}(AB')}} \qquad \textbf{(Equation 5)}$$

In **Chapter 5**, the double mutant cycle analysis strategy was used to examine the possible contribution of R101 in gating. The analysis that permits establishing the coupling of amino acid residues to gating using EC_{50} values is termed “elucidating long-range functional coupling in allosteric receptors” (ELFCAR) (Gleitsman *et al.*, 2009). Even though EC_{50} values represent both the binding of agonist and gating, by assessing how a gating reporter mutation alters the effects of the target mutation (in this case R101), it is possible to determine the coupling of the target residue to gating. The gating reporter mutation used in this analysis is L9’T. L9’ is situated at the 9th position of the pore-lining M2 helix and it is known to be implicated in the gating process. L9’ is part of the hydrophobic occlusion region of the channel and its substitution to a more hydrophilic amino acid such as serine or threonine leads to an increase in the agonist EC_{50} (Revah *et al.*, 1991; Chang and Weiss, 1999; Moroni *et al.*, 2006). Estimated EC_{50} values were used to calculate **Ω** using the double-mutant cycle analysis equation (**Fig. 2.3**), where AB corresponds to wild type receptor, A’B’ to the double mutant α7R101A, L9’T receptor, A’B to α7R101A receptor and AB’ to α7L9’T receptor. A coupling value $\Omega > 2$ is considered as significant coupling between the two residues.

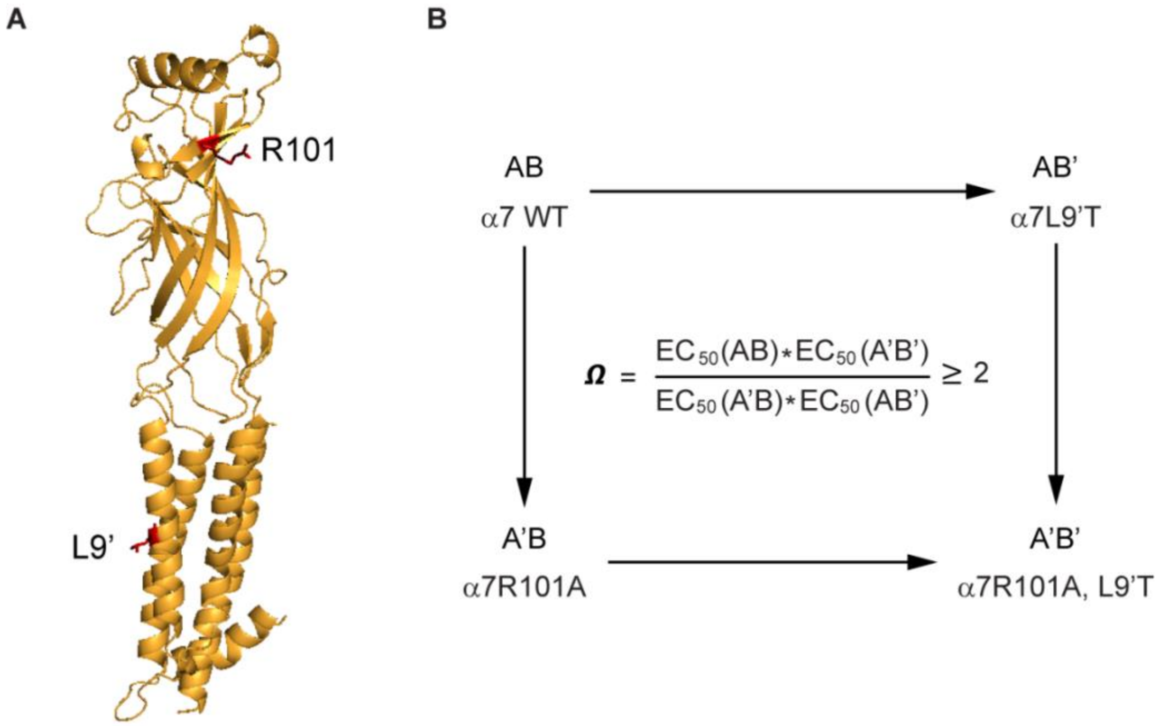

Figure 2.3. The elucidating long-range functional coupling of allosteric receptors (ELFCAR). **A)** Lateral side view showing the residue R101 at the ECD and the residue L9´at the TMD domains of the α7 nAChR. **B)** Diagram for the ELFCAR analysis and equation to calculate the coupling parameter, Ω.

2.8. Statistical analysis

Whole-cell recording data and statistical analysis comply with the recommendations on experimental design and analysis in pharmacology (Curtis *et al*., 2015). Data are presented as arithmetic mean ± 95% confidence interval (95% CI) of at least 5 independent experiments (n) carried out on oocytes from a minimum of 3 different *Xenopus* donors (N). Statistical and non-linear regression analyses of the data from concentration-response curves and single exponential decay were performed using GraphPad Prism5® (San Diego, CA). An F-test determined whether the one-site or biphasic model best fit the concentration response data; the simpler one-component model was preferred unless the extra sum-of-squares F test had a value of p less than 0.05. Data homogeneity was tested using three different normality tests (KS test, D'Agostino & Pearson omnibus test and Shapiro-Wilk test). Unpaired Student's t-tests was used for comparison between two groups (control and test) whereas one-way ANOVA with post-hoc Dunnett's test for comparison involving more than two groups. Statistical tests with $p < 0.05$ were considered significant.

2.9. Studies carried out in collaboration with external research groups

2.9.1. Computational biology

Computational biological approaches were used to identify structural elements involved in the selectivity of C(10) Cyt derivatives for nAChRs, particularly the α7 and α4β2 subtypes. These techniques comprised i) examination of homology models and crystal structures, ii) molecular docking studies and iii) molecular dynamic (MD) simulations that capture the dynamic behaviour of the bound agonists as well as the agonist site. Of these, ii) and iii) were carried out in collaboration with Dr Sofia Oliveira and Professor Adrian Mullohand from the School of Chemistry at the University of Bristol. Details of the procedures used in these three types of studies are described below.

2.9.1.a. Comparative Modelling and Molecular Docking

The homology model of α7 nAChR and the recently available X-ray structure of the human $(\alpha4)_2(\beta2)_3$ nAChR with Nic (Morales-Perez *et al.*, 2016) were visualized and compared using PyMol® (http://www.pymol.org). The α7 nAChR homology model was constructed by Dr

Sofia Oliveira. Briefly, the model was based on the crystal structure of the $(\alpha4)_2(\beta2)_3$ nAChR (5KX.pdb) (Morales-Perez *et al*., 2016) using ClustalOmega (McWilliam *et al.*, 2013) for sequences alignment, Scwrl4 (Krivov *et al*., 2009) for packing the side chains and Modeller (Webb *et al.,* 2014) for building the loops. The models comprise the ECD but not its TMD.

The α4β2 nAChR crystal structure and the α7 nAChR homology model detailed above together with the Cyt skeleton were prepared for molecular docking using Autodock Tools (Morris *et al*., 2009) and docking calculations were performed with Autodock Vina (Trott and Olson, 2010). A box of 14x14x14 $Å^3$ placed in the middle of the agonist binding pocket at the interface α4(+)/β2(-) of α4β2 nAChR and the interface α7(+)/α7(-) of α7 nAChR was used as the search space for docking calculations. The docking poses corresponding to those observed in the crystal structures of the AChBP with Cyt (4bqt.pdb; Rucktooa *et al*., 2012) were chosen and the resulting complexes were relaxed by energy minimisation.

2.9.1.b. Molecular Dynamic simulations

MD simulations simulations were performed using the ECD of the α4β2 crystal structure (Morales-Perez *et al*., 2016) and the α7 homology model, and the mutants were built usingPyMol® (http://www.pymol.org). All MD simulations were performed using GROMACS (van der Spoel *et al*., 2005) on the University of Bristol's High-Performance Computer, BlueCrystal (Phase 4). All systems were energy minimised, equilibrated and simulated according to the protocol described in Oliveira *et al.* (2019). Five unrestrained MD simulations, each 100 ns long in a total of 500 ns, were performed for each of the following protein-agonist complexes: α4β2WT, α7WT, α7G174D and α7R101A, each bound to ACh, Cyt or BS40.

2.9.2. Radioligand binding assays

Radioligand binding studies were kindly carried out by Cecilia Gotti from CNR, Institute of Neuroscience, Biometra Department, University of Milan, I-20129 Milan (Italy), although most of the analysis of the data was carried out at Oxford Brookes University. The radioligand studies were undertaken to determine whether the C(10) Cyt derivatives exerted their functional effects by binding the agonist site of nAChRs.

HEK 293 cells were used for heterologous expression of α4β2 and α3β4 nAChRs whereas for α7 nAChR heterologous expression, SH-SY5Y cells were used (Rego-Campello *et al.*, 2018). All the cDNAs used for these studies were cloned at Brookes University. HEK 293 cells and the SH-SY5Y clonal cell lines were supplied by Oxford Brookes University. cDNAs encoding human nAChR subunits (α3 and β4, α4 and β2 or α7) were transfected into HEK 293 cells or SH-SY5Y cell sat 30% confluency. The cells were maintained in Dulbecco's modified Eagle medium (supplemented with 10% foetal bovine serum, 1% L-Glutamine, 100 units/mL penicillin G and 100 µg/mL streptomycin) an environment of 37 °C containing 5% CO_2. Cells were then harvested by scraping, sedimented (800 rpm, 3 min), diluted with 50 mM TRIS–HCl, pH 7.4, and stored at −25°C until use in binding assays.

2.9.2.a. Saturation binding assays

The saturation (±)-[^{3}H]Epi binding experiments were performed by incubating aliquots of α4β2 and α3β4 membrane of transfected cells with 0.01-2.5 nM concentrations of (±)-[^{3}H]Epi overnight at 4 °C. Nonspecific binding was determined in parallel by means of incubation in the presence of 100 nM unlabelled Epi. At the end of the incubation, the samples were filtered on a GF/C glass microfiber filter (Whatman, UK) soaked in 0.5% polyethylenimine and washed with 15 mL ice-cold phosphate-buffered saline (PBS) and the filters were counted in a β counter. The saturation [^{125}I]α-Bgt binding experiments were performed using membrane of α7-transfected SH-SY5Y incubated overnight with 0.1-1.0 nM concentrations of [^{125}I]α-Bgt at r.t. Nonspecific binding was determined in parallel by means of incubation in the presence of 1 µM unlabelled α-Bgt. After incubation, the samples were filtered as described above and the bound radioactivity was directly counted in a β counter. Specific radioligand binding was defined as total binding minus the nonspecific binding determined in the presence of 1 µM unlabelled α-Bgt. Nonspecific binding averaged around the 20-30% of total binding.

2.9.2.b. Competition binding assays

The competition of [^{3}H]Epi and [^{125}I] α-Bgt binding was measured by incubating the membranes transfected with the appropriate subtype with increasing concentrations of Cyt or BS40 for five minutes followed by overnight incubation at 4 °C, with [^{3}H]Epi 0.1 nM or at r.t. with [^{125}I]α-Bgt 2-3 nM in the case of the α7 subtype. After incubation, the membrane-bound α4β2 or α7 subtypes were washed five times with ice-cold PBS. [^{3}H]Epi binding was determined by means of liquid scintillation counting in a γ counter, and [^{125}I]α-Bgt binding by means of direct counting in an α counter.

2.9.2.c. Binding assays statistics

Data from radioligand binding were evaluated by one-site competitive binding curve-fitting procedures using GraphPad Prism version 5 (GraphPad Software, Inc, US). In the saturation binding assay, the maximum specific binding (B_{max}) and the equilibrium binding constant (K_d) values were calculated using one site–specific binding with Hill slope – model. K_i values were obtained by fitting three independent competition binding experiments, each performed in duplicate for each compound on each subtype.

CHAPTER 3. PHARMACOLOGICAL CHARACTERIZATION OF C(10) CYT DERIVATIVES

3.1. Introduction

Modulating the activity of nAChRs is considered a valid strategy to aid tobacco smoking cessation and intervene therapeutically in a number of brain diseases, including Alzheimer's and Parkinson's disease, schizophrenia and depression (see **Chapter 1**, **section 1.7.7**). Drug discovery programs have shown interest in emulating the functional effects of natural compounds such as Nic, Cyt or Epi. However, these compounds bind the agonist site of all subtypes of nAChRs due to the conserved nature of the aromatic box (Cecchini and Changeux, 2015). For some brain disorders nAChR cross-reactivity may be desirable; however for clinical scenarios such as Nic addiction subtype specificity may increase clinical efficacy. The ability to design and tune a smoking cessation ligand to achieve high levels of selectivity for α4β2, the subtype that is necessary and sufficient to cause Nic addition (Picciotto and Kenny, 2020), may be critically important to avoid the off-target effects often seen with Var or Nic-replacement therapies.

Current pharmacotherapies prescribed in the UK for smoking cessation include Nic replacement therapy (e.g., Nic patches, gums, lozenges, inhalers or nasal sprays), the anti-depressant bupropion (see **Chapter 1**, **section 1.5.2**) and Var (Chantix®). Of these, Var is the most effective, but most expensive, smoking cessation medication. In this respect, cuts (close to 50%) in the funding for smoking cessation programs by the NHS (Cancer Research UK, 2017) makes it urgent to develop cheaper alternative therapies.

One such alternative is Cyt. This compound has been used as a smoking cessation treatment in several Central and Eastern European countries since the 1960s (Etter *et al.*, 2008). It is a natural product that is easily extracted from *Laburnum* plants and seeds, making it significantly cheaper than Var-based therapies. The cost of Var full treatment in the UK is around £160 while a Cyt-based treatment could potentially cost a quarter of this value (e.g., in Poland Cyt-based smoking cessation approaches cost around £6). Like Var, Cyt partially blocks the effects of Nic on the brain and has been shown to be more effective than Nic replacement therapy (Aubin *et al.*, 2008; Cahill *et al.*, 2016) or bupropion (Gonzales *et al.*, 2006) at helping people quit smoking.

Despite the cost-effectiveness of Cyt-based smoking cessation therapies (Leaviss *et al.*, 2014), Cyt may display similar off-target effects as Var. Both activate most nAChRs, including the α7 and α3β4 subtypes (Amar *et al.*, 1993; Rollema *et al.*, 2007a). Potential side effects include nausea, constipation, increased risk of heart complications (such as a heart attack) in people who have existing cardiovascular diseases and behavioural or mood changes (agitation, depressed mood or suicidal thoughts) (Moore *et al.*, 2011; Cahill *et al.*, 2016). Therefore, decreasing the activation of the off-target nAChR subtypes by Cyt is of great therapeutic interest.

A well-established strategy to increase receptor specificity and reduce receptor cross-reactivity is to modify the structure of a lead compound. For example, introducing alkyl groups at the C(10) position of Cyt enhances the selectivity of Cyt for α4β2 nAChRs, compared to other nAChR subtypes (Chellappan *et al.*, 2006; Kozikowski *et al.*, 2007). The C(10) methyl analogue (racemic variant of BS40, see **Table 3.1** below) shows a 3500-fold selectivity in binding affinity for the α4β2 (relative to α3β4) nAChR subtype (Kozikowski *et al.*, 2007). This provides an impetus to explore modification of the pyridone moiety of Cyt as an attractive avenue for further enhancing nAChR subtype selectivity. However, the synthesis of C(10) Cyt derivatives requires lengthy synthetic sequences (≥10 chemical steps) limiting both the number and variety of C(10) options available. This is mostly because C(3) and C(5) are also functionalised, producing multiple compounds. Additionally, only racemic ligands have been reported to date (Chellappan *et al.*, 2006; Kozikowski *et al.*, 2007; Durkin *et al.*, 2010), while the (+)-enantiomer lacks a nicotinic profile (Gray and Gallagher, 2006), the broader characteristics (e.g. toxicology) of (+)-Cyt remain unclear, highlighting the value of targeting enantiomerically pure variants. More recently, Professor Tim Gallagher and his team at Bristol University used a highly efficient iridium-catalyzed borylation that provides access to pure (−)-Cyt derivatives (Miura *et al.*, 2017). The key difference with other approaches is that with the Ir-catalyzed borylation it is possible to control the site where the substituent is introduced by the judicious choice of ligand and solvent (Miura *et al.*, 2017). Rego-Campello *et al.*, (2018) used this approach to selectively activate the C(10) within the pyridone ring of Cyt by introducing a boronate ester or derived bromide (**Fig. 3.1**). Exploiting the reactivity profiles of these functionalities introduced provides unlimited possibilities of C(10) substituent variations. The resultant set of C(10) Cyt derivatives synthesized by Tim Gallagher and his team (see **Table 3.1** below) were functionally characterised and reported in this chapter. Overall, C(10) Cyt derivatives showed an increased selectivity for α4β2 nAChRs, compared to α3β4 and α7 nAChRs.

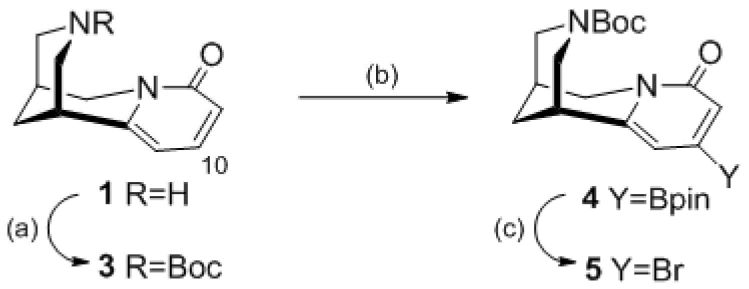

Figure 3.1. Ir-catalyzed borylation of the C(10) within the pyridone ring of Cyt. In (a) and (b) steps, the C-H activation of the C(10) within the pyridone ring of Cyt. Boc is a protecting group for the N(3) site that will result in NH or NH.HCl at the end of the process. (c) The resultant boronate ester can be modified to a derived bromide. Details of synthesis process can be found at Rego-Campello *et al.*, 2018.

3.2. Results

The C(10) Cyt derivatives reported in this chapter were named by Tim Gallagher and his team as BS followed by the number of synthesis order, as shown in **Table 3.1**.

Radioligand binding assays and two electrode voltage-clamp studies established the superior selectivity of C(10) Cyt derivatives for human α4β2 nAChR, supporting their potential as candidates for smoking cessation. Then, molecular docking studies were performed to insight the structural elements that define this selectivity.

Table 3.1. C(10) Cyt derivatives along with their chemical structures.

Agonist	Chemical structure	Nomenclature
BS01	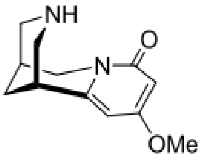	(–)-10-Methoxycytisine
BS07	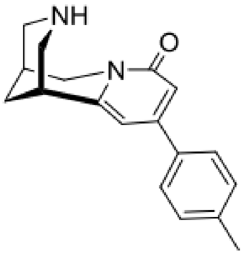	(+)-10-(4-Tolyl)cytisine
BS13	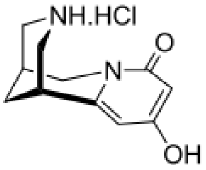	(+)-10-Hydroxycytisine hydrochloride
BS34	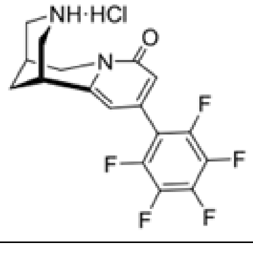	(–)-10-(Perfluorophenyl)cytisine hydrochloride
BS36	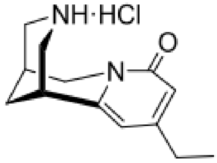	(–)-10-Ethylcytisine hydrochloride

BS40	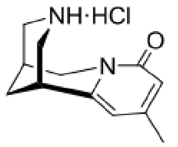	(–)-10-Methylcytisine hydrochloride
BS47	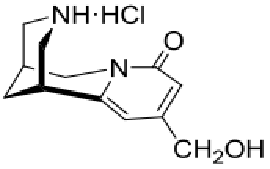	(–)-10-(Hydroxymethyl)cytisine hydrochloride
BS60	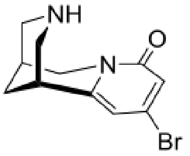	(–)-10-Bromocytisine
BS79	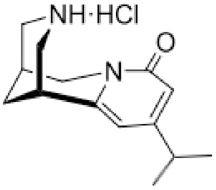	(–)-10-Isopropylcytisine hydrochloride
BS80	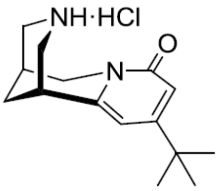	(–)-10-Tert-butylcytisine hydrochloride

3.2.1. Radioligand binding studies

Binding affinity profiles across three nAChR human subtypes (α4β2, α3β4 and α7) for the single (-) enantiomers of C(10) Cyt derivatives shown in **Table 3.1** are presented in **Table 3.2**, together with values for (–)-Cyt for comparison. BS40 and BS47 were previously reported as racemic ligands by Kozikowski *et al.* (2007), and their binding affinity data using rat nAChR subtypes are included for comparison in **Table 3.2**. The modest differences in K_i values between the present study and the one reported earlier may be accounted for by species (rat vs. human) differences and/or their use of racemic ligands.

The data documented in **Table 3.2** confirm that C(10) Cyt derivatives have preferential binding affinity for α4β2 nAChRs, in comparison to α3β4 or α7 nAChRs. All C(10) ligands bind to α3β4 and α7 nAChR with a lower affinity than Cyt, except BS34 which has a similar affinity at α3β4 as Cyt, and BS60 which has a (modestly) higher affinity for α7 than does Cyt. Moreover, binding affinities in the high nanomolar range are retained for the α4β2 nAChR subtype, with BS60, and the BS40 and BS36 having affinities comparable to Cyt. Increasing the size of the C(10)-alkyl substituent shows that, while there is a small loss of potency at the α4β2 nAChR subtype associated with the BS79 and BS80 analogues, these two ligands show markedly increased levels of selectivity (5000-7000 fold) against the α7 subtype.

Table 3.2. Binding affinities (K_i) of C(10) Cyt derivatives for α4β2, α3β4 and α7 nAChR subtypes. [b] Binding affinities (K_i) based on α4β2 and α3β4 rat subtypes reported by Kozikowski *et al*. (2007) for Cyt and racemic ligands (±)-BS40 and (±)-BS47 are shown in italics here for comparison; corresponding data for α7 nAChR subtype were not reported.

Ligand	**α4β2**	**α3β4**	**α7 nAChR**	**Binding ratios**	
	K_i (nM)	**K_i (nM)**	**K_i (nM)**	**α3β4/α4β2**	**α7/α4β2**
Cyt	1.27±0.1 *1.5*[b]	103±16.4 *220*[b]	691±16.4 -	81.1 *147*[b]	544 -
BS01	41±6.7	8452±2220	21300±7976	206	520
BS07	14.1±4.1	2280±760	5630±1747	162	399
BS13	14.7±3.4	8951±2434	15000±2526	609	1017
BS34	19.1±5.7	154±33	10980 ±4485	8.1	575
BS36	3.01±0.4	5723±1660	6928±2326	1901	2301
BS40	2.60±0.5 *1.9*[b]	2273±868 *6700*[b]	5027±1978 -	864 *3526*[b]	1911 -
BS47	36.8±9.4 *11*[b]	2685±910 *10000*[b]	116000±48750 -	73 *909*[b]	3152 -
BS60	1.77±0.4	537±131	323±127	303	182
BS79	12.5±3.0	20390±5150	96500±34050	1622	7677
BS80	26.4±4.8	70620±15050	134600±60275	2675	5098

3.2.2. Functional assays

The functional potency and efficacy of the C(10) Cyt derivatives shown in **Table 3.1** at human α4β2, α3β4 or α7 nAChRs expressed heterologously in *Xenopus* were measured by voltage-clamp procedures (**Table 3.3; Fig. 3.2**). ACh was assayed in parallel as a fully efficacious, non-selective agonist. Nic, Cyt and Var were also included for comparative purposes. The two stoichiometries of the α4β2 nAChR were examined by expressing separately the $(\alpha4)_2(\beta2)_3$ (high sensitivity for ACh and Nic) and the $(\alpha4)_3(\beta2)_2$ (low sensitivity for ACh and Nic) human nAChRs (Moroni *et al.*, 2006).

The C(10) Cyt derivatives evaluated behaved as partial agonists at both $(\alpha4)_2(\beta2)_3$ and $(\alpha4)_3(\beta2)_2$ nAChRs, producing very small responses compared with ACh, but of similar magnitude to those currents produced by Cyt (**Fig. 3.2.A**). Maximal responses were achieved by concentrations of 30-100 μM, indicating a potency comparable to that of the parent Cyt. The C(10) Cyt compounds also activated α3β4 nAChRs but with markedly lower efficacy than that observed for Cyt (**Fig. 3.2.B**).

Table 3.3. Comparison of agonist activity of ACh, Nic, Var, Cyt and (10) Cyt derivatives (BS01, BS07, BS13, BS34, BS36, BS40, BS47, BS60) at $(\alpha4)_2(\beta2)_3$, $(\alpha4)_3(\beta2)_2$, α3β4 and α7 nAChR subtypes. EC_{50} and relative efficacies are calculated as shown in **Chapter 2, section 2.8.1**. Values are the mean ± SEM of 6-7 independent experiments carried out on oocytes from 5-6 different Xenopus donors.

Ligand	**$(\alpha4)_2(\beta2)_3$**		**$(\alpha4)_3(\beta2)_2$**		**α3β4**		**α7**	
	EC_{50} μM	**Relative Efficacy**	**EC_{50} μM**	**Relative Efficacy**	**EC_{50} μM**	**Relative Efficacy**	**EC_{50} μM**	**Relative Efficacy**
ACh	6 ±1	1	95 ±8	1	101 ±15	1	100 ±5	1
Nic	2.1 ±0.6	0.31 ±0.07	5.1 ±0.1	0.48 ±0.3	81 ±5	0.71 ±0.07	110 ±12	0.96 ±0.1
Var	0.07 ±0.002	0.14 ±0.03	0.96 ±0.06	0.4 ±0.09	31.3 ±12	0.51 ±0.09	19 ±5	0.96 ±0.03
Cyt	ND	0.02 ±0.001	5.3 ±0.6	0.19 ±0.07	71 ±5	0.61 ±0.5	73 ±5	1.01 ±0.08
BS01	ND	0.009 ±0.0008	ND	0.071 ±0.009	ND	0.044 ±0.059	ND	0.01 ±0.0006
BS07	ND	0.030 ±0.013	ND	0.017 ±0.019	ND	0.076 ±0.093	1548 ±345	0.31 ±0.1
BS13	ND	0.005 ±0.0001	ND	0.07 ±0.009	ND	0.047 ±0.036	NE	NE
BS34	ND	0.050 ±0.071	ND	0.011 ±0.010	12.4 ±2	0.120 ±0.039	ND	0.01 ±0.0009
BS36	ND	0.062 ±0.025	ND	0.036 ±0.055	ND	0.086 ±0.106	1700 ±178	0.37 ±0.007
BS40	ND	0.041 ±0.004	ND	0.014 ±0.007	ND	0.0708 ±0.059	1600 ±200	0.21 ±0.02

BS47	ND	0.025 ±0.000	ND	0.058 ±0.057	ND	0.015 ±0.020	ND	0.02 ±0.0006
BS60	ND	0.01 ±0.009	ND	0.101 ±0.09	ND	0.121 ±0.08	1578 ±150	0.38 ±0.1
BS79	ND	0.018 ±0.009	ND	0.022 ±.0.007	ND	0.069 ±.0.001	ND	0.047 ±.0.009
BS80	ND	0.062 ±0.01	ND	0.039 ±0.001	ND	0.056 ±0.009	ND	0.033 ±0.008

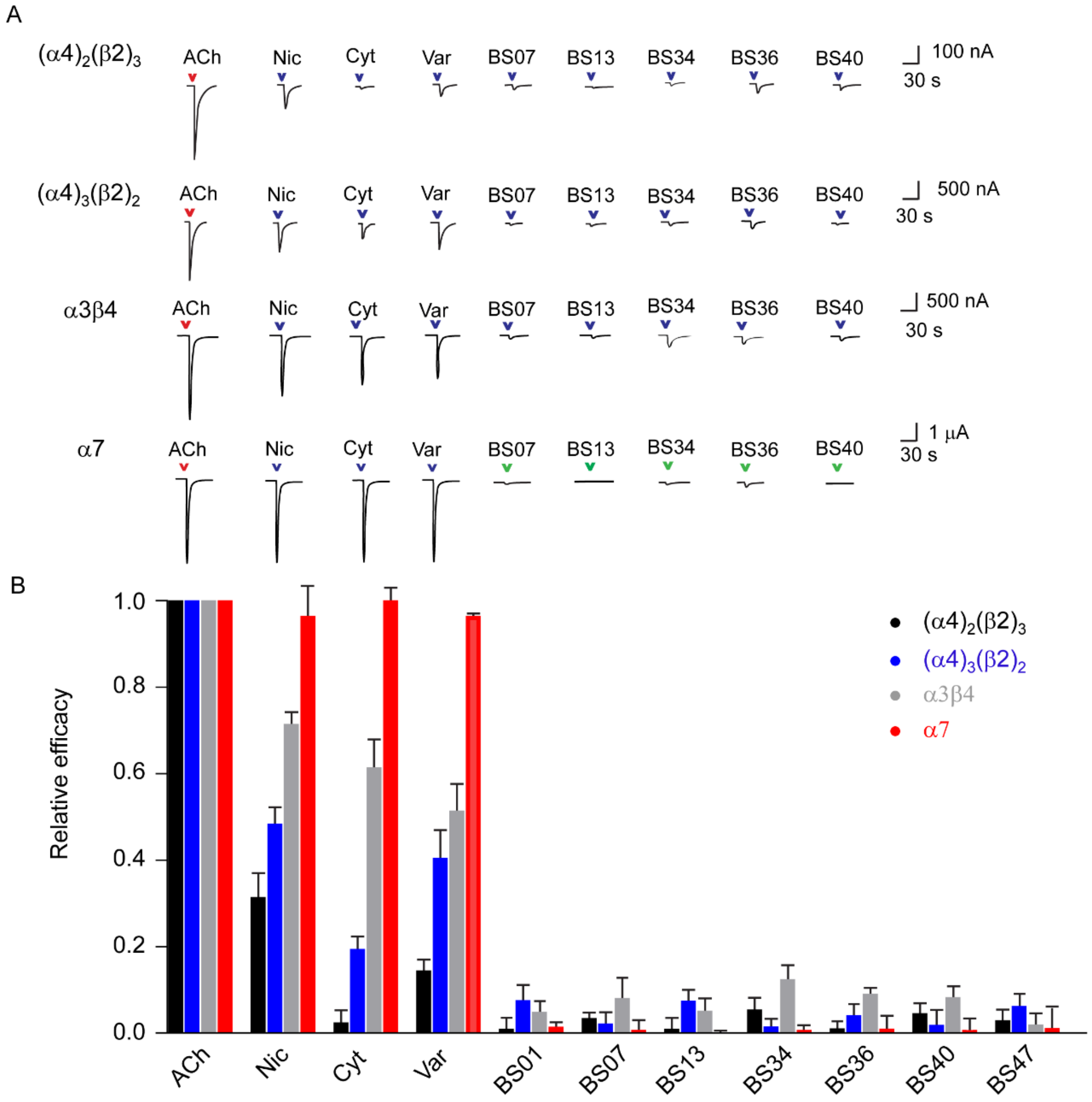

Figure 3.2. Functional effects of C(10) Cyt derivatives on nAChR subtypes. **A)** Representative traces of the current responses of $(\alpha4)_2(\beta2)_3$, $(\alpha4)_3(\beta2)_2$, α3β4 and α7 nAChR subtypes elicited by C(10) Cyt derivatives with the highest binding affinities for α4β2 nAChRs (BS07, BS13, BS34, BS36 and BS40) tested at 100 µM. For comparison, traces of the maximal current responses for ACh, Nic, Cyt and Var are included. **B)** Relative efficacies of C(10) Cyt derivatives for activating $(\alpha4)_2(\beta2)_3$, $(\alpha4)_3(\beta2)_2$, α3β4 and α7 nAChR subtypes; comparison with ACh, Nic, Cyt and Var. Values are the mean ± SEM of 6-7 independent experiments carried out on oocytes from 5-6 different Xenopus donors.

For α7 nAChRs, the same concentration range of C(10) Cyt derivatives (1 nM-100 μM) induced current responses that were less than 1% of the maximal ACh response. With the exception of ligand BS13 that had no effect (NE), higher concentrations of ligand (up to 3 mM) increased the amplitude of the current responses. For compounds BS01, BS34, BS47, BS79 and BS80 the amplitudes of the responses were too low to construct full concentration-response curves. In contrast, for compounds BS07, BS36, BS40 and BS60, it was possible to generate full concentration-response curves but the estimated efficacy was 20-40% of that of ACh and the potency was at mM level: BS07: 1.55 ± 0.35 mM; BS36: 1.70 ± 0.18 mM; BS40: 1.60 ± 0.20 mM; BS60: 1.58 ± 0.15 mM (**Fig. 3.3**; **Table 3.3**). This is in marked contrast to the more than 2 orders of magnitude greater potency and full agonism of Cyt and Var at human (see **Fig. 3.3**), chick (Amar *et al.*, 1993) and rat (Mihalak *et al.*, 2006) α7 nAChR.

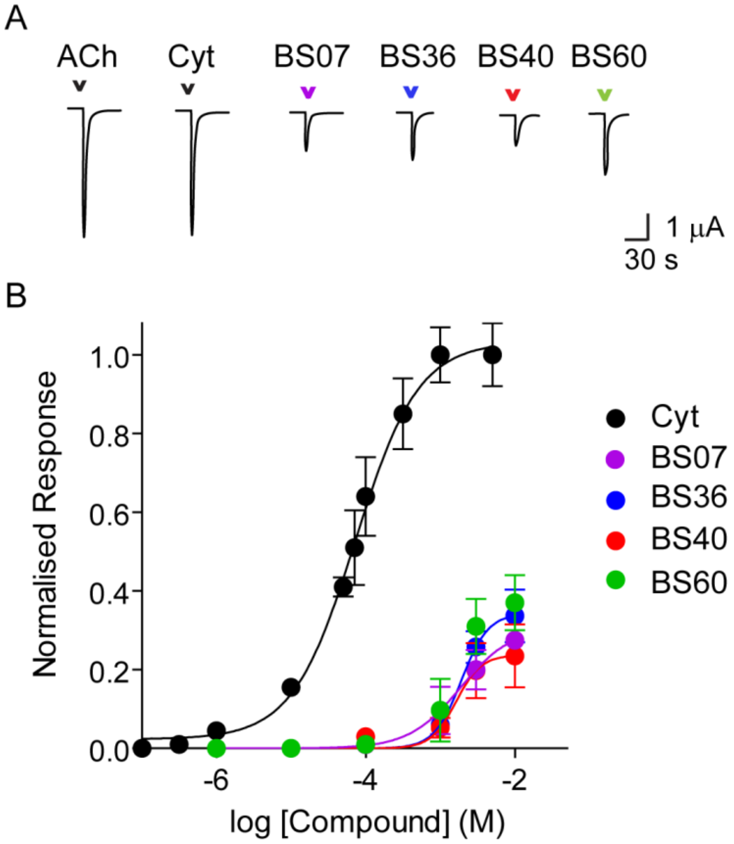

Figure 3.3. Agonist effects of C(10) Cyt derivatives at α7 nAChR subtype. **A)** Representative current traces for C(10) Cyt derivatives BS07, BS36, BS40 and BS60 at 3 mM, with responses to maximally effective concentrations of ACh and Cyt 1 (1 mM) shown for comparison. **B)** CRCs show ligands BS07, BS36, BS40 and BS60 to be weak agonists at α7 nAChR: estimated EC_{50} values were: BS07: 1.55 ± 0.35 mM; BS36: 1.70 ± 0.18 mM; BS40: 1.60 ± 0.20 mM; BS60: 1.58 ± 0.15 mM. For comparison purposes, the CRC for Cyt is included (EC_{50} = 73 ± 5 μM). EC_{50} and relative efficacies are calculated as shown in **Chapter 2, section 2.8.1**. Values are the mean ± SEM of 6-7 independent experiments carried out on oocytes from 5-6 different Xenopus donors.

3.2.2.a. C(10) Cyt derivatives as antagonists of nAChRs

Although the data shown in **Fig. 3.2** and **Table 3.3** clearly demonstrate the partial agonist profiles of the C(10) Cyt derivatives at α4β2 nAChRs, the limited agonist efficacy observed confounds accurate determination of their potency when the maximal current is less than 10% of that achieved by a full agonist like ACh. As a result, further characterisation of these C(10) Cyt derivatives at α4β2 nAChRs was undertaken to explore their partial agonism and obtain quantitative determinations of functional potency. This was achieved by assessing ability of these ligands to act as competitive antagonists. This is illustrated in **Fig. 3.4** for inhibition by Cyt of ACh-evoked responses of $(\alpha4)_2(\beta2)_3$ and $(\alpha4)_3(\beta2)_2$ nAChRs. Note that the inhibition curve falls short of 100% inhibition, consistent with the partial agonist action of Cyt. The inhibition curve allows determination of the concentration of Cyt producing 50% inhibition (IC_{50} 0.61 μM and 7.30 μM for $(\alpha4)_2(\beta2)_3$ and $(\alpha4)_3(\beta2)_2$ nAChR respectively, **Table 3.4**). The latter value accords well with the directly estimated EC_{50} of 5.3 μM for activation of $(\alpha4)_3(\beta2)_2$ nAChR by Cyt (**Table 3.3**), which validates this approach for assessing potency.

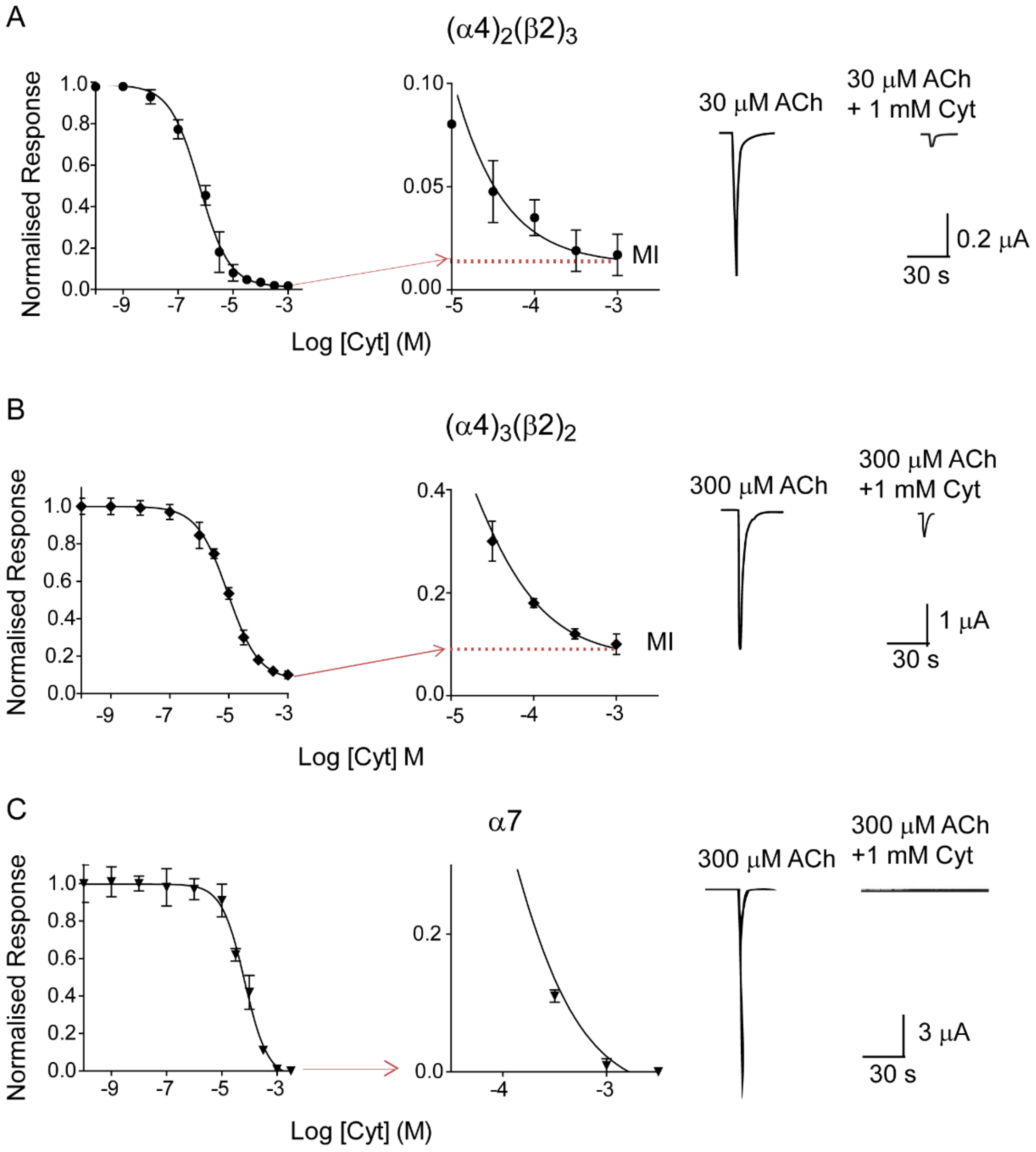

Figure 3.4. Cyt inhibits the ACh-evoked responses of nAChRs subtypes. CRCs for the inhibitory effects of Cyt at **A)** $(\alpha4)_2(\beta2)_3$, **B)** $(\alpha4)_3(\beta2)_2$ and **C)** α7 nAChRs. CRC were obtained as explained in **Chapter 2, section 2.8.2**. The fit curves are shown in the left panel. The central panel shows a magnified version of the lower part of the concentration response curves to highlight the maximal inhibition (MI) of the ACh responses induced by Cyt. Representative traces are shown in the right panel. MI, maximal inhibition.

Similar to Cyt, C(10) Cyt derivatives inhibited ACh-evoked responses of $(\alpha4)_2(\beta2)_3$ and $(\alpha4)_3(\beta2)_2$ nAChR expressed in *Xenopus* oocytes. The maximal inhibition (MI) correlates with the directly determined agonist efficacy (**Table 3.4**; see also **Table 3.3**). In all cases, ligands were more potent inhibitors of the $(\alpha4)_2(\beta2)_3$ stoichiometry. Consistent with the binding data (**Table 3.1**), the most potent inhibitors of α4β2 nAChR were the BS36 and BS40, which gave IC_{50} values (0.88 μM and 0.95 μM respectively) comparable to Cyt (IC_{50} = 0.61 μM; **Table 3.4**).

Table 3.4. Comparison of antagonist activity of, Cyt and (10) Cyt derivatives (BS01, BS07, BS13, BS34, BS36, BS40, BS47, BS60) on $(\alpha4)_2(\beta2)_3$ and $(\alpha4)_3(\beta2)_2$ nAChR subtypes. CRC were obtained as explained in **Chapter 2, section 2.8.2**. Values are the mean ± SEM of 6-7 independent experiments carried out on oocytes from 5-6 different Xenopus donors. K_i and MI, inhibitory constant and maximal inhibition, respectively.

Ligand	**$(\alpha4)_2(\beta2)_3$**			**$(\alpha4)_3(\beta2)_2$**		
	IC_{50} µM	**K_i µM**	**MI**	**IC_{50} µM**	**K_i µM**	**MI**
Cyt	0.61±0.05	0.10±0.009	0.019±0.01	7.30±1.1	1.75±0.15	0.11±0.08
BS01	11.02±1.2	1.8±0.19	0.009±0.00	37.31±4	8.97±0.11	0.077±0.09
BS07	5.41±2	0.9±0.28	0.033±0.01	35.01±6	8.41±3.1	0.022±0.01
BS13	9.41±1	1.60±0.2	0.081±0.00	28.2±3.5	7.0±0.7	0.081±0.01
BS34	7.6±1.1	1.26±0.3	0.059±0.01	115±43	27.64±7.9	0.013±0.01
BS36	0.95±0.1	0.16±0.02	0.061±0.01	18.26±3	4.38±0.7	0.018
BS40	0.88±0.09	0.15±0.02	0.066±0.01	8.6±2	2.07±0.6	0.022±0.01
BS47	9.51±2	1,58±0.4	0.022±0.01	40.15±10	9.65±2.3	0.034±0.01

The ability of C(10) Cyt derivatives BS40 and BS36 to inhibit ACh-evoked responses at α7 nAChRs is shown in **Fig. 3.5**. This experiment clearly demonstrated that neither of these ligands have any antagonist activity at concentrations below 1 mM. This confirms that these ligands lack the ability to interact productively with α7 nAChRs at sub-mM concentrations. This is consistent with the low affinity binding constants shown in **Table 3.1**, and in marked contrast to Cyt. Given the series of alkyl derivatives tested, this correlation between affinity and α7 nAChR function appears to extend to more sterically demanding substituents, such as those present in BS79 and BS90 and 22 (see **Tables 3.1-3.3**). However, it would be premature to attribute (or indeed limit) this selectivity effect to substituent volume.

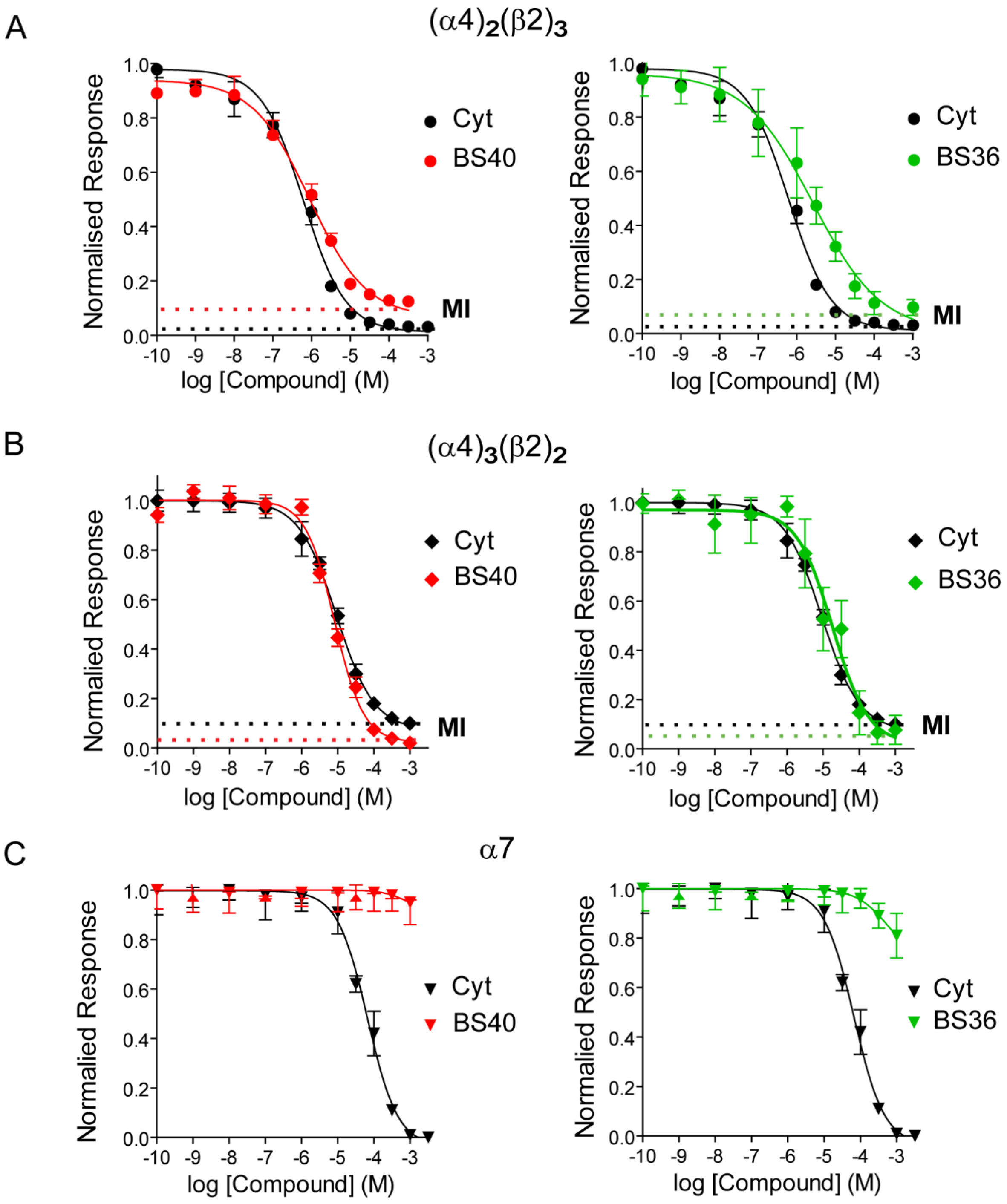

Figure 3.5. Competitive antagonist activity of C(10) Cyt derivatives BS40 and BS36 on $(\alpha4\beta2)_2\beta2$, $(\alpha4\beta2)_2\alpha4$ and α7 nAChR subtypes. The ability of BS40 and BS36 to inhibit current responses elicited by ACh in *Xenopus* oocytes expressing **A)** $(\alpha4)_2(\beta2)_3$, **B)** $(\alpha4)_3(\beta2)_2$ and **C)** α7 nAChR subtypes was determined as shown in **Chapter 2, section 2.8.2**. Values are the mean ± SEM of 6-7 independent experiments carried out on oocytes from 5-6 different Xenopus donors. MI, maximal inhibition.

3.3. Discussion

The findings reported in this chapter show that the C(10) Cyt derivatives tested retain the potent partial agonism of Cyt at α4β2 nAChR. Partial agonism at α4β2 nAChRs is considered as a fundamental property for successful smoking cessation agents (Rollema *et al.*, 2007b). Significantly, these ligands display selectivity for the $(\alpha4)_2(\beta2)_3$ nAChR and that selectivity can be attenuated by variation, for example, of the size of a C(10) substituent. In contrast to Cyt, C(10) Cyt derivatives lack the ability to activate (or inhibit) α7 nAChR at therapeutically meaningful concentrations, eliminating an interaction considered to be off-target for smoking cessation (Rollema *et al.*, 2007b; Rollema *et al.*, 2009b). Furthermore, although these C(10) Cyt derivatives are also weak partial agonists at α3β4 nAChRs, observed efficacies at this subtype are consistently lower than those of Cyt and Var at α3β4 nAChR (Mihalak *et al.*, 2006). Moreover, the binding affinity of α3β4 nAChR for the C(10) Cyt derivatives (with the exception of BS34) is markedly lower than for Cyt. As a consequence, these novel C(10) Cyt derivatives (exemplified by the C(10)-alkyl series BS36, BS40, BS79 and BS80) combine potent partial agonism with exceptional selectivity for α4β2 nAChR, with making them excellent lead candidates for further structural and pharmacological development.

The functional data clearly shows that the C(10) Cyt derivatives maintain the same pattern of potency and efficacy at α4β2 nAChRs displayed by the parent compound. Moreover, the competitive antagonism of Cyt is also preserved, as expected for partial agonists. C(10) Cyt derivatives display a preference for the $(\alpha4)_2(\beta2)_3$ receptor stoichiometry, as indicated by the IC_{50} values obtained in the inhibition of ACh responses by the C(10) Cyt derivatives. The basis for this stoichiometry-discrimination are not clear but the presence of an alkyl group at C(10) may decrease access to the agonist site present in the α4/α4 subunit interface of the $(\alpha4)_3(\beta2)_2$, which may decrease the sensitivity of the receptors to the C(10) Cyt derivatives due to the greater size of these compounds, in comparison to Cyt. Unlike the agonist sites on the α4/β2 interfaces found in both stoichiometries, the agonist site at the α4/α4 interface of the $(\alpha4)_3(\beta2)_2$ receptor does not bind ligands with a size greater than ACh, Cyt or Var (Mazzaferro *et al.*, 2014), which may lead to an overall decrease in the sensitivity of the receptors to ligands, in comparison to $(\alpha4)_2(\beta2)_3$ receptor stoichiometry (Mazzaferro *et al.*, 2014). An alternative explanation is that non-conserved residues in loop E in the α4 subunit (H142, Q150 and T152) create a more hydrophilic environment in the agonist site at the α4/α4 interface than in the agonist sites at the α4β2 interfaces. Here the corresponding E loop residues are V, L and F, which create a hydrophobic environment. This difference has been postulated to play a pivotal role in the ligand sensitivity of the alternate forms of the α4β2 nAChR (Harpsøe *et al.*, 2011; Lucero *et al.*, 2016). Further experimental studies should define better the structural determinants of the C(10) Cyt derivatives for α4β2 nAChR stoichiometry selectivity.

Although α3β4 receptors are activated by Cyt and its C(10) derivatives, the potency is much lower than that at α4β2 nAChR. Interestingly, the efficacy of these compounds at α3β4 nAChR is consistently higher than at α4β2 subtype. The structural basis for partial agonism have not been elucidated yet, although it has been suggested that the degree of loop C capping induced by agonist binding (Lape *et al.*, 2008) may be an important determinant. Others have suggested that interactions with the complementary side of the agonist binding site may play a role. From a series of AChBP crystal structures in complex with partial agonist activity at nAChRs, it has been suggested that partial agonists bind the complementary side through a water bridge: water interacts with the ligand and the complementary side (Hibbs and Gouaux, 2011; Billen *et al.*, 2012). Subsequent studies that analysed the interactions between agonists and α4β2 nAChRs by unnatural amino acid mutagenesis confirmed the presence of hydrogen bonds between the complementary side of the agonist site and the hydrogen-bond acceptor moieties of the agonists. However, these studies were not able to determine whether this hydrogen bond was mediated by a water molecule (Tavares *et al.*, 2012). Furthermore, the crystal structure of the $(\alpha4)_2(\beta2)_3$ shows no evidence of hydrogen bonds in this region (Morales-Perez *et al.*, 2016) although it is present in the recent crystal structure of the α3β4 nAChR (Gharpure *et al.*, 2019). Whether interactions between Cyt and its (C10) derivatives with the complementary side are through direct hydrogen bonds or through water molecules, it seems reasonable to speculate that differences in agonist efficacy at α4β2 and α3β4 receptors may stem from differences in the complementary side of the agonist sites in these two receptor types. Modelling comparison between α4β2 and α3β4 nAChR (Rego-Campello *et al.*, 2018) suggests that loop E in α3β4 is more hydrophilic than in α4β2 receptors, which would affect profoundly hydrogen bonding or other type of ionic interactions. Since partial agonism reflects the ability of ligands to transit through shut states to reach the open configuration, the strength of the binding interactions with the complementary side may influence this step. More recently, the resolution of the crystal structure of the α3β4 subtype revealed a hydrogen bond between loop C and a conserved Asp on loop F, which may be an important element for distinguishing α3β4 from α4β2 nAChR (Gharpure *et al*., 2019).

Remarkably, despite Cyt being a moderate and full agonist at α7 nAChR, its C(10) derivatives have no agonist activity on this nAChR subtype, at least at pharmacological relevant concentrations. This finding suggests that substitution at C(10) may hinder binding of the compounds to the α7 nAChR agonist site. Indeed, the radioligand binding studies carried out show a remarkable decrease in binding affinity. The structural basis for this behaviour will be explored in the next chapter.

In conclusion, C(10) substitution of Cyt has been validated as a viable strategy for (i) achieving increased selectivity for α4β2 over α3β4 and, in particular, α7 nAChR subtypes and (ii) suppressing α7 agonism. The critical challenge of accessing this class of Cyt derivative has been solved by site-specific C–H functionalisation of (–)-Cyt using Ir-catalysed borylation. This makes C(10) Cyt derivatives available directly from the parent compound (i.e. Cyt), in enantiomerically pure form, and the tractability associated with this chemistry opens up the range of structural variation that is accessible. In addition, given the relatively lower lipophilicity of Cyt compared to both Nic and Var (Rollema *et al*., 2007a) the flexibility enabled by C-H chemistry provides an opportunity to identify new Cyt-based ligands with improved penetration across the blood-brain barrier to achieve a more effective therapeutic benefit.

CHAPTER 4. MOLECULAR DETERMINANTS OF THE NACHR SUBTYPE SELECTIVITY OF C(10) CYT DERIVATIVES

4.1. Introduction

The previous chapter described a family of novel C(10) derivatives of Cyt that retain the potency and efficacy of Cyt at α4β2 nAChRs but show mM affinity for α7 nAChRs. [^{125}I]α-Bgt binding studies indicated that the C(10) Cyt derivatives have limited ability to displace the binding of [^{125}I]α-Bgt to α7 nAChR. This finding strongly suggest that the C(10) Cyt derivatives have restricted access to the agonist binding site in the α7 nAChR. Even small substituents such as the methyl group in BS40 greatly decreased binding affinity and functional potency, compared to Cyt. Identification of the structural elements that restrict access of the C(10) Cyt derivatives to the agonist site in α7 nAChR would aid the development of more specific nAChR ligands as well as provide further insights on the receptor function in the nAChR family.

What structural elements may prevent C(10) Cyt ligands accessing the aromatic box in α7 nAChRs? Studies using unnatural amino acid experimental strategies to explore the interaction of Cyt and its C(10) derivatives with the agonist binding site of the α4β2 nAChR showed that the aromatic box accommodates the (protonated) N(3) of Cyt (Van Arnam and Dougherty, 2014; Dougherty, 2008; Tavares *et al.*, 2012) and C(10) Cyt derivatives (Blom *et al.*, 2019) through both cation-π and hydrogen-bonding interactions. Unlike ACh or Nic, Cyt and its C(10) derivatives do make cation-π interaction with both TrpB and TyrC2 (Blom *et al.*, 2019). Also, the pyridone moiety of Cyt makes contacts with LeuE in the complementary side provided by the adjacent β2 subunit (**Fig. 4.1**). C(10) substituents generally strengthens the second cation-π interaction with TyrC2 but weaken the hydrogen bond typically seen to LeuE in the complementary side (Blom *et al.*, 2019).

Unnatural amino acid strategies have not been applied to define the binding interactions of the C(10) Cyt ligands with α7 nAChRs but molecular docking exercises suggest that substituents in C(10) orientate towards the complementary side of the agonist binding site (Rego-Campello *et al.*, 2018). Thus, the structural determinants responsible for the poor affinity of the C(10) Cyt derivatives for α7 nAChR may lie on the complementary side of this receptor subtype. Previous studies have identified residues at the complementary side that behave differently in α4β2 and α7 nAChRs. For example, residues in loop E (AsnE and LeuE) that in the α4β2 binding sites of the α4β2 nAChR interact with the hydrogen bond acceptor of some agonists, do not appear to be important in α7 nAChRs (Van Arnam *et al.*, 2013; Van Arnam and Dougherty, 2014). It has also been reported that equivalent mutations in TrpD have different pharmacological effects in α4β2 and α7 nAChRs (Williams *et al.*, 2009), further highlighting complementary residues as important determinants of receptor subtype selectivity.

This chapter focuses on the identification of possible structural elements in the α7 nAChR that may modulate access to the agonist binding site.

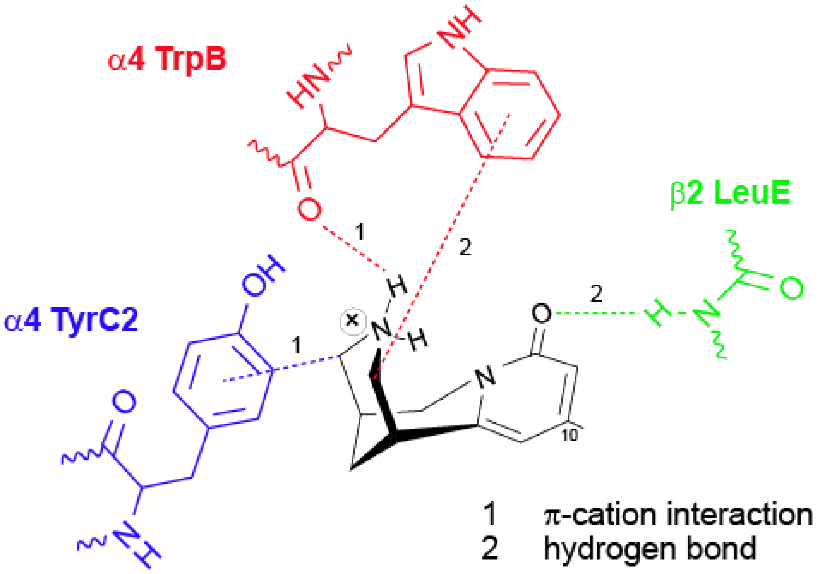

Figure 4.1. Cyt binding interactions at the α4β2 nAChR agonist binding site. The main interactions with Cyt are numbered by 1) cation-π interaction through TrpB 2) hydrogen bond through TrpB, TyrC1 and LeuE. Introduction of a substituent in C(10) of Cyt skeleton strengthens the cation-π interaction with TyrC2 while weakens the hydrogen bond to LeuE.

4.2. Results

4.2.1. Searching for agonist discriminatory elements using molecular docking

To insight the structural elements that define the receptor selectivity of the C(10) Cyt derivatives, computational modelling analysis of Cyt- and BS40-bound nAChRs (α4β2 and α7) was carried out. BS40 was selected for these studies on the basis that this compound has the smallest substituent and displays the highest α7/α4β2 binding affinity ratio (see **Table 3.2** in **Chapter 3**). The molecular docking studies were carried out using published crystallographic data (Morales-Perez *et al.*, 2016) to derive human homology models in order to dock ligands into the binding sites of α4β2 and α7 nAChRs in poses corresponding to those observed in the crystal structures of the AChBP with Cyt (4bqt.pdb; Rucktooa *et al.*, 2012) (see section **2.9.1.a** in **Chapter 2**). Note that the structure from Morales-Perez *et al.* (2016) corresponds to the $(\alpha4)_2(\beta2)_3$ stoichiometry in a non-conducting, desensitised conformation.

The modelled complexes of Cyt- and BS40-bound (**Fig. 4.2**) α7 nAChR share the core interactions observed in the AChBP-Cyt complex (Rucktooa *et al.*, 2012) and as described by Van Arnam and Dougherty (2014) and Dougherty (2008). The protonated secondary amine N(3) binds with a combination of a cation-π interaction and hydrogen bonding within the principal side of the α subunit (Tavares *et al.*, 2012). Hydrogen bonds to the side chain of TyrA and the amide carbonyl of TrpB are also present. The pyridone carbonyl oxygen of Cyt (and BS40) is orientated towards the amide nitrogen and carbonyl of LeuE within the protein backbone with space for bridging water molecules (as present in Billen *et al.*, 2012). According to the complexes, the C(10) substituent project into the aperture of the active site pocket enabling interactions with residues in the C-loop or the neighbouring subunit.

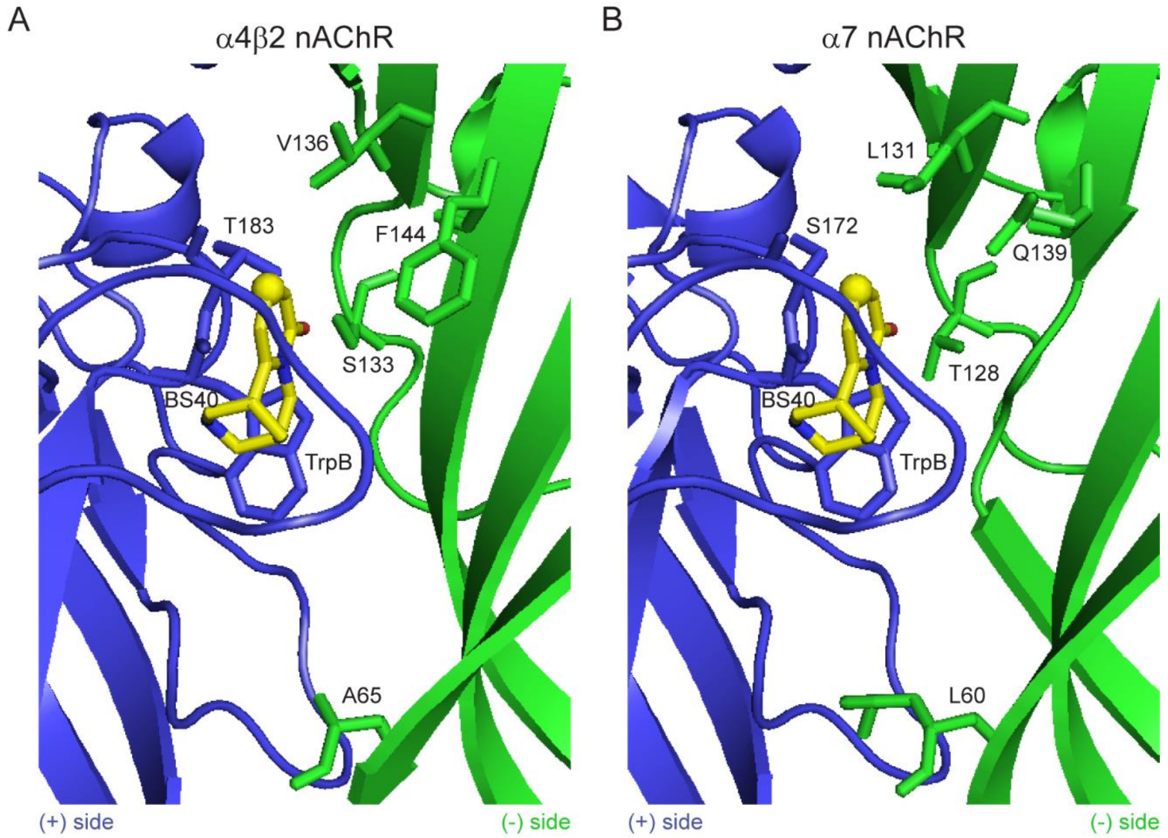

Figure 4.2. Binding site orientations of BS40 in α4β2 and α7 nAChRs highlighting the structural differences among them. **A)** BS40 docked into the binding pocket of α4β2. **B)** BS40 docked into the model of the human α7 nAChR. The residues that are different between the two subtypes are highlighted with sticks along with TrpB as reference residue. The principal and complementary subunits are coloured in blue and green, respectively. The solid sphere corresponds to the C(10) position within Cyt. The residue numbering refers to the following UniProt sequence codes: P43681 (α4 subunit), P17787 (β2 subunit) and P36544 (α7 subunit).

Closer examination of the agonist bound models revealed three factors that may differentiate the immediate environment of the agonist sites of the two nAChR subtypes and that could therefore affect the affinity of Cyt and C(10) Cyt for these receptor subtypes. First, the residue immediately lining the binding pocket; phenylalanine F144 in α4β2 nAChR is substituted by a polar glutamine Q139 in α7 nAChR, which modify the hydrophobicity of the binding pocket. Second, alanine A65 at the bottom and valine V136 on top of the binding site of the α4β2 nAChR are substituted by two leucine residues in α7 nAChR (L60 and L131) (**Fig 4.2**). The two bulkier residues (leucines) in these regions may modulate the volume of the agonist binding pocket and may be less accommodating of the more sterically demanding C(10) Cyt derivatives. And third, the residues serine S133 and threonine T183 in α4β2 nAChR are changed at the same positions to T128 and S172 in α7 nAChR, which may affect the hydrogen-bonding network around the Cyt carbonyl (**Fig. 4.2**).

Site-directed mutagenesis of these residues at the α7 nAChR was carried out in order to transform this receptor into an α4β2-like receptor (α7Q139F, α7T128S,S172T and α7L60A,L131V). However, subsequent two-electrode voltage clamp functional assays showed that none of these mutations increased BS40 potency, compared to wild type (**Table 4.1**). Moreover, mutant receptors α7Q139F and α7T128S,S172T displayed decreased potency for all agonists tested (ACh, Cyt and BS40) (**Table 4.1**). These findings are consistent with Q139 and T128 and S172 being part of the receptor machinery that sustain agonist binding in α7 receptors, although their role does not seem to be related to size discrimination because the mutations do not appear to increase BS40 access to the agonist pocket. Previous studies have shown that S172T has no functional effects in α7 receptors (Marotta *et al*., 2015), suggesting that the detrimental effects of α7T128S,S172T were mediated by T128S. Double mutant α7L60A,L131V did not alter agonist potency, discarding the possibility that these residues may influence the binding of BS40 to the α7 subtype (**Table 4.1**).

Table 4.1. Agonist sensitivity to activation of α7 WT and mutants α7 nAChRs. Whole-cell current responses to agonist (ACh, Cyt or BS40) were measured using *Xenopus laevis* oocyte two electrode voltage clamping electrophysiology. Data were fitted to the empirical Hill equation using non-linear regression and are presented with 95% confidence interval (95% CI) as EC_{50} in µM and relative maximal efficacy I_{max}/I_{AChmax} from at least five independent experiments carried out using at least 3 different *Xenopus* donors. Statistical analysis was performed by comparing the estimated values of wild type and mutant EC_{50} and I_{max}/I_{AChMax} using ANOVA followed by Dunnett's post-test. Significant differences, compared to control were considered as significant if $p < 0.05$ (noted by *). ND, not determined.

Receptor	**ACh**		**Cyt**		**BS40**	
	EC_{50} (µM) (95% CI)	**I_{max}/I_{AChmax} (95% CI)**	**EC_{50} (µM) (95% CI)**	**I_{max}/I_{AChmax} (95% CI)**	**EC_{50} (µM) (95% CI)**	**I_{max}/I_{AChmax} (95% CI)**
α7 WT	82.4 (71-95)	1	29.64 (24-37)	0.93 (0.9-0.94)	643 (493-837)	0.55 (0.4-0.7)
α7L60A, L131V	50.0 (19-134)	1	66.2 (23-191)	0.9 (0.7-1.2)	ND	0.7
α7Q139F	462* (340-628)	1	137* (21-254)	1.11 (1.0-1.2)	504 (301-545)	0.35 (0.1-0.6)
α7T128S, S172T	367.3* (232-581)	1	91.2* (57-271)	1.10 (0.8-1.4)	972.7* (321-2944)	0.74 (0.5-1.0)

The studies described above indicate that none of the residues that were identified by molecular docking as potential modulators of C(10) Cyt derivatives binding to α7 nAChR. One of the major limitations of molecular docking is that the data produced corresponds to dead-end, static structures. Thus, the temporal changes brought about by agonist binding, which may be crucial to decipher the molecular mechanisms underpinning agonist receptor specificity, are not captured by molecular docking. Therefore, detecting those temporal changes may permit a better insight of the dynamic behaviour of agonist binding residues and non-agonist binding residues that may modulate access to the binding pocket or the binding interactions between agonists and the aromatic box. More advanced computational approaches such as molecular dynamics (MD) simulations can overcome the limitations of docking by revealing the dynamics of agonists within the agonist site of the α7 and α4β2 nAChRs. Comparison of the dynamical behaviour of bound ligands in both receptor subtypes may reveal how α7 nAChRs discriminate against C(10) Cyt derivatives. The application of this approach to BS40- and Cyt-bound α7 and α4β2 nAChR is described below.

4.2.2. MD simulations identify an arginine residue as a critical element of agonist selectivity

Molecular dynamics (MD) simulations revealed contrasting patterns of dynamic behaviour of bound BS40 in α7 and α4β2 nAChRs. In the α4β2 simulated complexes, ACh exhibited a highly dynamical behaviour, adopting many different binding modes while inside the agonist binding cleft. As expected from their more rigid structures, Cyt and BS40 showed limited mobility, generally remaining in the same orientation throughout the simulation time (**Fig. 4.3**). In contrast, in the α7 complexes, there is no clear difference between the dynamical behaviour of ACh, Cyt or BS40 (**Fig. 4.3**).

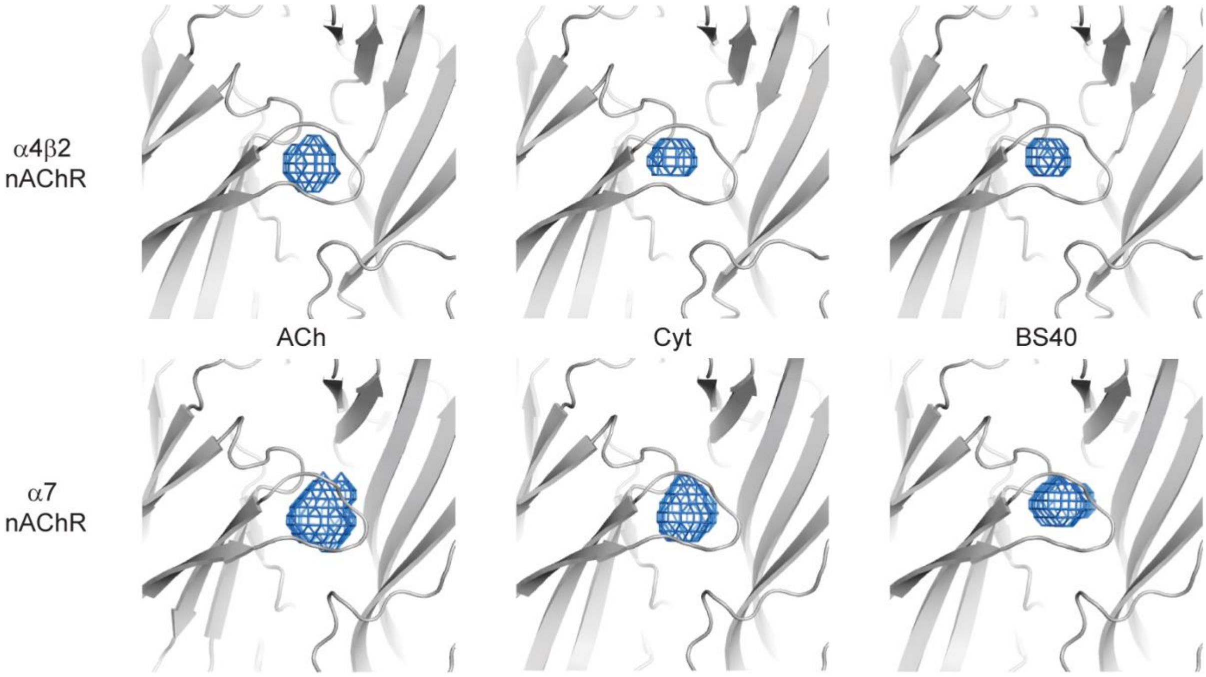

Figure 4.3. Dynamical behavior of the agonists in α4β2 and α7 nAChRs. Probability density maps (with a 0.0 Å−3 contour) for the positively charged group of acetylcholine, Cyt and BS40 in the first binding pocket are depicted as a blue mesh. The structure used as the starting point for the simulations is shown in grey.

A key element underpinning the subtype-specific ligand dynamics is an arginine residue in β3-strand in the complementary side of α7 (R101) or β2 (R106). In α4β2, β2R106 establishes an inter-subunit electrostatic interaction with an aspartate residue (α4D185) in loop B (**Fig. 4.4A**). This inter-subunit interaction is present in all heteromeric nAChR, except the α9α10 nAChR subtype (**Fig. 4.4B**). In loop B of the α7 subtype, there is a glycine residue (G174) in the position equivalent to that of α4D185. As a consequence, the side chain of R101 in α7 is not stabilised by strong electrostatic interactions, which makes it highly mobile. This mobility allows the side chin of R101 to orientate downwards towards the inside of the binding pocket establishing transient interactions with loop C, notably with the side chain of E215. In the BS40-bound α7 model, the side chain of R101 approaches the C(10) moiety, which results in the loss of interactions between BS40 and the conserved aromatic residues at the binding pocket (**Fig. 4.5**).

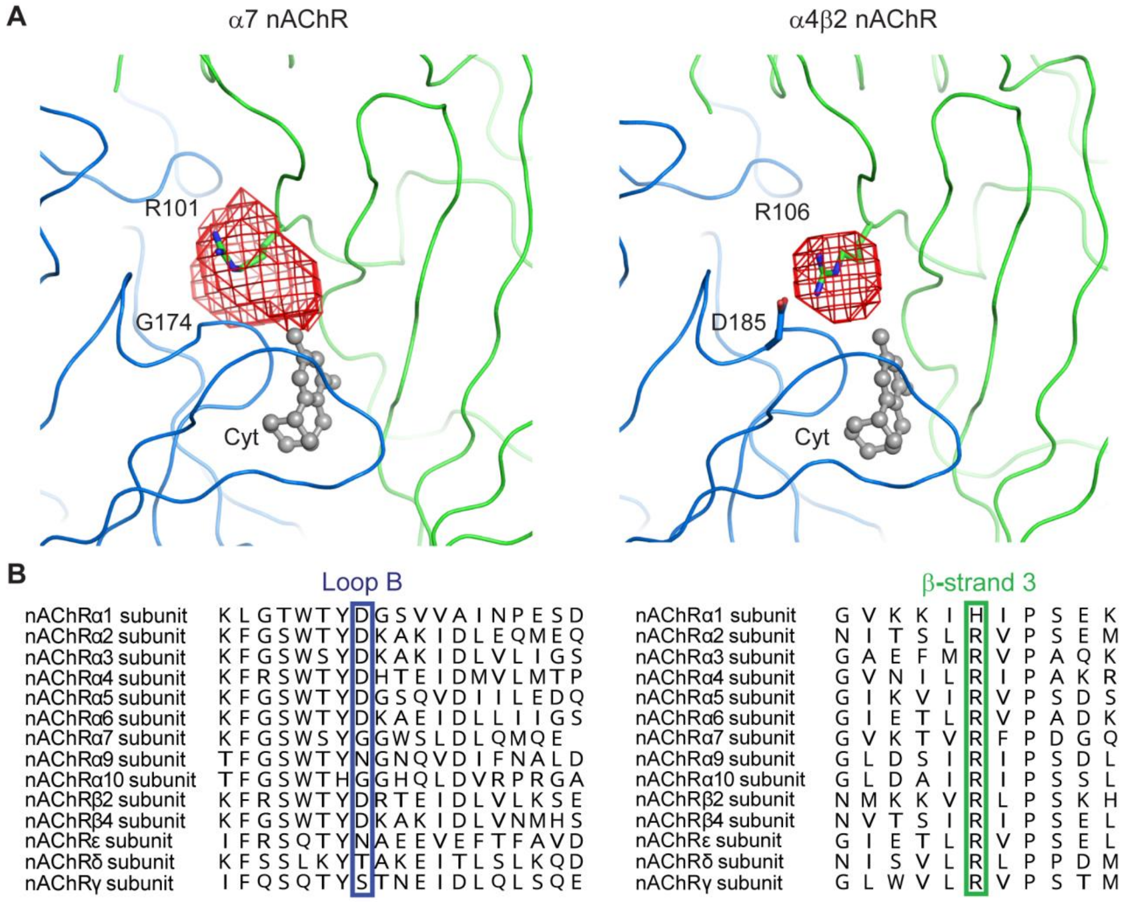
A
α7 nAChR
α4β2 nAChR
R101
G174
Cyt
R106
D185
Cyt
B
Loop B
nAChRα1 subunit KLGTWTYDGSVVAINPESD
nAChRα2 subunit KFGSWTYDKAKIDLEQMEQ
nAChRα3 subunit KFGSWSYDKAKIDLVLIGS
nAChRα4 subunit KFRSWTYDHTEIDMVLMTP
nAChRα5 subunit KFGSWTYDGSQVDIILEDQ
nAChRα6 subunit KFGSWTYDKAEIDLLIIGS
nAChRα7 subunit KFGSWSYGGWSLDLQMQE
nAChRα9 subunit TFGSWTYNGNQVDIFNALD
nAChRα10 subunit TFGSWTHGGHQLDVRPRGA
nAChRβ2 subunit KFRSWTYDRTEIDLVLKSE
nAChRβ4 subunit KFGSWTYDKAKIDLVNMHS
nAChRε subunit IFRSQTYNAEEVEFTFAVD
nAChRδ subunit KFSSLKYTAKEITLSLKQD
nAChRγ subunit IFQSQTYSTNEIDLQLSQE
β-strand 3
nAChRα1 subunit G V K K I H I P S E K
nAChRα2 subunit N I T S L R V P S E M
nAChRα3 subunit G A E F M R V P A Q K
nAChRα4 subunit G V N I L R I P A K R
nAChRα5 subunit G I K V I R V P S D S
nAChRα6 subunit G I E T L R V P A D K
nAChRα7 subunit G V K T V R F P D G Q
nAChRα9 subunit G L D S I R I P S D L
nAChRα10 subunit G L D A I R I P S S L
nAChRβ2 subunit N M K K V R L P S K H
nAChRβ4 subunit N V T S I R I P S E L
nAChRε subunit G I E T L R V P S E L
nAChRδ subunit N I S V L R L P P D M
nAChRγ subunit G L W V L R V P S T M

Figure 4.4. A conserved arginine in β3-strand in nAChR shows subtype-specific dynamical behaviour. **A)** Probability density maps for the side chain of the β3-strand arginine located in the binding pocket of α4β2 and α7 nAChRs for BS40 during MD simulations. The area in which the side chain of arginine moves during the MD simulations is coloured in red. The principal and complementary subunits are coloured in blue and green, respectively. The agonist, BS40, is represented with balls-and-sticks and coloured in grey. **B)** Sequences alignment for loop B and β-strand 3 of the nAChR subunits.

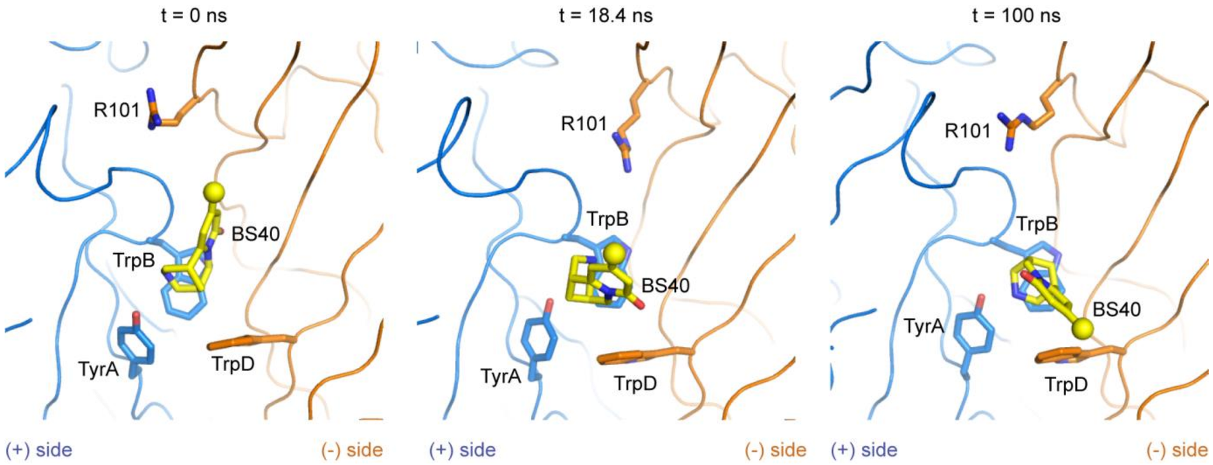
t = 0 ns
t = 18.4 ns
t = 100 ns
R101
BS40
TrpB
TyrA
TrpD
R101
TrpB
BS40
TyrA
TrpD
R101
TrpB
TyrA
BS40
TrpD
(+) side
(-) side
(+) side
(-) side
(+) side
(-) side

Figure 4.5. Changes in BS40 binding orientation in α7 nAChR. The (+) and (-) subunits are coloured in blue and orange, respectively. BS40 is represented in yellow with sticks and the solid sphere highlights the methyl group at C(10) position. Note that after 18.4 ns, the side chain of R101 rotates downward to the inside of the binding pocket thus forcing a change in the binding mode of BS40.

4.2.3. G174D increases agonist potency in α7 nAChR.

As discussed above, MD simulations suggested that the movement of α7R101 disturbed the binding of BS40 to the aromatic box. Therefore, reducing the mobility of R101 by introducing a residue with which R101 can establish strong electrostatic interactions may increase the affinity of BS40 for the α7 subtype. This was achieved by mutating G174 to D. Recall that G174 occupies in α7 the position equivalent to D185 in α4. α7G174D mutant receptor was expressed in *Xenopus* oocytes and its sensitivity to activation by agonists (ACh, Cyt or BS40) was assessed using two electrode voltage-clamping. As expected, α7G174D increased by ~ 4-fold the potency and almost doubled the relative efficacy (I_{max}/I_{AChmax}) of BS40 (**Fig. 4.6**; **Table 4.2A**). To a lesser extent, but significantly, the potency of Cyt was also increased (EC_{50} value goes from 29.6 μM in the wild type to 8.5μM in the α7G174D mutant). The relative efficacy of Cyt remained unchanged (**Fig. 4.6**; **Table 4.2A**). The mutant α7G174D did not produce a significant change in ACh potency (**Fig. 4.6**; **Table 4.2A**), probably because the high mobility and small size of ACh makes the binding of this agonist more tolerant of structural changes. Interestingly, alanine substitution of G174 (G174A) had no effects on the potency of ACh, Cyt or BS40 (**Table 4.2A**), suggesting that this residue does not play an important role in α7 nAChR function.

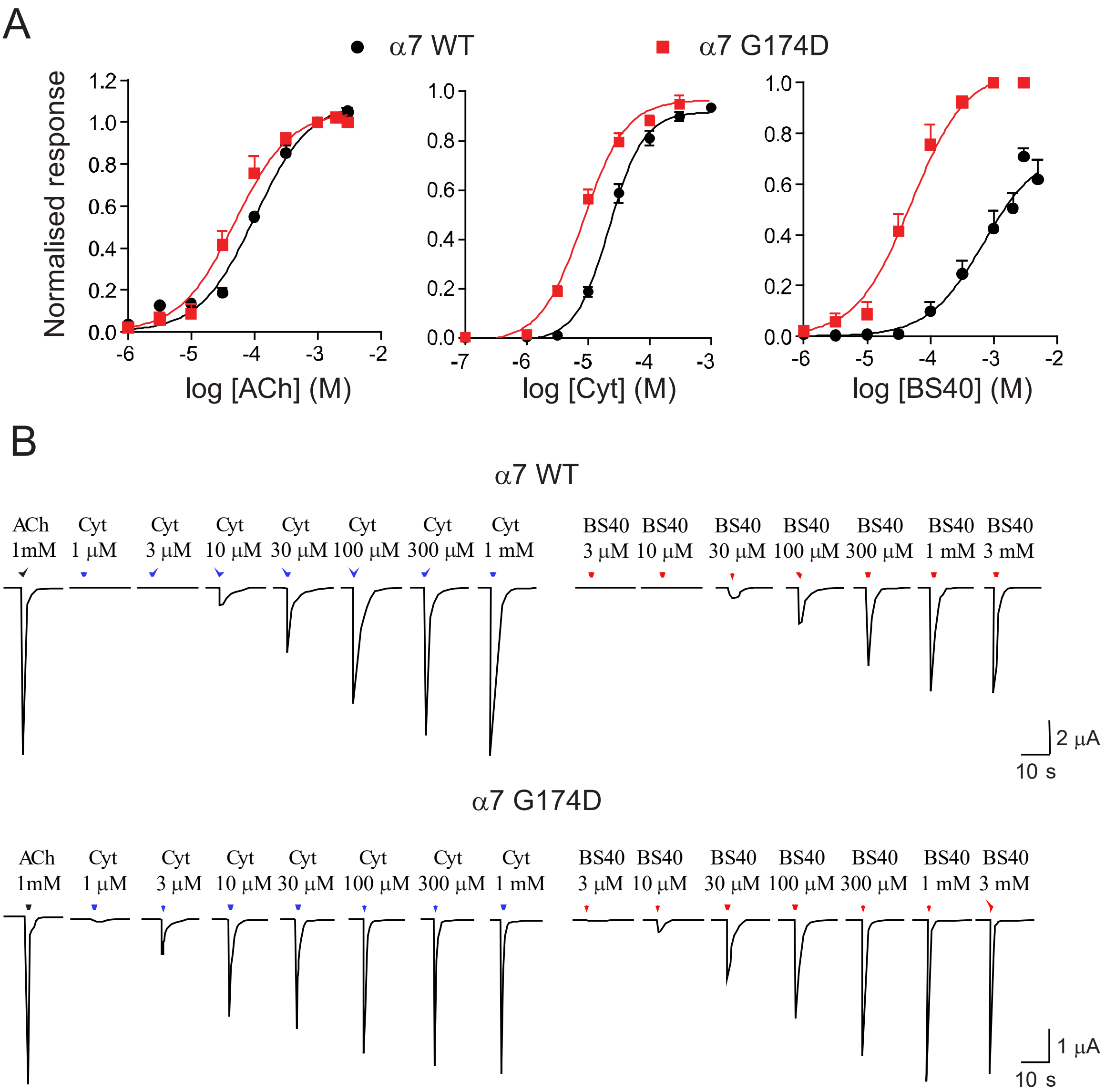

Figure 4.6. Functional effects of the mutant α7G174D on receptor activation. **A)** Activation concentration response curves by ACh, Cyt and BS40 for α7 WT (in black) and α7G174D (in red) nAChRs expressed heterologously in *Xenopus* oocytes. Data were fitted to the empirical Hill equation using non-linear regression and error bars indicate SEM. Values are the mean ± SEM of 11-12 independent experiments carried out on oocytes from 5-6 different Xenopus donors. **B)** Representative traces of the responses elicited by ACh, Cyt and BS40 at α7 WT and α7G174D nAChRs.

[^{125}I]α-Bgt binding assays were carried out to establish the affinity of αG174D receptors for Cyt and BS40. The studies revealed a significant increase in agonist binding affinity (K_i) in α7G174D mutant compared to α7 WT. The ability of both Cyt and BS40 to displace [^{125}I]α-Bgt from the binding site was enhanced by respectively, 5- and 12-fold, compared to wild type ($p < 0.05$; Student's t test; n = 3) (**Table 4.2B**), indicating that these agonists bind the site with higher affinity when an aspartate residue is introduced at position 174 in the α7 nAChR.

Table 4.2. Glycine to aspartate exchange in loop B increase agonist potency and binding affinity in α7 nAChR. **A)** Whole-cell current responses to agonist (ACh, Cyt or BS40) were measured using *Xenopus* oocyte two electrode voltage clamping electrophysiology. Data were fitted to the empirical Hill equation using non-linear regression and are presented with 95% confidence interval (95% CI) as EC_{50} in μM and relative maximal efficacy I_{max}/I_{AChmax} from a minimum of five independent experiments carried out using at least 3 different *Xenopus* donors. Statistical analysis was performed by comparing the estimated values of wild type and mutant EC_{50} and I_{max}/I_{AChMax} using ANOVA followed by Dunnett's post-test. **B)** Saturation binding affinities of [^{125}I]α-Bgt (K_d) and competition binding affinities of BS40 and Cyt (K_i) for α7 WT and α7G174D. Human a7 WT and mutant were expressed in SH-SY5Y cells (n=3). Data were fitted to the one site–specific binding with Hill slope – model and are presented as the mean with 95% confidence interval (95% CI). Statistical analysis was performed by comparing the estimated values of wild type and mutant using Student's t-test. Significant differences, compared to control were considered as significant if $p < 0.05$ (noted by *).

A) Whole-cell recordings						
	ACh		**Cyt**		**BS40**	
Receptor	**EC_{50} (μM) (95% CI)**	**I_{max}/I_{AChMax} (95% CI)**	**EC_{50} (μM) (95% CI)**	**I_{max}/I_{AChMax} (95% CI)**	**EC_{50} (μM) (95% CI)**	**I_{max}/I_{AChMax} (95% CI)**
α7 WT	82.4 (71-95)	1	29.64 (24-37)	0.93 (0.90-0.94)	643 (493-837)	0.55 (0.4-0.7)
α7G174D	66.9 (37-120)	1	8.5* (5.4-7.4)	0.95 (0.8-1.1)	139.6* (100-190)	0.92* (0.8-1.0)
α7G174A	86 (38-194)	1	60.11 (19-191)	1.40 (1.0-1.8)	891 (545-1459)	0.40 (0.2-0.6)

B) [^{125}I]α-Bgt binding assays			
	Saturation binding assays	**Competition binding assays**	
Receptor	**K_d (nM) (95% CI)**	**K_i Cyt (nM) (95% CI)**	**K_i BS40 (nM) (95% CI)**
α7 WT	0.32	855 (528-1386)	5371 (2650-10880)
α7G174D	0.33	169* (108-865)	458* (275-760)

4.2.4. G174D and R101 establish de novo electrostatic interactions

As shown in the previous section, α7G174D causes an increase in both agonist potency and binding affinity for Cyt and BS40. Considering that the equivalent arginine residue in α4β2 nAChRs is stabilised by electrostatic interactions with α4D185, it is likely that the effects of

G174D stem from the formation of an electrostatic interaction between G174D and R101. To test the validity of this view, the stability of the "*de novo*" formed electrostatic interaction was assessed by substituting R101 or G174 with shorter or longer charged residues (R101K and G174E) to alter the stability of the interaction. If the effects of G174D solely stem from the "*de novo*" electrostatic interaction, changes in the stability of the interaction should produce corresponding changes in agonist potency. Oocytes expressing the α7 mutant or α7 WT nAChRs were functionally characterised using two electrode voltage-clamp. The impact of the mutations on agonist potency and efficacy is shown in **Table 4.3**.

Table 4.3. Effects of mutating 101 and 174 positions at α7 nAChR on agonist sensitivity. **A)** Whole-cell current responses to agonist (ACh, Cyt or BS40) were measured using *Xenopus* oocyte two electrode voltage-clamping electrophysiology. Data were fitted to the empirical Hill equation using non-linear regression and are presented with 95% confidence interval (95% CI) as EC_{50} in μM and relative maximal efficacy I_{max}/I_{AChmax} from a minimum of 11-12 independent experiments carried out using at least 3 different *Xenopus* donors. Statistical analysis was performed by comparing the estimated values of wild type and mutant EC_{50} and I_{max}/I_{AChMax} using ANOVA followed by Dunnett's post-test. NE, no functional expression.

	ACh		**Cyt**		**BS40**	
Receptor	**EC_{50} (μM) (95% CI)**	**I_{max}/I_{AChMax} (95% CI)**	**EC_{50} (μM) (95% CI)**	**I_{max}/I_{AChMax} (95% CI)**	**EC_{50} (μM) (95% CI)**	**I_{max}/I_{AChMax} (95% CI)**
α7 WT	82.4 (71-95)	1	29.64 (24-37)	0.93 (0.90-0.94)	643 (493-837)	0.55 (0.4-0.7)
α7G174R, R101D	NE	NE	NE	NE	NE	NE
α7R101K	741.3* (506-1086)	1	121.6* (63-236)	1.05 (0.8-1.3)	3228* (2523-4130)	0.56 (0.2-0.9)
α7G174D, R101K	349.1* (222-550)	1	54 (25-112)	1.26 (1.1-1.5)	1303.2* (902-1888)	0.96* (0.7-1.2)
α7G174E	322 * (181-568)	1	272.9* (161-463)	1.17 (0.8-1.5)	1025.6* (120-8749)	0.75 (0.5-0.9)
α7G174E, R101K	54 (36-79)	1	7.81* (3-20)	1.04 (0.8-1.3)	69.34* (36-132)	0.68 (0.5-0.8)

Swapping R101 for the shorter residue K decreased the sensitivity of α7G174D receptors to activation by all agonist tested, including ACh (**Fig. 4.7A**; **Table 4.3**). To understand the effects of the R to K substitution, the distance between the interacting moieties in the α7 nAChR homology model was measured using PyMol and its mutagenesis option. As shown in **Fig. 4.7B**, the distance between the side chains of G174D and R101K is 5.4 Å, almost twice longer than the distance that separates G174D from R101 (2.5 Å). Since a distance of less than approx. 4 Å is needed for stable electrostatic interactions between charged amino acid, a distance of 5.4 Å would prevent the formation of salt bridges or hydrogen bonds between G174D and R101K. Interestingly, replacing G174 for E also decreased agonist potency (**Table 4.3**), even though for mutant G174E, the distance separating the side chains of E and R are predicted to be (~1.1 Å) (**Fig. 4.7B**). Such short distance would cause overlapping of the charged moieties, which would in turn impede the formation of stable electrostatic interaction between them. In accord with this possibility, α7G174E,R101K, in which the distance between G174E and R101K is only 0.6 Å greater than that between D and R in α7G174D (**Fig. 4.7B**), displayed affinities for Cyt or BS40 that were not different from those exhibited by α7G174D receptors (**Fig. 4.6A; Table 4.2**).

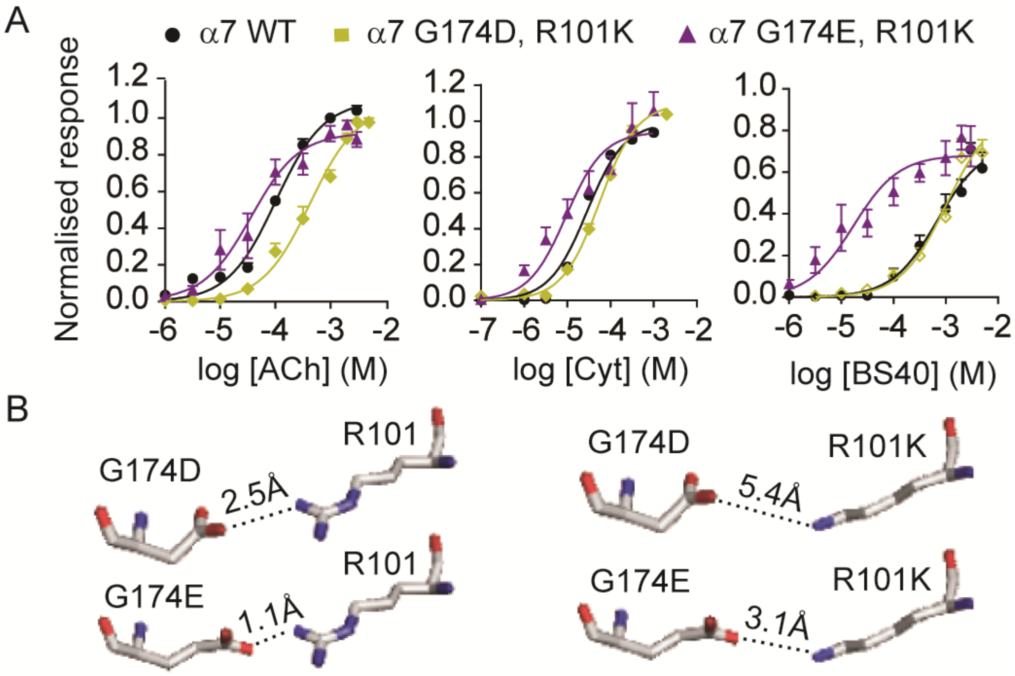

Figure 4.7. Functional effects of changes in distance between the charged moieties at the position 174 in loop B and 101 in β3-strand of α7 nAChR. **A)** Activation concentration responses curves for α7 WT (in black) and double mutants (α7G174D, R101K in yellow and α7G174E, R101K in purple). Data were fitted to the empirical Hill equation using non-linear regression and error bars indicate SEM. Values are the mean ± SEM of 11-12 independent experiments carried out using at least 3 different *Xenopus* donors. **B)** Distances between R101 and G174 residues and their respective mutations.

The findings reported above show that the greater decreases in agonist potency are caused by mutations that are unlikely to promote the stabilisation of R101 through electrostatic interactions (G174D-R101K or G174E-R101). This finding suggests that R101 may have a more fundamental role in the function of α7 nAChR than solely obstructing access of bulky agonists to the agonist site. To test this possibility, the functional effects of α7R101K were assayed. As shown in **Table 4.3**, α7R101K receptors displayed significantly reduced sensitivity to activation by all agonist tested (ACh, Cyt and BS40). Furthermore, reversal of charges (α7G174R,R101D) ablated function (**Table 4.3**). If the effects of R101 on function were due solely to its steric effect, reversal of charge should have preserved the agonist potency displayed by G174D. Collectively, therefore, the findings suggest that the functional effects may be more complex than exerting a "gatekeeper" effect in the agonist site.

4.2.5. α4D185-β2R106 electrostatic interaction regulates cell surface expression of α4β2 nAChR

To test whether the α4D185-β2R106 interaction in the α4β2 nAChR affects agonist potency, the interaction was ablated by introducing an α4D185G mutation and its effects on activation by agonists (ACh, Cyt or BS40) was assessed using two electrode voltage-clamping and compared to both α4β2 WT. The mutation β2R106A was also introduced for a better understanding of the role of this residue in the receptor. The effects of the mutations were studied in the two stoichiometries of the α4β2 nAChR, $(\alpha4)_2(\beta2)_3$ and $(\alpha4)_3(\beta2)_2$. Both mutations ablated the functional expression of $(\alpha4)_2(\beta2)_3$ and markedly decreased that of $(\alpha4)_3(\beta2)_2$ by 80 ± 24% (N = 10; p <0.001; Student's *t*-test) (**Table 4.4A; Fig. 4.8**). The reduced level of functional expression impeded the construction of reliable activation concentration-effects relationships for both receptor ensembles; however, because Cyt and BS40 display high affinity but very poor efficacy at the α4β2 nAChR, we determined the ability of Cyt and BS40 to inhibit the agonist responses elicited by the full agonist ACh to assess the effect of dismantling the α4D185-β2R106 interaction on agonist binding (as in **Chapter 3**, **section 3.2.2.a**). Neither $(\alpha4D185G)_3(\beta2)_2$ nor $(\alpha4)_3(\beta2R106A)_2$ affected the inhibitory potency of Cyt or BS40, compared to wild type (**Table 4.4A; Fig. 4.8**).

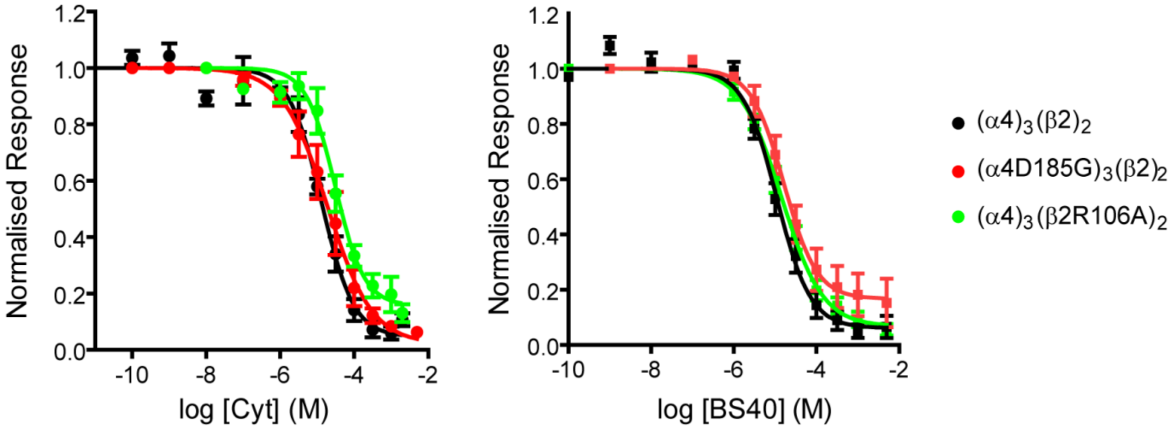

Figure 4.8. Functional effects of disrupting the α4D185-β2R106 interaction in $(\alpha4)_2(\beta2)_3$ nAChR. Activation concentration responses curves for $(\alpha4)_3(\beta2)_2$ WT coloured in black and the mutants $(\alpha4D185G)_3(\beta2)_2$ and $(\alpha4)_3(\beta2R106A)_2$ coloured in red and green, respectively. Human wild type and mutants nAChR subunits α4 and β2 are injected in a ratio 10:1 to express the $(\alpha4)_3(\beta2)_2$ nAChRs heterologously in *Xenopus* oocytes. Data were fitted to the empirical Hill equation using non-linear regression and error bars indicate SEM. Values are the mean ± SEM of 5-6 independent experiments carried out using at least 3 different *Xenopus* donors.

Table 4.4. Effects of ablatating the α4D185-β2R106 interaction on the receptor function and agonist binding of α4β2 WT and mutants. **A)** The agonist activity of ACh and the antagonist activity of Cyt or BS40 were measured using *Xenopus* oocyte two electrode voltage clamping electrophysiology at $(\alpha4)_2(\beta2)_3$ and $(\alpha4)_3(\beta2)_2$ WT and D185G or R106A mutants. Increasing concentrations (1 nM to 3 mM) of Cyt and BS40 were co-applied with ACh EC_{80}: 30 µM for $(\alpha4)_2(\beta2)_3$ receptors; 300 µM for $(\alpha4)_3(\beta2)_2$ receptors. The peak of the current responses obtained in this manner were then normalised to the peak of the responses elicited by ACh EC_{80} alone. The normalised data were then fit by non-linear regression to the Hill equation. There was no statistical difference between mutants and wild type (OneWay Anova, n = 8; N= 5). Data are presented with 95% confidence interval (95% CI) as IC_{50} in µM from a minimum of 5-6 independent experiments carried out using at least 3 different *Xenopus* donors. NE, not functional expression (less than ~ 50 nA). **B)** Saturation binding affinities of [^{3}H]Epi (K_d) and competition binding affinities of BS40 and Cyt (K_i) for α4β2 WT and α4D185G mutant. Human α4β2 WT and α4D185G mutant were expressed in HEK 293 cells (n=3). Data were fitted to the one site–specific binding with Hill slope – model and are presented as the mean with 95% confidence interval (95% CI). Statistical analysis was performed by comparing the estimated values of wild type and mutant using Student's *t*-test. Significant differences, compared to control were considered as significant if $p < 0.05$ (noted by *).

A) Whole-cell recordings			
	ACh	**Cyt**	**BS40**
Receptor	**ACh EC_{50} (µM) (95% CI)**	**Cyt IC_{50} (µM) (95% CI)**	**BS40 IC_{50} (µM) (95% CI)**
$(\alpha4)_3(\beta2)_2$	57.7 (48-69)	13 (9-19)	13 (6-28)
$(\alpha4D185G)_3(\beta2)_2$	67.3 (54-84)	21 (11-40)	14 (7-29)
$(\alpha4)_3(\beta2R106A)_2$	34.8 (26-47)	25 (10-61)	14 (11-18)

$(\alpha4)_2(\beta2)_3$	6.5 (5.2-8.2)	0.56 (0.3-1.0)	0.73 (0.3-2.1)
$(\alpha4D185G)_2(\beta2)_3$	NE	NE	NE
$(\alpha4)_2(\beta2R106A)_3$	NE	NE	NE
B) [^{3}H]Epi binding assays			
	Saturation binding assays		**Competition binding assays**
Receptor	**K_d (nM) (95% CI)**	**B_{max} (fmol/mg of protein) (±SD)**	**K_i BS40 (nM) (95% CI)**
α4β2	0.106	1219 ± 68	2.8 (2.1-3.7)
α4D185Gβ2	0.149	269* ± 107	4.1 (3.0-5.0)

Thus, together, the results show that ablation of the electrostatic interaction between α4D185 and β2R106 impairs cell surface expression but not agonist binding. To test further this possibility we carried out [^{3}H]Epi binding assays on cells expressing α4β2 receptors. The data showed a 5-fold decrease in B_{max} but no changes in K_d in saturation studies or BS40 K_i in competition studies (**Table 4.4B**), in accord with our conclusion that abolishing the α4D185-β2R106 electrostatic interaction disturbs cell surface expression only.

4.3. Discussion

The main finding of this chapter is that a conserved arginine residue in β3-strand (R101) influences agonist potency in α7 nAChRs. In agreement with the view that complementary residues are important for agonist specificity, R101 is contributed by the complementary side of the agonist binding domain in the α7 nAChR.

Molecular docking failed to identify R101 as a key determinant of C(10) Cyt derivatives specificity. Instead, it suggested complementary residues that may affect diverse characteristics of the binding pocket such as hydrophobicity, volume or hydrogen bonding networks. However, making the complementary side of the α7 agonist site to resemble that of the α4β2 receptor in well-established agonist selectivity residues (eg., β2F144) had either no effect or a detrimental effect on agonist potency. Despite there being more divergent residues in loop E, only residues that appear to be close enough to interact with the compounds docked into the receptor binding pocket were reported in this thesis. Mutating Q139 residue from α7 loop E to resemble its β2 subunit counterpart (Q139F) decreased agonist affinity, even though this residue appears to make significant contribution to the hydrophilicity of the agonist site in the α4β2 subtype. Thus, several studies of α4β2 nAChRs have proposed that differences in the hydrophobicity of the agonist sites in the α4β2 and α4/α4 interfaces account for the lower agonist affinity displayed by the $(\alpha4)_3(\beta2)_2$ stoichiometry, compared to the $(\alpha4)_2(\beta2)_3$ (Harpsøe *et al.*, 2011; Lucero *et al.*, 2016). The key differences are H142, Q150, T152 in α4 and V136, F144, L146 in β2, and interchanging them converts the alternate stoichiometries in their counterparts, at least in respect of their agonist affinity (Harpsøe *et al.*, 2011; Lucero *et al.*, 2016). It is surprising therefore that mutation Q139F, which would change the environment around position 139 from hydrophilic to hydrophobic (Kyte and Doolittle, 1982; Rose *et al.*, 1985), had a detrimental effect on agonist potency. Double mutant α7T128S,S172T, which may likely affect the extensive hydrogen bond networks observed in this part of the agonist binding site (Unwin, 2005) also decreased agonist potency. Overall the mutagenesis studies directed by observations made using molecular docking approaches failed to approximate the potency of C(10) Cyt derivatives at α7 nAChR to that exhibited at the α4β2 subtype.

To overcome the limitations of molecular docking, other computational techniques such as MD simulations were used. MD simulations take into account the natural motion of the protein and examine agonist dynamics within the binding site. Extending MD simulations to identify the structural underpinnings of C(10) Cyt derivatives selectivity led to the identification of arginine residue in the β3-strand that defines the selectivity of these compounds in nAChRs. In α4β2 nAChR and all heteromeric nAChRs, except α9α10, the side chain of this arginine is stabilised by electrostatic interactions with an aspartate residue in loop B of the principal subunit. In α7 nAChR, the aspartate residue is substituted by a glycine (G174), which cannot stabilise R101 through electrostatic interactions. As a consequence the side chain of R101 is highly mobile and orients towards the agonist binding site searching for compatible residues to form electrostatic interactions, which impairs the binding of the C(10) Cyt derivatives to the binding pocket in α7 nAChR. In accord with this view, decreasing the mobility of the side chain of R101 by introducing electrostatic interactions with G174D markedly increased the affinity of BS40 for the α7 nAChR.

Disruption of the electrostatic interactions between α4D185 and β2R106 in α4β2 nAChR impairs functional expression but not function. This suggest that the α4D185-β2R106 interaction is important for receptor assembly and/or trafficking to the membrane, as it is the case in the $GABA_A$ receptor where the disruption of a homologue interaction ablates biogenesis and as a consequence produces a type of familial epilepsy (Sancar and Czajkowski, 2004; Hales *et al.*, 2005). Remarkably, the R-D electrostatic interaction observed in α4β2 nAChR is highly conserved among the heteromeric members of the nAChR family, with the exception of the α9α10 nAChR. It is tempting to suggest that the acquisition of the loop B-β3-strand interaction during the evolution of the nAChR family was driven by the necessity to create functional diversity through the assembly of heteromeric receptors. Perhaps, assembling homologue subunits is more energetically demanding than the assembly of identical subunits and, introducing inter-subunit salt bridges would give greater stability to the ensemble (Sokalingam *et al.*, 2012). Thus, in the case of the nAChR family, which shows a high degree of sequence conservation in the agonist binding site, functional divergence seems to have been achieved thanks to the introduction of inter-subunit interactions that stabilised the multimeric complexes. Interestingly, the α9α10 subtype lacks the loop B-β3-stand interaction. This may be due to that neither the α9 nor the α10 subunits followed the same evolutionary trajectory of the other members of the nAChR family; α9 and α10 subunits show great divergence in coding sequence and a highly restrictive ability to assemble with other nAChR subunits (Marcovich *et al.*, 2019).

In conclusion, the findings described here show that the arginine residue in β3-strand in nAChR is a conserved residue with a non-conserved function. In heteromeric receptors such as the α4β2 nAChR, this arginine forms an electrostatic interaction with aspartate that is essential for the assembly and/or trafficking of the receptor but not for receptor function. In contrast, in the homomeric α7 subtype the arginine in β3-strand does not affect the biogenesis of the receptor. However, its mobility, brought about by the absence of strong electrostatic interactions, places this residue as a key discriminator of agonist size. C(10) Cyt derivatives even with small substituents such as in BS40 are expelled from the agonist binding pocket due to the action of α7R101. However, as suggested by mutagenesis exercises, R101 appears to have a more profound effect on α7 nAChR function than merely acting as an agonist size discriminator. For example, exchanging R101 for the smaller K residue, markedly impaired receptor activation, regardless of the presence or absence of a D residue in loop B position 174. The role of R101 in the function of the α7 nAChR will be explored in **Chapter 5**.

CHAPTER 5. ROLE OF R101 IN α7 NACHRS

5.1. Introduction

The findings reported in the previous chapter identify R101, a residue located in β3-strand, as a key element of C(10) Cyt derivatives discrimination in the α7 nAChR. Surprisingly, the arginine in β3-strand is conserved among the nAChR family, although its contribution to receptor function is not. In the α4β2 nAChR, and indeed in all heteromeric nAChRs, except the α9α10 subtype, the arginine is stabilised through inter-subunit electrostatic interaction with an aspartate residue in loop B, and this interaction is obligatory for the assembly/trafficking of the receptor complexes. Unlike its equivalent in β2, α7R101 is not stabilised through pairwise electrostatic interactions. As a consequence, the side chain of R101 is highly mobile, searching for polar atoms to satisfy the propensity of its guanidinium moiety to donate hydrogen bonds or establish salt-bridges. In this search, the side chain of R101 can orientate downwards towards the binding pocket establishing short-lived interactions with E215 in loop C. In BS40-bound α7 nAChRs, the side chain of R101 approaches the C(10) position of BS40 and Cyt, which eventually perturbs the interaction of these ligands with the conserved aromatic residues at the agonist binding site. In accord with this observation, stabilisation of R101 through inter-subunit electrostatic interactions with G174D in loop B, increased the affinity of BS40 and Cyt for α7 nAChR.

Unsurprisingly, further studies that examined the functional effects of charge substitutions on R101 suggested a complex role for this residue on receptor function, comprising agonist selectivity as well as receptor activation. Of all the charged amino acids, arginine is frequently found as a key player of the mechanisms driving protein functions (Harms *et al.*, 2011). For example, arginines enable the voltage sensor of voltage-sensitive Na^+ channels to sense changes in the voltage across the plasma membrane (Armstrong *et al.*, 2016). In the Cys loop receptor family, the ability of the side chain of arginine to form salt bridges frequently sustain the stability of proteins, which is important for functional expression, as shown for the α4β2 nAChR (**Chapter 4**) or the $GABA_A$ (Sancar and Czajkowski, 2004; Hales *et al.*, 2005). In some cases, arginines are an essential component of agonist recognition; for example, in GluCl receptors, glutamate recognition requires arginine residues in the agonist site establishing hydrogen bonds with glutamate and a threonine residue in the agonist site (Lynagh *et al.*, 2017). Also, granisetron, a competitive inhibitor of the 5-HT_3 receptor is stabilised within the agonist site of this receptor through a cation-π with an arginine residue (Kesters *et al.*, 2013). Moreover, a highly conserved arginine residue at the end of β10-strand of nAChRs forms a salt bridge with a glutamate residue in the β1-β2 linker that is part of the transduction mechanism in the family (reviewed by Gay and Yakel, 2007).

The diverse functions that arginine exhibited in protein stem from the charged nature of its side chain and its unusual ability to retain its positive charge, even in microenvironments that are considered incompatible with charge (Fitch *et al.*, 2015). Additionally, the guanidinium group can establish interactions in three possible directions through its three asymmetrical nitrogen atoms (Sokalingam *et al.*, 2012). In comparison, the basic functional group of lysine allows only one direction of interaction and its pKa value can shift to neutral state depending on the environment (Fitch *et al.*, 2015). These unique properties enable arginine to participate in numerous stabilizing noncovalent interactions such as salt-bridges and hydrogen bonds (Harms *et al.*, 2011). This chapter explores the functional consequences of the mobile side chain of R101 on the overall function of α7 nAChRs.

5.2. Results

5.2.1. α7R101 mutations affect agonist potency and onset of current decay

To test whether R101 influences α7 nAChR function, the residue was replaced with alanine via site-directed mutagenesis and the functional consequences of this replacement were assayed by measuring agonist (ACh, Cyt or BS40) induced current responses with two electrode voltage-clamping procedures. Given the effects of stabilising R101 through electrostatic interactions with G174D on the binding of Cyt and BS40 to α7 nAChRs, one would expect Cyt and BS40 sensitivity of α7R101A to approximate that of α7G174D and the sensitivity for ACh to reflect that of α7 WT. Unexpectedly, however, α7R101A decreased the potency of all agonist tested, including ACh. The potency of both ACh and Cyt decreased by about 11-fold and that of BS40 by 3-fold (**Fig. 5.1A**; **Table 5.1**). Moreover, R101A increased the relative efficacy of Cyt by ~4-fold (**Fig. 5.1A**; **Table 5.1**) whereas that of BS40 was decreased (**Fig. 5.1A**; **Table 5.1**). These findings suggest that steric effects alone are not sufficient to account for the effects of R101 on Cyt or BS40 potency: the decrease in agonist affinity was more marked than the increase in agonist affinity observed for mutant α7G174D receptors (See **Chapter 4, Table 4.2**).

How could R101 influence agonist sensitivity in α7 nAChRs? The detrimental effects of R101K on agonist sensitivity described in **Chapter 4** (see also **Table 5.1**) suggest that the unvariable positive charge on the side chain of R101 may be necessary for agonist function at α7 receptors. (Recall that the side chain of arginine is positively charged even in microenvironments that are considered incompatible with charge). Therefore, sensitivity to activation by agonists would be expected to decrease markedly if positive charge were the main contribution of the side chain of R101 to agonist effects. To test this possibility, the charge at position 101 was reversed by mutating R101 residue to aspartate (R101D). α7R101D reduced the amplitude of the currents elicited by maximal ACh concentrations (1-2 mM) to less than ~ 50 nA, as it was the case for double mutant α7G174R,R101D described in **Chapter 4** (see also **Table 5.1**). These findings suggest that the positive charge of R101 plays a pivotal role in the sensitivity of α7 receptors to activation by agonists.

Table 5.1. Functional effects of substituting R101 in α7 nAChR on receptor activation. **A)** Whole-cell current responses to agonist (ACh, Cyt or BS40) of α7 WT and mutants were measured using *Xenopus* oocyte two electrode voltage-clamping electrophysiology. Data were fitted to the empirical Hill equation using non-linear regression and are presented with 95% confidence interval (95% CI) as EC_{50} in μM and relative maximal efficacy I_{max}/I_{AChmax} from a minimum of five independent experiments carried out using at least 3 different *Xenopus* donors. Statistical analysis was performed by comparing the estimated values of wild type and mutant EC_{50} and I_{max}/I_{AChmax} using ANOVA followed by Dunnett's post-test. Significant differences, compared to control were considered as significant if $p < 0.05$ (noted by *). LE, very low functional expression (maximal ACh, 1 mM, produced currents with amplitudes not greater than ~ 50 nA).

Whole-cell recordings						
	ACh		**Cyt**		**BS40**	
Receptor	**EC_{50} (μM) (95% CI)**	**I_{max}/I_{AChmax} (95% CI)**	**EC_{50} (μM) (95% CI)**	**I_{max}/I_{AChmax} (95% CI)**	**EC_{50} (μM) (95% CI)**	**I_{max}/I_{AChmax} (95% CI)**
α7WT	82.4 (71-95)	1	29.64 (24-37)	0.93 (0.90-0.94)	643 (493-837)	0.55 (0.4-0.7)
α7R101A	887.2* (565-1393)	1	389* (299-504)	4.10* (2.4-6.0)	2075* (440-7943)	0.16 (0.1-0.22)
α7R101K	741.3* (506-1086)	1	121.6* (63-236)	1.05 (0.8-1.3)	3228* (2523-4130)	0.56 (0.2-0.9)
α7R101D	LE	LE	LE	LE	LE	LE
α7E215A	148* (83-260)	1	85.9* (52-140)	1.12 (1.0-1.3)	1140* (756-1713)	0.95 (0.6-1.2)

Surprisingly, R101A, R101K and R101D slowed down the onset of decay of the current responses stimulated by ACh in α7 nAChRs by 3-fold, compared to wild type (**Fig. 5.1B**). Two-phase decay fits to the data indicated that R101A increased the half-life constant of the fast decay phase (α7 WT 0.37 s *vs* α7R101A 1.01 s) but not that of the slow decay phase (**Table 5.2**). R101K also decreased the half-life constant of the fast decay phase (T½ = 0.62 s) but this decrease was not significant (**Fig. 5.1B; Table 5.2**). The reduced amplitudes of the current responses in α7R101D prevented estimating the half-life constant for this mutant. However, visual inspection of the current responses, indicate that R101D also slowed down the onset of current decay (**Fig. 5.1B**). The effects of the reversal of charge are specific to the side chain of R101: G174D has no impact on the onset of current decay (**Table 5.2**).

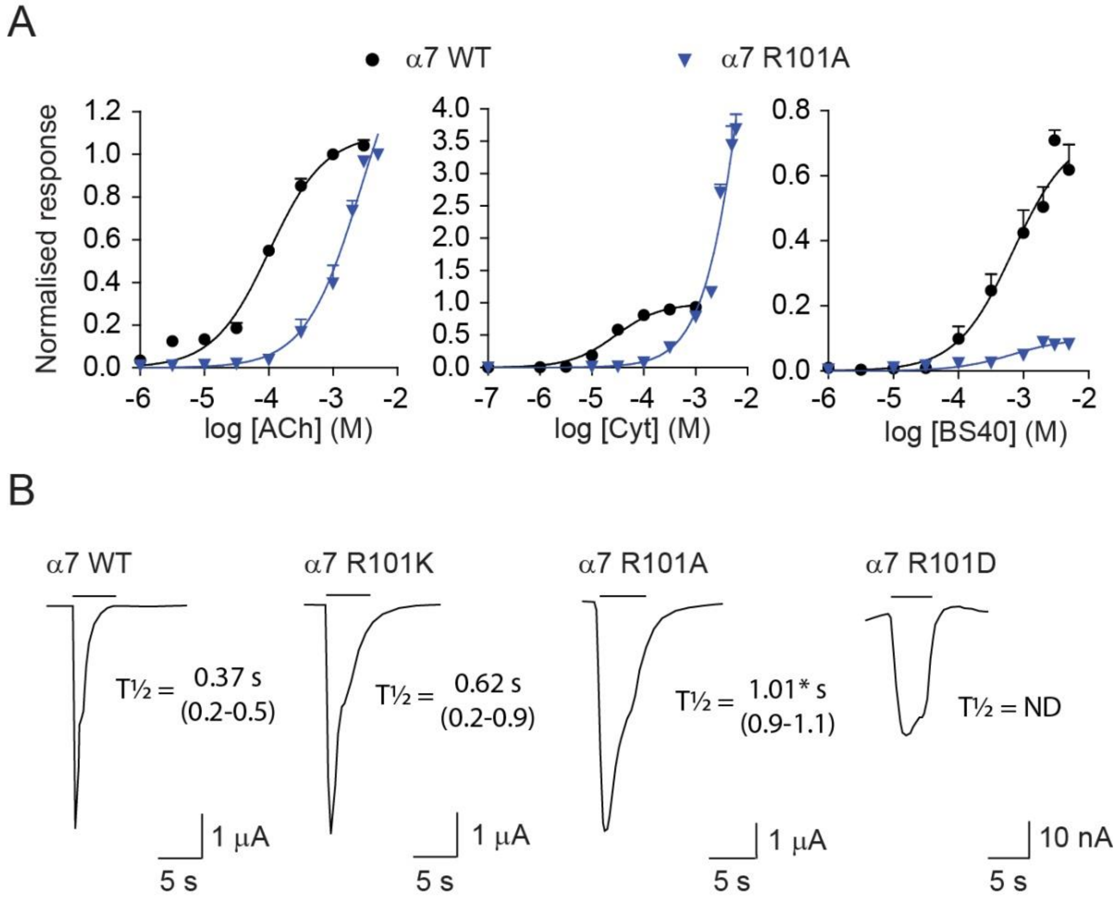

Figure 5.1. Functional effects of substituting R101 in α7 nAChR on receptor activation. **A)** Activation concentration response curves by ACh, Cyt and BS40 for α7 WT (in black) and α7R101A (in blue) nAChRs expressed heterologously in *Xenopus* oocytes. Data were fitted to the empirical Hill equation using non-linear regression and error bars indicate SEM. Values are the mean ± SEM of 11-12 independent experiments carried out on oocytes from 5-6 different Xenopus donors **B)** Representative traces of the responses elicited by 1 mM ACh at α7 WT and mutants α7R101A, α7R101K and α7R101D.Data were fitted to the two-phase decay equation to calculate the half-life constant (T½) with 95% confidence interval (95% CI). ND, not determined.

Table 5.2. Functional effects of substituting R101 in α7 nAChR on onset of current decay. Onset of current response decay in α7 WT and mutants α7G174D, α7R101A, α7R101K and α7R191D. Data were fitted to the two-phase decay equation and are presented with 95% confidence interval (95% CI) as half-life constant from 11-12 independent experiments carried out using at least 3 different *Xenopus* donors. ND, not determined. Statistical analysis was performed by comparing the estimated values of wild type and mutant half-life using ANOVA followed by Dunnett's post-test. Significant differences, compared to control were considered as significant if $p < 0.05$ (noted by *).

Onset of current response (two-phase decay)		
Receptor	**Slow half-life (CI)**	**Fast half-life (CI)**
α7 WT	1.887 (0.6-3.1)	0.365 (0.2-0.5)
α7G174D	1.117 (0.3-2.4)	0.331 (0.27-0.39)
α7R101A	2.769 (0.9-4.6)	1.013* (0.9-1.1)
α7R101K	1.724 (0.7-2.8)	0.615 (0.2-1.0)
α7R101D	ND	ND

5.2.2. α7R107A changes the dynamics of coupling elements in the agonist site

In order to insight the mechanisms underlying the functional effects of α7R101A, its dynamical behaviour in agonist-bound α7R101A was compared to α7 WT. The average structures of α7 WT and α7R101A during MD simulations shows a change in loop C capping with bulkier ligands such as Cyt and BS40 (**Fig. 5.2**). As described in **Chapter 4**, the mobile side chain of R101 can orientate downwards towards the agonist site, establishing short-lived interactions with loop C E215. In addition to loop C, changes in Cys-loop and loop F can also be observed (**Fig. 5.2**).

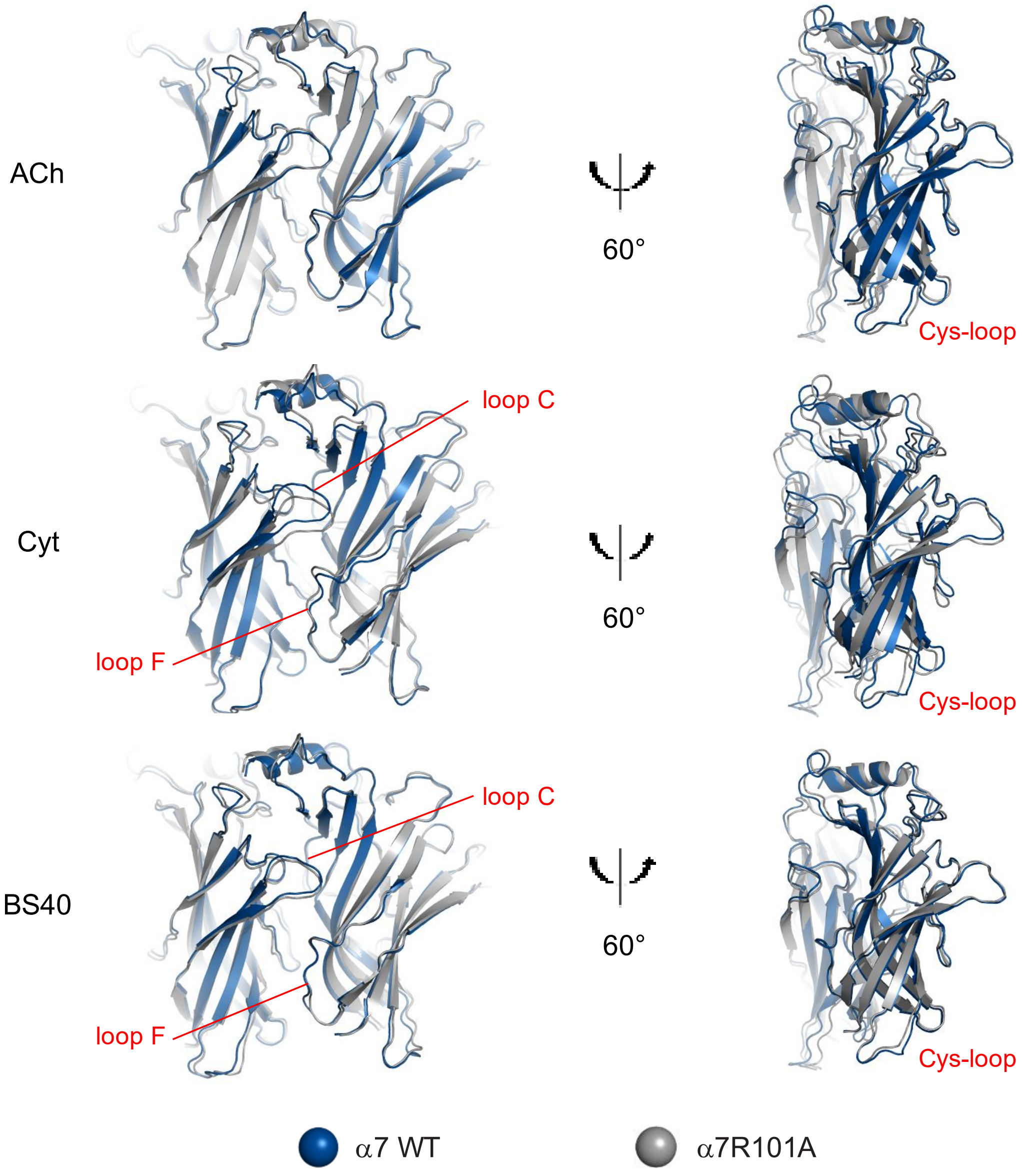

Figure 5.2. α7 WT and α7 R101A average structures of MD simulations of the first binding pocket for ACh, Cyt and BS40. Note that R101A induces a small change in the extent of loop C capping in the cytisine-bound complex. The significance of this change was determined by the residue root mean square fluctuation (RMSF) analysis.

The transient interaction of the side chain of R101 and loop C E215 may be important for modulating loop C capping and the size of the ligand clearly affects access to E215 (**Fig. 5.3A-B**). In α7R101A the E215-R101 interaction is lost, suggesting that the functional effects of R101A stem from this loss. In accord with this possibility, alanine substitution of E215 decreased the functional potency of ACh, Cyt and BS40 (**Table 5.1**), although not to the same extent as R101A (**Table 5.1**). Interestingly, to compensate for the loss of the E215-R101 contact, in the α7R101A complex, E215 transiently forms a salt bridge with K98 (located close to R101) in (**Fig. 5.3C**). However, this new interaction is not stable enough to allow wild type closing of loop C.

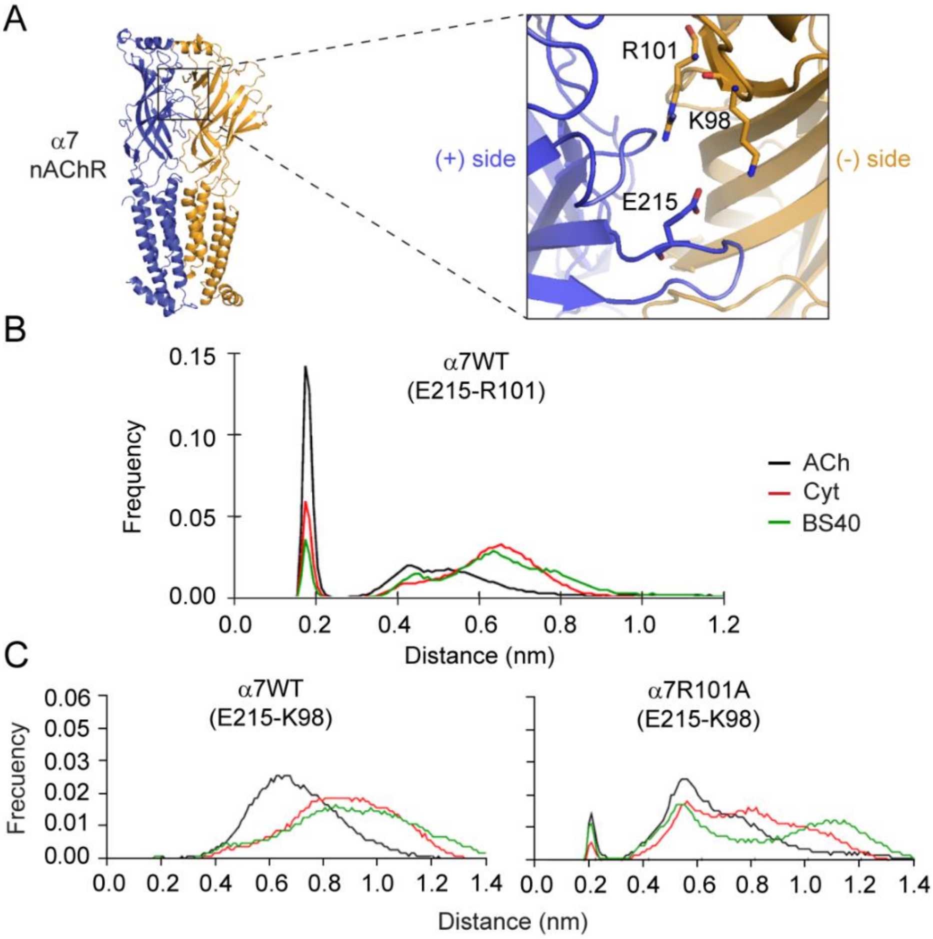

Figure 5.3. Interactions between R101 and loop C in α7 nAChR and the effects of α7R101A mutation. **A)** Location of R101, E215 and K98 in the ECD of α7WT nAChR. The principal and complementary subunits are coloured in blue and orange, respectively. The residues numbering refers to the following UniProt sequence codes: P36544 (α7 subunit). **B)** Overall distribution of the minimum distance between the side chains of R101 and E215 in α7WT receptor. **C)** Overall distribution of the minimum distance between the side chains of E215 and K98 in α7WT and α7R101A receptors. All histograms reflect the distances over the two binding pockets.

5.2.3. α7R107 is coupled to receptor gating

Given the effects of R101A in the dynamics of the Cys-loop and loops C and F, R101 would be expected to affect the process of coupling agonist binding to gating. The Cys-loop, loop C and the lower part of loop F have been implicated in coupling (Jha *et al.*, 2007; Bouzat *et al.*, 2008; Lee *et al.*, 2009; Khatri and Weiss, 2010; Oliveira *et al.*, 2019). To test this possibility, ELFCAR analysis was applied to R101. As described in **Chapter 2**, **Section 2.7**, ELFCAR analysis can establish whether a residue in the ECD couples to gating by using the well-established L9'T gating reporter mutation (Gleitsman *et al.*, 2009) (**Fig. 5.4**). α7L9' is part of the gating machinery of the α7 receptor and, swapping the hydrophobic leucine with a more hydrophilic amino acid such as threonine leads to an decrease in the agonist EC_{50} (Revah *et al.*, 1991). If the two residues are functionally coupled, double mutant α7R101,L9'T should yield EC_{50} values that are greater than the product of the single mutant EC_{50} values, producing functional coupling (Ω) values greater than 1. Coupling values lower than one are typical of close interactions between residues (e.g., salt bridges, hydrogen bonds) but for long range coupling, such as coupling of ECD residues with gating elements, values are greater than 2 (Gleitsman *et al.*, 2009). As shown in **Fig. 5.4**, ELFCAR analysis showed functional coupling between R101 and L9'T (Ω = 2.38).

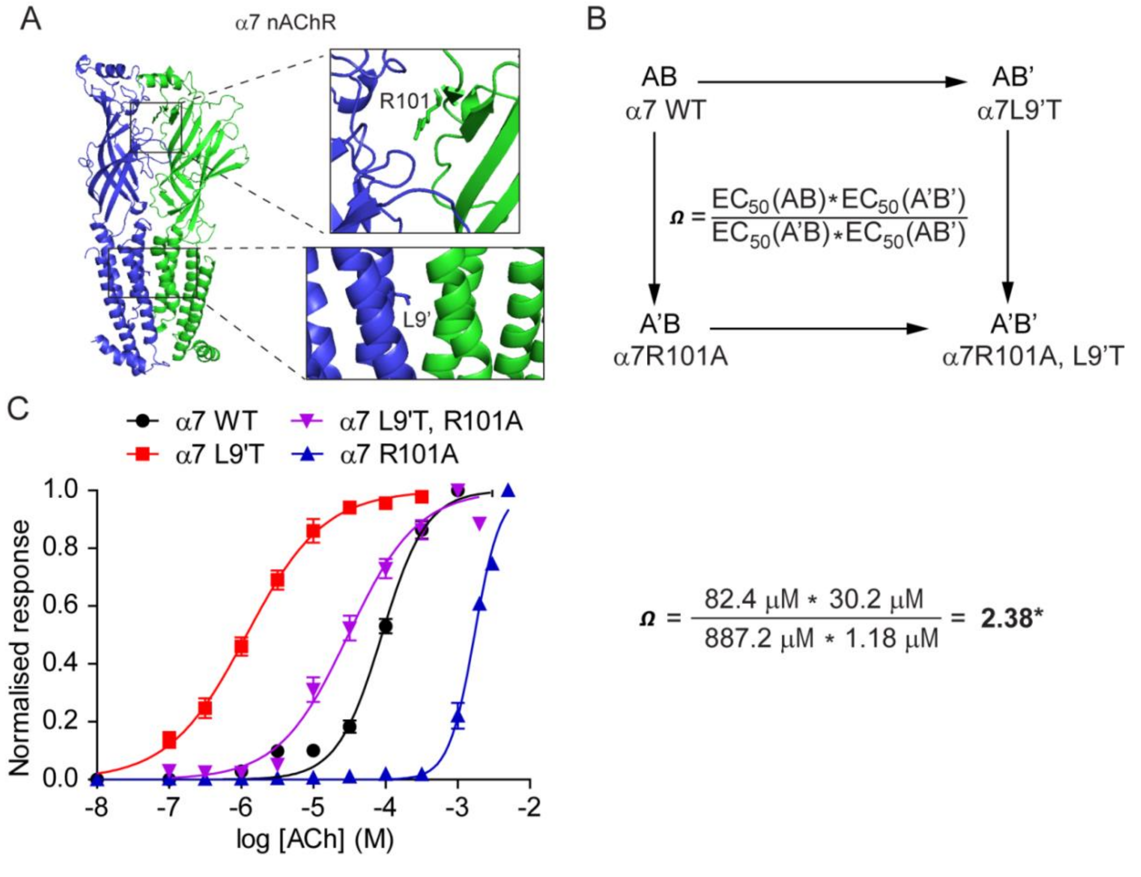

Figure 5.4. α7R101 is functionally couple to L9' in the ion channel. **A)** Lateral side view of the α7 nAChR (left) and magnified versions of the ECD showing the residue R101 and the TMD showing residue L9' (right). **B)** Long-range functional coupling of allosteric receptors analysis. Scheme for double mutant cycle analysis where A and B represent amino acid positions (R101 and L9') and A' and B' represent mutations at these sites. The coupling parameter, Ω, is calculated from the given equation. A value of Ω higher than 2 is considered as meaningful coupling (Gleitsman *et al.*, 2009). **C)** Activation concentration response curves by ACh α7 WT (in black), α7L9'T (in red), α7R101A (in blue) and α7L9'T,R101A (in purple) nAChRs expressed heterologously in *Xenopus* oocytes. Data were fitted to the empirical Hill equation using non-linear regression and error bars indicate SEM from a minimum of five independent experiments carried out using at least 3 different *Xenopus* donors. Ω is equal 2.38 suggesting that R101 and L9' residues are coupled.

5.2.4. α7R101 dominates the electrostatic landscape near loop C

The detrimental effects of E215A on agonist effects do not compare to the devastating effects of R101A on receptor function. Given that R101 is only able to establish short-lived interactions with loop C E215, the highly mobile side chain of R101 likely acts as charge carrier setting the electrostatic landscape of the region reached by the side chain. To examine this possibility, the electrostatic maps of WT and R to A mutant nAChRs were compared. As shown in **Fig. 5.5**, the electrostatic map of the region accessible to the side chain of α7R101 reverses its charge, compared to α7 WT. This finding supports the view put forward above that the ability of the side chain of R101 to carry positive charges may define the electrostatic landscape in the region of the agonist site reached by the side chain. Unlike α7 nAChR, in α4β2 nAChR, the mutation β2R106A has little effect on the electrostatic of the region. It is likely that this is due to the presence of an extra lysine residue (K104) close to R106 in β2, which could ameliorate the consequences of the loss of charges brought about by β2R106A (see β3-strand alignment in **Chapter 4**).

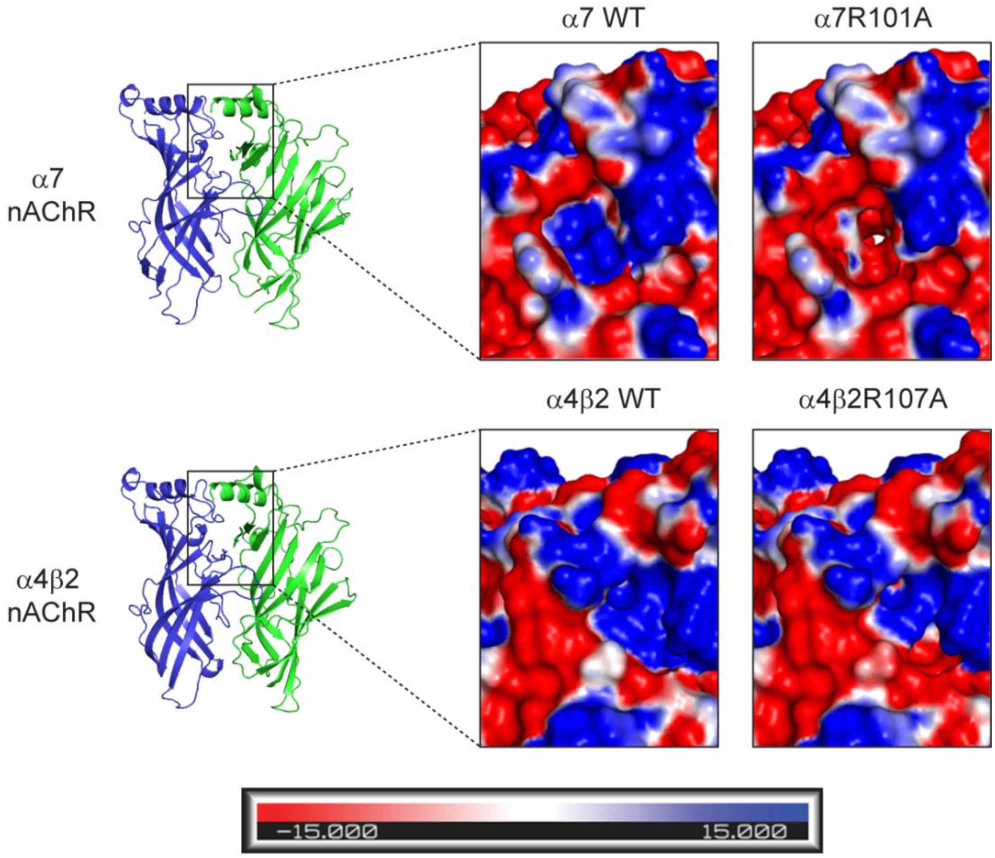

Figure 5.5. Electrostatic maps for α7 WT and mutant α7R101A and α4β2 WT and α4β2R107A nAChRs. R101 dominates the electrostatic landscape on the top of the agonist site in α7nAChR. Zoom of the electrostatic potential distribution on the top of the of the agonist site. The potential varies between -15 and +15 KT/e, as shown in the colours bar, with red and blue representing negative and positive potentials, respectively.

5.3. Discussion

The main finding of this chapter is that R101 is not only an important element of agonist specificity through its ability to disrupt the binding of bulky agonists, but also influences the process of receptor activation and possibly desensitization through its ability to act as a charge carrier. This ability makes it largely responsible for defining the electrostatic environment of the regions reached by the side chain of R101, notably around loop C.

Alanine substitution of R101 markedly impaired the sensitivity of the receptor to activation by agonists and MD simulations of α7R101A showed conformational rearrangements in loop C (uncapping), as well as the Cys-loop and loop F. These loops are considered as key elements of the pathway that couples agonist binding to gating (Mukhtasimova *et al*. 2005; Mukhtasimova and Sine, 2013; Oliveira *et al*., 2019), suggesting that R101 influences this process. In support of this possibility, EFSCAR analysis showed R101 functionally coupled to L9'T in the ion channel. This mutation is known to affect directly the gating of the ion channel (Revah *et al*., 1991).

How could R101 affect coupling? The role of R101 in receptor gating may be due to not only direct interactions between R101 and residues in loop C like E215 but also to its contribution to the electrostatic field around loop C. In α7 nAChR, unlike in the α4β2 nAChR, R101 is the major determinant of the electrostatic landscape around loop C. The electrostatic field around the agonist binding site is an important element in receptor activation, steering the agonist to the agonist site (Carpenter and Lightstone, 2016) and increasing the ligand association rate (Meltzer *et al*., 2006). Additionally, overall electrostatic interactions in the gating domain of Cys loop receptors play a critical role in gating (Xiu *et al*., 2005: Lee and Sine, 2005; Sine *et al*., 1994). Even more relevant, the crystal structure of the α9-ECD (Zouridakis *et al*., 2014) has revealed an uncommon accumulation of arginine residues on the complementary sides of α9, which define the physicochemical properties of the α9-containing nAChRs. Furthermore, molecular dynamic calculations indicate that these arginines could interfere with the loop C closure (Azam *et al*., 2015), which could explain the conversion of nAChR agonists such as Nic and Cyt into antagonists at α9 and α9α10 nAChRs (Verbitsky *et al*., 2000).

The second finding of this Chapter is that α7R101A also slowed down the onset of ACh-elicited current decay by 3-fold. This suggests that R101 may influence receptor desensitisation. To date, several different mutations in α7 nAChRs have been shown to delay the rate of desensitization. Mutations within the TM2 lining the channel pore cause the most profound effects on desensitisation (Revah *et al.*, 1991). Other studies have shown that residues in ECD regions, such as TrpD (Gay *et al.*, 2008) or a proline residue near the middle of β9-strand of the outer β-sheet (McCormak *et al.*, 2010) also slow down desensitisation. The proline residue in β8-strand is particularly interesting because this region links loops C and F, domains known to affect the activation of nAChRs (Celie *et al.*, 2004; Hansen *et al.*, 2005; Hibbs *et al.*, 2006; McLaughlin *et al.*, 2006; Oliveira *et al.*, 2019). In this scenario, it is notable that R101A alters the dynamics of loops C and F. However, *Xenopus* oocytes are not a good model to investigate the role of R101 in α7 nAChR desensitization due to the slow perfusion of the system. Therefore, microscopic studies to determine the receptor kinetics should be undertaken.

In conclusion, our findings reveal that R101 sets the electrostatic field on the top region of the agonist site, which appears to influence the fundamental processes of α7 nAChR function. R101 is a novel element of α7 nAChR gating forming part of the loop C capping mechanism. The effects of α7R101 on loop C may be also implicated somehow in α7 nAChR desensitization, however more studies should be undertaken in order to confirm this. MD simulations have been shown to be a powerful technique that, in combination with functional assays, help to insight the molecular mechanisms of receptor function. These studies suggest that R101 contributes to the gating process in the α7 nAChR, likely through its effects on the dynamics of loop C and other structural elements (i.e., Cys-loop and loop F) of the pathway coupling agonist binding to channel gating.

CHAPTER 6. FINAL DISCUSSION

Since they were first identified (Langley, 1905), nAChRs have been under the gaze of physiologists and pharmacologists. However, nAChRs only became a major focus of drug discovery efforts from the late 1980’s, when the gene family that encodes for neuronal nAChR subunits was identified and the subsequent realisation that these subunits form multiple subtypes of nAChR, all expressed differentially in the brain and involved in diverse brain functions and pathologies. Drug discovery programs have shown interest in emulating the functional effects of natural compounds such as Nic, Cyt or Epi. However, only smoking cessation drugs such as Var (approved by the US FDA) and Cyt (approved in East Europe) have been marketed so far. The reason for these unsatisfactory results lies on the narrow therapeutic range of the ligands developed. In clinical trials, the nicotinic ligands tested to date have displayed an insufficient potency and/or low selectivity for the target subtype or they have not shown to be better than other available drugs. The most common adverse effects appear to gastrointestinal but neuropsychiatric and cardiovascular events may occur. Even the already approved Var causes some of these side effects (McClure *et al.*, 2009; Moore *et al.*, 2011; Ware *et al.*, 2013).

As addressed throughout this thesis, a strategy to overcome cross-reactivity in nAChR drugs to reduce off-target effects is to identify unique drug-discriminatory elements in nAChR subtypes to guide the design of more selective drugs. There has been a tremendous leap forward in the understanding of the molecular mechanisms that drive nAChR selectivity with the resolution of a number of atomic structures of nAChRs and their homologues bound to diverse nicotinic ligands (Brejc *et al.*, 2001; Unwin, 2005; Hilf and Dutzler, 2008; 2009; Morales-Perez *et al.*, 2016; Gharpure *et al.*, 2019). The critical role of the aromatic box in agonist binding has been firmly established, but critically several non-conserved residues within the binding site, mostly in the loop E in the complementary side, have been identified as key elements of ligand selectivity in the neuronal nAChR family (Harpsøe *et al.*, 2011; Blum *et al.*, 2013; Mazzaferro *et al.*, 2014; Van Arnamand Dougherty, 2014).

However, these residues do not fully account for the selectivity of some nicotinic ligands. For example, the C(10) Cyt derivatives characterised in **Chapter 3** show an enhanced selectivity for α4β2 nAChR over α3β4 and α7 nAChR, which cannot be explained by differences in loop E. The C(10)-substituents are predicted to orientate towards the complementary side of the agonist binding site but none of the already known determinants of agonist selectivity could explained the dramatic decrease of α7 nAChR activation displayed by the C(10) Cyt derivatives.

Sequence and structure comparisons may be useful when the determinants are non-conserved residues between the nAChR subtypes. However, identification of conserved residues that may influence agonist binding through orientation of the side chains contacting the ligands or the shape of the aromatic box (Puskar *et al.*, 2012) will require more advanced computational approaches based on receptor changes over time. In **Chapter 4**, MD stimulations were able to identify an arginine residue in the β3-strand (Argβ3-strand) that defines the differential sensitivity to C(10) Cyt derivatives at α7 and α4β2 nAChRs. This arginine is conserved among the nAChR family but its function is not. In α4β2 nAChRs, there is a strong electrostatic interaction between Argβ3-strand and an aspartate residue in loop B (AspB) which is not present in the α7 nAChRs due to the substitution of AspB for a glycine residue. The lack of stabilisation of Argβ3-strand in α7 nAChR allows its side chain to move freely. As a consequence, the side chain of Argβ3-strand orients towards the agonist binding site perturbing the access of agonists, particularly C(10) Cyt derivatives such as BS40. In agreement, introducing mutations that allow the stabilisation of Argβ3-strand in α7 nAChR increases both agonist binding affinity and potency.

Remarkably, contrary to the α7 homomeric nAChRs, the Argβ3-strand - AspB electrostatic interaction observed in α4β2 nAChRs is present in all heteromeric nAChRs with the exception of the α9α10 nAChRs. A plausible explanation is that Argβ3-strand - AspB interaction appears during evolution to confer protein stability and permit the assembly and trafficking of heteromeric ensembles. In accord with this view, ablation of the electrostatic interaction in the α4β2 subtype decreases functional expression but not the ability of the receptor to elicit current responses upon exposure to agonists. The same phenomenon has been observed for the GABA$_A$ receptor (Sancar and Czajkowski, 2004; Hales *et al.*, 2005). Surprisingly α9α10 receptors do not conserve the electrostatic interaction. Interestingly, the primary sequence of neither the α9 nor the α10 is conserved, in respect to that of the other nAChR subunits. Consistently with this observation, the pharmacological properties of the α9α10 subtype are quite different from that of the other nAChRs subtypes; for example, Nic and Cyt are competitive inhibitor at the α9α10 subtypes. Perhaps then, the electrostatic interaction of the heteromeric nAChRs is not conserved in the α9α10 subtype because the α9 and α10 subunits followed different evolutionary trajectories as the remaining members of the nAChR family, it would be interesting to explore the role of the arginine residue in the α9α10 subtype. Identifying its role may shed some light on why Nic and Cys behave as competitive antagonists at α9 and α9α10 nAChRs (Verbitsky *et al.*, 2000).

The unique properties of an arginine residue such as the ability to retain its positive charge, even in incompatible microenvironments (Fitch *et al.*, 2015), as well as establish interactions in different directions through its guanidinium group (Sokalingam *et al.*, 2012), make this residue critical for diverse receptor functions. The dramatic effect of mutating Argβ3-strand to alanine in the α7 nAChR indicated that this residue is not only an important element of agonist specificity but also of receptor function. In **Chapter 5** of this thesis, MD simulations combined with mutagenesis and electrophysiological techniques revealed that Argβ3-strand is involved in α7 nAChR gating not only through direct interactions with residues in loop C but also to its contribution to the electrostatic field around loop C. Moreover, the Argβ3-strand may also be involved in α7 nAChR desensitization as its mutation to alanine slowed down the onset of ACh-elicited current decay. However, more studies should be undertaken in order to confirm this.

The importance of the findings collected in this thesis is that Argβ3-strand may be a good target to increase receptor subtype-specificity. The different dynamic behaviour of Argβ3-strand can be exploited to separate the activation of the α7 subtype and heteromeric nAChRs in the brain. More specifically, Argβ3-strand can guide the design of new drugs for the treatment of brain disorders that required the activation of only heteromeric nAChRs. For example, in smoking cessation a higher clinic efficacy may be achieved by avoiding the activation of α7 nAChR (McClure *et al.*, 2009; Moore *et al.*, 2011). The C(10) Cyt derivatives are an example of this type of compounds. Going further, substituents that directly interact with α7 Argβ3-strand can potentially modulate receptor function as this residue is involved in the gating process and possibly desensitisation of α7 nAChR. The strong positive charge of Argβ3-strand can be targeted by compounds containing a negatively charged moiety. For example a C(10) carboxylate Cyt ligand could potentially interact with the arginine residue and this could perhaps have an allosteric effect that may be useful for therapeutic purposes.

In conclusion, Argβ3-strand is a conserved residue with a non-conserved function in the nAChR family that has the potential to become a target for the design of novel subtype-selective ligands for nAChRs. This residue was identified by applying novel dynamic computational approaches in combination with classical functional assays and mutagenesis to nAChRs, a combination that provides a new impetus to drug discovery programs. For the first time "the rational design of drugs" seems to be a certain possibility.

ACKNOWLEDGEMENTS

This Thesis would not have been possible without the dedication and support of my supervisor Isabel Bermudez. I would like to thank her for being an inspiration not only as a scientist but as a person. Isabel awaked my interest for research during my Erasmus internship and that made me have no doubt about starting my PhD studies in her lab. I do not exaggerate if I say that these three years here were truly enjoyable. She taught me how to do good science: the importance of controls and statistics, to collaborate, to help everyone and not to publish until I am sure. I really appreciate her listening to my ideas, taking them into account and giving me the feedback to improve. Also, she taught me many other things apart from science. I really enjoyed the moments sharing music, books, films, laughs and political ideas trying to make “la revolución”.

I also would like to thank to all the present and past members of the lab: Andrea Rodero, Joe Hawkins, Connie Alcaino, Simone Mazzaferro, Eleanor Mitchell and Andy Jones. Thanks to Silvia García del Villar for sharing my first years in the lab and the unforgettable conference trips to Chile and Crete.

My special thanks are extended to our collaborators from University of Bristol Sofia Oliveira and Tim Gallagher, University of Milan Cecilia Gotti, University of Bath Sue Wonnacott and CONICET Bahia Blanca Elizabeth Nielsen and Cecilia Bouzat, for contributing to this thesis with ideas and experiments.

Thanks to the people that made me enjoy my time in Oxford forming my temporary family: melocotoños, itanolos, ruta en bici por Summertown and my very best housemates at Morrell Avenue Elise and Konrad. Special mention to my friend and housemate Patri for all the laughs and conversations about life and science that we shared: she is a reference of woman in science that makes me wish to be there as well. Thanks also to my friends from Spain (spread throughout Toledo, Madrid, Galicia, Barcelona or Luxemburg) for their support despite the distance and making me feel at home every time we are together. Celia, you are the next one!

To my “compañero de lucha”, who helped me to go through this Thesis with his generosity, dedication and support. A piece of this thesis is yours (especially the bibliography). Thanks

for taking the most from what we have and demonstrating that the distance is only physical. I want to continue learning together.

Finally, I will switch to Spanish to thank my family. Gracias a mis padres, por apoyarme en todas y cada una de las decisiones que he tomado incluso cuando significaban separarnos. Estoy muy agradecida por la educación que me habéis dado y los valores que me habéis enseñado. A mi hermano Jaime, por enseñarme a trabajar duro y hacerme feliz con esas dos brujitas. A mi hermano Alfonso, por despertarme la curiosidad por aprender y enseñarme a pensar de forma crítica. También gracias a mis abuelos Feli, Samuel y Florentina por su cariño y ejemplo de vida. Gran parte de lo que soy es gracias a todos vosotros.

BIBLIOGRAPHY

Abdrakhmanova GR, Blough BE, Nesloney C, Navarro HA, Damaj MI and Carroll FI (2010). In vitro and in vivo characterization of a novel negative allosteric modulator of neuronal nAChRs. *Neuropharmacology*, 59(6): 511–517.

Ahmed NY, Knowles R and Dehorter N (2019). New Insights Into Cholinergic Neuron Diversity. *Frontiers in Molecular Neuroscience*, 12: 204.

Akk G, Zhou M and Auerbach A (1999). A mutational analysis of the acetylcholine receptor channel transmitter binding site. *Biophys J*, 76: 207–218.

Alburquerque EX, Pereira EF, Alkondon M and Rogers SW (2009). Mammalian Nicotinic Acetylcholine Receptors: From Structure to Function. *Physiol Rev*, 89(1): 73–120.

Alcaino C, Musgaard M, Minguez T, Mazzaferro S, Faundez M, Iturriaga-Vasquez P, Biggin PC and Bermudez I (2017). Role of the cys loop and transmembrane domain in the allosteric modulation of α4β2 nicotinic acetylcholine receptors. *J Biol Chem*, 292(2): 551-562.

AlSharari SD, Freitas K and Damaj MI (2013). Functional role of alpha7 nicotinic receptor in chronic neuropathic and inflammatory pain: studies in transgenic mice. *Biochemical Pharmacology*, 86(8): 1201–1207.

Althoff T, Hibbs RE, Banerjee S and Gouaux E (2014). X-ray structures of GluCl in apo states reveal a gating mechanism of Cys-loop receptors. *Nature*, 512: 333–337.

Amar M, Thomas P, Johnson C, Lunt GG and Wonnacott S (1993). Agonist pharmacology of the neuronal alpha-7 nicotinic receptor expressed in *Xenopus*-oocytes. *FEBS Lett*, 327: 284-288.

Armstrong CT, Mason PE, Anderson JLR and Dempsey CE (2016). Arginine side chain interactions and the role of arginine as a gating charge carrier in voltage sensitive ion channels. *Sci Reports*, 6(1).

Andreasen JT, Olsen GM, Wiborg O and Redrobe JP (2009). Antidepressant-like effects of nicotinic acetylcholine receptor antagonists, but not agonists, in the mouse forced swim and mouse tail suspension tests. *J Psychopharmacol*, 23(7): 797-804.

Aubin HJ, Bobak A, Britton JR, Oncken C, Billing CB Jr, Gong J, Williams KE and Reeves KR (2008). Varenicline versus transdermal nicotine patch for smoking cessation: Results from a randomised open-label trial. *Thorax*. 63(8):717–724.

Azam L and McIntosh JM (2009). Alpha-conotoxins as pharmacological probes of nicotinic acetylcholine receptors. *Acta Pharmacol Sin*, 30(6): 771–783.

Azam L, Papakyriakou A, Zouridakis M, Giastas P, Tzartos SJ and McIntosh JM (2015). Molecular Interaction of α-Conotoxin RgIA with the Rat α9α10 Nicotinic Acetylcholine Receptor. *Molecular Pharmacology*, 87(5): 855–864.

Bannon AW, Decker MW, Curzon P, Buckley MJ, Kim DJ, Radek RJ, Lynch JK, Wasicak JT, Lin NH, Arnold WH, Holladay MW, Williams M and Arneric SP (1998). ABT-594 [(R)-5-(2-azetidinylmethoxy)-2-chloropyridine]: a novel, orally effective antinociceptive agent acting via neuronal nicotinic acetylcholine receptors: II. In vivo characterization. *J PArmacol Exp Ther*, 285(2): 787-794.

Basak S, Gicheru Y, Rao S, Sansom MSP and Chakrapani S (2018). Cryo-EM reveals two distinct serotonin-bound conformations of full-length 5-HT3A receptor. *Nature,* 563: 270–274.

Benowitz NL (2010). Nicotine Addiction. *New England Journal of Medicine*, 362(24): 2295–2303.

Bertrand S, Weiland S, Berkovic SF, Steinlein OK and Bertrand D (1998). Properties of neuronal nicotinic acetylcholine receptor mutants from humans suffering from autosomal dominant nocturnal frontal lobe epilepsy. *Br J Pharmacol,* 125(4): 751-760.

Billen B, Spurny R, Brams M, van Elk R, Valera-Kummer S, Yakel JL, Voets T, Bertrand D, Smit AB and Ulens C (2012). Molecular actions of smoking cessation drugs at alpha 4 beta 2 nicotinic receptors defined in crystal structures of a homologous binding protein. *PNAS*, 109: 9173-9178.

Blom AEM, Rego-Campello H, Lester HA, Gallagher T and Dougherty DA (2019). Probing Binding Interactions of Cytisine Derivatives to the α4β2 Nicotinic Acetylcholine Receptor. *J Am Chem Soc*, 140(40): 15840-15849.

Blum AP, Van Arnam EB, German LA, Lester HA and Dougherty DA (2013). Binding Interactions with the Complementary Subunit of Nicotinic Receptors. *Journal of Biological Chemistry*, 288(10): 6991–6997.

Bocquet N, Nury H, Baaden M, Le Poupon C, Changeux JP, Delarue M and Corringer PJ (2009). X-ray structure of a pentameric ligand-gated ion channel in an apparently open conformation. *Nature*, 1: 457(7225).

Bodnar AL, Cortes-Burgos LA, Cook KK, Dinh DM, Groppi VE, Hajos M, Higdon NR, Hoffmann WE, Hurst RS, Myers JK, Rogers BN, Wall TM, Wolfe ML and Wong E (2005). Discovery and Structure−Activity Relationship of Quinuclidine Benzamides as Agonists of α7 Nicotinic Acetylcholine Receptors. *J Med Chem*, 48(4): 905–908.

Bordia T, Grady SR, McIntosh JM and Quik M (2007). Nigrostriatal damage preferentially decreases a subpopulation of a6b2* nAChRs in mouse, monkey and Parkinson’s disease striatum. *Mol Pharmacol*, 72: 52-61.

Bouzat C, Bren N and Sine SM (1994). Structural basis of the different gatingkinetics of fetalandadult acetylcholinereceptors. *Neuron*, 13; 1395–1402.

Bouzat C, Bartos M, Corradi J and Sine SM (2008). The interface between extracellular and transmembrane domains of homomeric Cys-loop receptors governs open-channel lifetime and rate of desensitization. *J Neurosci*, 28: 7808–7819.

Brams M, Pandya A, Kuzmin D, Van Elk R, Krijnen L, Yakel JL, Tsetlin V, Smit AB and Ulens C (2011). A Structural and Mutagenic Blueprint for Molecular Recognition of Strychnine and d-Tubocurarine by Different Cys-Loop Receptors. *PLoS Biology*, 9(3): e1001034.

Brejc K, Van Dijk WJ, Klaassen RV, Schuurmans M, Van Der Oost J, Smit AB and Sixma TK (2001). Crystal structure of an ACh-binding protein reveals the ligand-binding domain of nicotinic receptors. *Nature,* 411(6835): 269-76.

Brown RW, Collins AC, Lindstrom JM, Whiteaker P (2007). Nicotinic α5 subunit deletion locally reduces high-affinity agonist activation without altering nicotinic receptor numbers. *J Neurochem,* 103: 204–215.

Cahill K, Lindson-Hawley N, Thomas KH, Fanshawe TR and Lancaster T (2016). Nicotine receptor partial agonists for smoking cessation. *Cochrane Database of Systematic Reviews*.

Calimet N, Simoes M, Changeux JP, Karplus M, Taly A and Cecchini M (2013). A gating mechanism of pentameric ligand-gated ion channels. *PNAS*, 110: E3987–E3996.

Campos-Caro A, Sala S, Ballesta JJ, Vicente-Agullo F, Criado M and Sala F (1996). A single residue in the M2-M3 loop is a major determinant of coupling between binding and gating in neuronal nicotinic receptors. *PNAS*, 93: 6118–6123.

Cancer Research UK and Action on Smoking and Health (2017). Feeling the Heat: The Decline of Stop Smoking Services in England. Cancer Research UK website. https://www.cancerresearchuk.org/sites/default/files/la_survey_report_2017.pdf

Carpenter TS and Lightstone FC (2016). An Electrostatic Funnel in the GABA-Binding Pathway. *PLoS Comput Biol*, 4(12): e1004831.

Cecchini M and Changeux JP (2015). The nicotinic acetylcholine receptor and its prokaryotic homologues: Structure, conformational transitions & allosteric modulation. *Neuropharmacology*, 96: 137–149.

Celie PH, Van Rossum-Fikkert SE, Van Dijk WJ, Brejc K, Smit AB and Sixma TK (2004). Nicotine and carbamylcholine binding to nicotinic acetylcholine receptors as studied in AChBP crystal structures. *Neuron*, 41(6): 907–14.

Chang Y and Weiss DS (1999). Channel opening locks agonist onto the $GABA_C$ receptor. *Nat Neurosci,* 2(3): 219-225.

Changeux J-P, Kasai M, Huchet M and Meunier J-C (1970). Extraction from electric tissue of Electrophorus of a protein presenting several typical properties characteristic of the physiological receptor of acetylcholine. *Comptes Rendus Hebd Seances Acad Sci*, 270: 2864–2867.

Changeux JP (2012). The Nicotinic Acetylcholine Receptor: The Founding Father of the Pentameric Ligand-gated Ion Channel Superfamily. *Journal of Biological Chemistry*, 287(48): 40207–40215.

CHANTIX®. What are the possible side effects of CHANTIX? CHANTIX® Official Site, 3 December 2019, www.chantix.com/support-for-taking-chantix/faqs#possible-side-effects-of-chantix.

Charles HC, Lazeyras F, Krishnan KRR, Boyko O, Payne M and Moore D (1994). Brain choline in depression: in vivo detection of potential pharmacodynamic effects of antidepressant therapy using hydrogen localized spectroscopy. *Prog Neuropsychopharmacol Biol Psychiat*, 18: 1121–1127.

Charlton, A. (2004). Medicinal uses of tobacco in history. *JRSM*, 97(6): 292–296.

Charvin D, Medori R, Hauser RA and Rascol O (2018). Therapeutic strategies for Parkinson disease: beyond dopaminergic drugs. *Nat Rev Drug Discov*, 19(11): 804-822.

Chellappan SK, Xiao YX, Tueckmantel W, Kellar KJ and Kozikowski AP (2006). Synthesis and pharmacological evaluation of novel 9- and 10-substituted cytisine derivatives. Nicotinic ligands of enhanced subtype selectivity. *J Med Chem*, 49: 2673-2676.

Colombo SF, Mazzo F, Pistillo F and Gotti C (2013). Biogenesis, trafficking and up-regulation of nicotinic ACh receptors. *Biochem Pharmacol*, 15; 86(8): 1063-1073.

Colquhoun D and Sakmann B (1985). Fast events in single-channel currents activated by acetylcholine and its analogues at the frog muscle end-plate. *J Physiology*, 369(1): 501–557.

Corrigal WA, Coen KM and Adamson KL (1994). Self-administered nicotine activates the mesolimbic dopamine system through the ventral tegmental area. *Brain research*, 653(1-2): 278-284.

Corringer PJ, Le Novere N and Changeux JP (2000). Nicotinic receptors at the amino acid level. *Ann Rev Pharmacol Toxicol*, 40: 431–458.

Corringer PJ, Poitevin F, Prevost MS, Sauguet L, Delarue M and Changeux JP (2012). Structure and pharmacology of pentameric receptor channels: from bacteria to brain. *Structure*, 6; 20(6): 941-56.

Court J, Spurden D, Lloyd S, McKeith I, Ballard C, Cairns N, Kerwin R, Perry R and Perry E (2002). Neuronal Nicotinic Receptors in Dementia with Lewy Bodies and Schizophrenia. *Journal of Neurochemistry*, 73(4): 1590–1597.

Curtis MJ, Bond RA, Spina D, Ahluwalia A, Alexander SP, Giembycz M, Gilchrist A, Hoyer D, Insel PA, Izzo AA, Lawrence AJ, MacEwan DJ, Moon LDF, Wonnacott S, Weston AH and McGrath JC (2015). Experimental design and analysis and their reporting: new guidance for publication in BJP. *Br J Pharmacol*, 172(14): 3461–3471.

Dani JA and Balfour DJK (2011). *Historical and current perspective on tobacco use and nicotine addiction. Trends in Neurosciences,* 34(7), 383–392.

De Leon J and Diaz FJ (2005). A meta-analysis of worldwide studies demonstrates an association between schizophrenia and tobacco smoking behaviors. *Schizophrenia Research*, 76 (2–3): 135–157.

Del Castillo J and Katz B (1957). Interaction at endplate receptors between different choline derivatives. *Proceedings of the Royal Society of London Series B*, 146: 369–381.

Dellisanti CD, Yao Y, Stroud JC, Wang Z-Z and Chen L (2007). Crystal structure of the extracellular domain of nAChR α1 bound to α-bungarotoxin at 1.94 Å resolution. *Nature Neuroscience*, 10(8): 953–962.

Deardorff WJ, Shobassy A and Grossberg GT (2015). Safety and clinical effects of EVP-6124 in subjects with Alzheimer’s disease currently or previously receiving an acetylcholinesterase inhibitor medication. *Exp Rev Neurother*, 15(1): 7–17.

Dineley KT, Pandya AA and Yakel JL (2015). Nicotinic ACh receptors as therapeutic targets in CNS disorders. *Trends in Pharmacological Sciences*, 36(2): 96–108.

Dougherty DA (2008). Cys-loop neuroreceptors: Structure to the rescue? *Chem Rev*, 108: 1642-1653.

Du J, Lu W, Wu S, Cheng Y and Gouaux E (2015). Glycine receptor mechanism elucidated by electron cryo-microscopy. *Nature*, 526: 224–229.

Durkin P, Magrone P, Matthews S, Dallanoce C and Gallagher T (2010). Lactam Enolate-Pyridone Addition: Synthesis of 4-Halocytisines. *Synlett*, 2789-2791.

Eggert M, Winterer G, Wanischeck M, Hoda J-C, Bertrand D and Steinlein O (2015). The nicotinic acetylcholine receptor alpha 4 subunit contains a functionally relevant SNP Haplotype. *BMC Genet*, 16: 46.

Elgoyhen AB, Vetter D, Katz E, Rothlin C, Heinemann S and Boulter J (2001) α10: a determinant of nicotinic cholinergic receptor function in mammalian vestibular and cochlear mechanosensory hair cells. *PNAS*, 98: 3501-3506.

Elgoyhen AB and Katz E (2012). The efferent medial olivocochlear-hair cell synapse. *Journal of Physiology-Paris*, 106(1-2): 47–56.

Etter JF, Lukas RJ, Benowitz NL, West R and Dresler CM (2008). Cytisine for smoking cessation: A research agenda. *Drug Alcohol Depend*, 92: 3-8.

Faiman GA and Horovitz A (1996). On the choice of reference mutant states in the application of the double-mutant cycle method. *Protein Eng*, 9: 315-316.

Fitch CA, Platzer G, Okon M, Garcia-Moreno EB and McIntosh LP (2015). Arginine: Its pKavalue revisited. *Protein Science*, 24(5): 752–761.

Fowler CD, Lu Q, Johnson PM, Marks MJ and Kenny PJ (2011). Habenular α5 nicotinic receptor subunit signalling controls nicotine intake. *Nature*, 471: 597–601.

Freedman R, Olincy A, Buchanan RW, Harris JG, Gold JM, Johnson L, Allensworth D, Guzman-Bonilla A, Clement B, Ball MP, Kutnick J, Pender V, Martin LF, Stevens KE, Wagner BD, Zerbe GO, Scoti F and Kem WR (2008). Initial Phase 2 Trial of a Nicotinic Agonist in Schizophrenia. *American Journal of Psychiatry*, 165(8): 1040–1047.

Freitas K, Carroll FI and Damaj MI (2013). The antinociceptive effects of nicotinic receptors α7-positive allosteric modulators in murine acute and tonic pain models. *J Pharmacol Exp Ther*, 344(1): 264–275.

Fryer J and Lukas RJ (1999). Noncompetitive Functional Inhibition at Diverse, Human Nicotinic Acetylcholine Receptor Subtypes by Bupropion, Phencyclidine, and Ibogaine. *J Pharmacol Exp Ther*, 288(1): 88-92.

Fucile S (2004). Ca2+ permeability of nicotinic acetylcholine receptors. *Cell Calcium*, 35(1): 1-8.

Fukuyama K, Fukuzawa M, Shiroyama T and Okada M (2020). Pathogenesis and pathophysiology of autosomal dominant sleep-related hypermotor epilepsy with S284L-mutant α4 subunit of nicotinic ACh receptor. *British Journal of Pharmacology*, 14974.

Galzi JL, Revah F, Black D, Goeldner M, Hirth C and Changeaux JP (1990). Identification of a novel amino acid α-tyrosine 93 within the cholinergic ligand-binding sites of the acetylcholine receptor by photolabeling. Additional evidence for a three-loop model of the cholinergic ligand-binding site. *J Bio Chem,* 265: 10430–10437.

Gao J, Adam BL and Terry AV (2014). Evaluation of nicotine and cotinine analogs as potential neuroprotective agents for Alzheimer's disease. *Bioorganic & Medicinal Chemistry Letters*, 24(6): 1472–1478.

Gately I (2001). *Tobacco: a cultural history of how an exotic plant seduced civilization.* London, England, UK: Simon & Schuster.

Gault J, Robinson M, Berger R, Drebing C, Logel J, Hopkins J, Moore T, Jacobs S, Meriwether J, Choi MJ, Kim EJ, Walton K, Buiting K, Davis A, Breese C, Freedman R and

Leonard S (1998). Genomic Organization and Partial Duplication of the Human α7 Neuronal Nicotinic Acetylcholine Receptor Gene (CHRNA7). *Genomics*, 52(2): 173–185.

Gay EA and Yakel JL (2007). Gating of nicotinic ACh receptors; new insights into structural transitions triggered by agonist binding that induce channel opening. *J Physiol*, 584(3): 727–733.

Gay EA, Giniatullin R, Skorinkin A and Yakel JL (2008). Aromatic residues at position 55 of rat α7 nicotinic acetylcholine receptors are critical for maintaining rapid desensitization. *J Physiol*, 586: 1105–1115.

Gee KW, Olincy A, Kanner R, Johnson L, Hogenkamp D, Harris J, Tran M, Edmonds SA, Sauer W, Yoshimura R, Johnstone T and Freedman R (2017). First in human trial of a type I positive allosteric modulator of alpha7-nicotinic acetylcholine receptors: pharmacokinetics, safety, and evidence for neurocognitive effect of AVL-3288. *J Psychopharmacol*, 31: 434–441.

George TP, Sacco KA, Vessicchio JC, Weinberger AH and Shytle RD (2008). Nicotinic Antagonist Augmentation of Selective Serotonin Reuptake Inhibitor-Refractory Major Depressive Disorder. *Journal of Clinical Psychopharmacology*, 28(3): 340–344.

Gharpure A, Teng J, Zhuang Y, Noviello CM, Walsh RM, Cabuco R, … Hibbs RE (2019). Agonist Selectivity and Ion Permeation in the α3β4 Ganglionic Nicotinic Receptor. *Neuron*, 104(3): 501-511.

Giacobini E (2004). Cholinesterase inhibitors: new roles and therapeutic alternatives. *Pharmacological Research*, 50(4): 433–440.

Gielen M and Corringer PJ (2018). The dual-gate model for pentameric ligand-gated ion channels activation and desensitization. *The Journal of Physiology*, 596(10): 1873–1902.

Gill JK, Savolainen M, Young GT, Zwart R, Sher E and Millar NS (2011). Agonist activation of α7 nicotinic acetylcholine receptors via an allosteric transmembrane site. *PNAS*, 108(14): 5867–5872.

Giniatullin R, Nistri A and Yakel J (2005). Desensitization of nicotinic ACh receptors: shaping cholinergic signaling. *Trends in Neurosciences*, 28(7), 371–378.

Giraudat J, Dennis M, Heidmann T, Chang JY and Changeux JP (1986). Structure of the high-affinity binding site for noncompetitive blockers of the acetylcholine receptor: serine-262 of the delta subunit is labeled by [^{3}H]chlorpromazine. *PNAS*, 83: 2719–2723.

Gleitsman KR, Shanata JAP, Frazier, SJ, Lester HA and Dougherty DA (2009). Long-Range Coupling in an Allosteric Receptor Revealed by Mutant Cycle Analysis. *Biophys J*, 96(8): 3168–3178.

Gonzales D, Rennard SI, Nides M, Oncken C, Azoulay S, Billing CB, Watsky EJ, Gong J, Williams KE and Reeves KR (2006). Varenicline, an α4β2 Nicotinic Acetylcholine Receptor Partial Agonist, vs Sustained-Release Bupropion and Placebo for Smoking CessationA Randomized Controlled Trial. *JAMA*, 296(1): 47.

Gotti C, Zoli M and Clementi F (2006a). Brain nicotinic acetylcholine receptors: native subtypes and their relevance. *Trends Pharmacol Sci*, 27: 482-491.

Gotti C, Moretti M, Bohr I, Ziabreva I, Vailati S, Longhi R, Riganti L, Gaimarri A, McKeith IG, Perry RH, Aarsland D, Larsen JP, Sher E, Beattie R, Clementi F and Court JA (2006b). Selective nicotinic acetylcholine receptor subunit deficits identified in Alzheimer's disease, Parkinson's disease and dementia with Lewy bodies by immunoprecipitation. *Neurobiol Dis*, 23: 481–9

Gotti C, Clementi F, Fornari A, Gaimarri A, Guiducci S, Manfredi I, Moretti M, Pedrazzi P, Pucci L and Zoli M (2009). Structural and functional diversity of native brain neuronal nicotinic receptors. *Biochem Pharmacol*, 78(7): 703-11

Grady SR, Salminen O, Laverty DC, Whiteaker P, McIntosh JM, Collins AC and Marks MJ (2007). The subtypes of nicotinic acetylcholine receptors on dopaminergic terminals of mouse striatum. *Biochem Pharmacol*, 74: 1235–1246

Grassi F, Palma E, Tonini R, Amici M, Ballivet M and Eusebi F (2003). Amyloid beta(1-42) peptide alters the gating of human and mouse alpha-bungarotoxin-sensitive nicotinic receptors. *J Physiol,* 547(1): 147-157.

Gray D and Gallagher T (2006). A Flexible Strategy for Tri- and Tetracyclic Lupin Alkaloids. Synthesis of (+)-Cytisine, (±)-Anagyrine and (±)-Thermopsine. *Angew Chem Int Ed Engl*, 45: 2419-2423.

Grønlien JH, Hakerud M, Ween H, Thorin-Hagene K, Briggs CA, Gopalakrishnan M and Malysz J (2007). Distinct Profiles of α7 nAChR Positive Allosteric Modulation Revealed by Structurally Diverse Chemotypes. *Molecular Pharmacology*, 72(3): 715–724.

Grosman C, Zhou M and Auerbach A (2000). Mapping the conformational wave of acetylcholine receptor channel gating. *Nature*, 403: 773–776.

Guan ZZ, Zhang X, Ravid R and Nordberg A (2000). Decreased protein levels of nicotinic receptor subunits in the hippocampus and temporal cortex of patients with Alzheimer´s disease. *J Neurochem*, 74(1): 237-43.

Haddad F, Sawalha M, Khawaja Y, Najjar A and Karaman R (2017). Dopamine and Levodopa prodrugs for treatment of Parkinson´s disease. *Molecules*, 23(1): 25.

Hales TG, Tang H, Bollan KA, Johnson SJ, King DP, McDonald NA, Cheng A and Connolly C (2005). The epilepsy mutation, γ2(R43Q) disrupts a highly conserved inter-subunit contact site, perturbing the biogenesis of $GABA_A$ receptors. *Mol Cell Neurosci*, 29: 120 – 127.

Hales TG, Dunlop JI, Deeb TZ, Carland JE, Kelley SP, Lambert JJ and Peters JA (2006). Common determinants of single channel conductance within the large cytoplasmic loop of 5-hydroxytryptamine type 3 and alpha4- beta2 nicotinic acetylcholine receptors. *J Biol Chem*, 281: 8062–8071.

Hamann SR and Martin WR (1992). Opioid and nicotinic analgesic and hyperalgesic loci in the rat brain stem. *J Pharma Exp Therap*, 261: 707–715.

Hamouda AK, Jayakar SS, Chiara DC and Cohen JB (2013). Photoaffinity Labeling of Nicotinic Receptors: Diversity of Drug Binding Sites! *Journal of Molecular Neuroscience*, 53(3): 480–486.

Hansen SB, SulzenbACher G, Huxford T, Marchot P, Taylor P, Bourne Y (2005). Structures of Aplysia AChBP complexes with nicotinic agonists and antagonists reveal distinctive binding interfaces and conformations. *EMBO Journal*, 24: 3635–3646.

Harms MJ, Schlessman JL, Sue GR and Garcia-Moreno EB (2011). Arginine residues at internal positions in a protein are always charged. *PNAS*, 108(47): 18954–18959.

Harpsøe K, Ahring PK, Christensen JK, Jensen ML, Peters D and Balle T (2011). Unravelling the high- and low-sensitivity agonist responses of nicotinic acetylcholine receptors. *J Neurosci*, 31: 10759–10766.

Harvey SC, Maddox FN and Luetje CW (1996). Multiple Determinants of Dihydro-β-Erythroidine Sensitivity on Rat Neuronal Nicotinic Receptor α Subunits. *J Neurochemistry*, 67(5): 1953–1959.

Hassaine G, Deluz C, Grasso L, Wyss R, Tol MB, Hovius R, Graff A, Stahlberg H, Tomizaki T, Desmyter A, Moreau C, Li X-D, Poitevin F, Vogel H and Nury H (2014). X-ray structure of the mouse serotonin 5-HT3 receptor. *Nature,* 21; 512(7514): 276-81.

Henault CM, Sun J, Therien JP, da Costa C, Carswell CL, Labriola JM, Juranka PF and Baenziger JE (2015). The role of the M4 lipid-sensor in the folding, trafficking and allosteric modulation of nicotinic acetylcholine receptors. *Neuropharmacol,* 96(Pt B): 157-68.

Hibbs RE, Johnson DA, Shi J and Taylor P (2006). Structural dynamics of the acetylcholine binding protein: hydrodynamic and fluorescence anisotropy decay analyses. *J Mol Neurosci*, 30: 73–74.

Hibbs RE and Gouaux E (2011). Principles of activation and permeation in an anionselective Cys-loop receptor. *Nature*, 474: 54–60.

Hidalgo P and MacKinnon R (1995) Revealing the architecture of a K^+ channel pore through mutant cycles with a peptide inhibitor. *Science,* 14; 268(5208): 307-10.

Hilf RJ and Dutzler R (2008). X-ray structure of a prokaryotic pentameric ligand-gated ion channel. *Nature,* 20; 452(7185): 375-9.

Hilf RJ and Dutzler R (2009). A prokaryotic perspective on pentameric ligand-gated ion channel structure. *Curr Opin Struct Biol*, 19(4): 418-24.

Hone AJ and McIntosh JM (2017). Nicotinic acetylcholine receptors in neuropathic and inflammatory pain. *FEBS Letters*, 592(7): 1045–1062.

Hone AJ, Servent D, McIntosh JM (2018). α9-containing nicotinic acetylcholine receptors and the modulation of pain. *Br J Pharmacol*, 175: 1915–1927.

Hsiao B, Dweck D and Luetje CW (2001). Subunit-dependent modulation of neuronal nicotinic receptors by zinc. *J Neurosci*, 21: 1848 –1856.

Huang X, Chen H, Michelsen K, Schneider S and Shaffer PL (2015). Crystal structure of human glycine receptor-α3 bound to antagonist strychnine. *Nature*, 526: 277–280.

Hucho F (1986). The nicotinic acetylcholine receptor and its ion channel. *European Journal of Biochemistry*, 158(2): 211–225.

Huganir RL and Greengard P (1990). Regulation of neurotransmitter receptor desensitization by protein phosphorylation. *Neuron*, 5: 555–567.

Hurst R, Rollema H and Bertrand D (2013). Nicotinic acetylcholine receptors: From basic science to therapeutics. *Pharmacology & Therapeutics*, 137(1), 22–54.

Janowsky DS, El-YousefMK, Davis JM, Sekerke HJ (1972). A cholinergic-adrenergic hypothesis ofmania and depression. *Lancet*, 2: 632–635.

Jha A, Cadugan DJ, Purohit P, Auerbach A (2007). Acetylcholine receptor gating at extracellular transmembrane domain interface: the Cys-loop and M2–M3 linker. *J Gen Physiol*, 130: 547–558.

Jones MV and Westbrook GL (1996). The impact of receptor desensitization on fast synaptic transmission. *Trends in Neurosciences*, 19(3): 96–101.

Jonge WJ and Ulloa L (2007). The alpha7 nicotinic acetylcholine receptor as a pharmacological target for inflammation. *Br J Pharmacol*, 151(7): 915-929.

Kao PN, Dwork AJ, Kaldany RR, Silver ML, Wideman J, Stein S and Karlin A (1984) Identification of the α -subunit half-cystine specifically labeled by an affinity reagent for the acetylcholine receptor binding site. *J Biol Chem*, 259: 11662–11665.

Katz B and Thesleff S (1957). A study of the “desensitization” produced by acetylcholine at the motor end-plate. *J Physiology*, 138(1): 63–80.

Kem WR, Olincy A, Johnson L, Harris J, Wagner BD, Buchanan RW, … Freedman R (2018). Pharmacokinetic Limitations on Effects of an Alpha7-Nicotinic Receptor Agonist in Schizophrenia: Randomized Trial with an Extended-Release Formulation. *Neuropsychopharmacology*, 43(3): 583–589.

Kesters D, Thompson AJ, Brams M, van Elk R, Spurny R, Geitmann M, … Ulens C (2012). Structural basis of ligand recognition in 5-HT3 receptors. *EMBO Reports*, 14(1): 49–56.

Khatri A, Sedelnikova A and Weiss DS (2009). Structural rearrangements in loop F of the GABA receptor signal ligand binding, not channel activation. *Biophys J*, 96: 45–55.

Khatri A and Weiss DS (2010). The role of loop F in the activation of the GABA receptor. *J Physiol*, 588: 59–66.

Khiroug SS, Harkness PC, Lamb PW, Sudweeks SN, Khiroug L, Millar NS and Yakel JL (2002). Rat nicotinic ACh receptor alpha7 and beta2 subunits co-assemble to form functional heteromeric nicotinic receptor channels. *J Physiol*, 540: 425–434.

Kim SY, Choi SH, Rollema H, Schwam EM, McRae T, Dubrava S and Jacobsen J (2014). Phase II Crossover Trial of Varenicline in Mild-to-Moderate Alzheimer's Disease. *Dementia and Geriatric Cognitive Disorders*, 37(3-4): 232–245.

Kozikowski AP, Chellappan SK, Xiao YX, Bajjuri KM, Yuan HB, Kellar KJ and Petukhov PA (2007). Chemical medicine: novel 10-substituted cytisine derivatives with increased selectivity for alpha 4 beta 2 nicotinic acetylcholine receptors. *Chem Med Chem*, 2: 1157-1161.

Krivov GG, Shapovalov MV and Dunbrack RL (2009). *Proteins Struct Funct Bioinf*: 77-778.

Kumari V and Postma P (2005). Nicotine use in schizophrenia: the self medication hypotheses. *Neurosci Biobehav Rev*, 29(6): 1021–1034.

Kuryatov A, Berrettini W and Lindstrom J (2011). Acetylcholine Receptor (AChR) α5 Subunit Variant Associated with Risk for Nicotine Dependence and Lung Cancer Reduces $(\alpha 4\beta 2)_2\alpha 5$ AChR Function. *Mol Pharmacol*, 79(1): 119–125.

Kyte J and Doolittle RF (1982). A simple method for displaying the hydropathic character of a protein. *J Mol Biol*, 157: 105-132.

Langley JN (1905). On the reaction of cells and of nerve-endings to certain poisons, chiefly as regards the reaction of striated muscle to nicotine and to curari. *J Physiol*, 33: 374–413.

Lape R, Colquhoun D and Sivilotti LG (2008). On the nature of partial agonism in the nicotinic receptor superfamily. *Nature*, 454: 722–727.

Leaviss J, Sullivan W, Ren S, Everson-Hock E, Stevenson M, Stevens J, Strong M and Cantrell A (2014). What is the clinical effectiveness and cost effectiveness of cytisine compared with varenicline for smoking cessation: a systematic review and economic evaluation? *Health Technol Assess*, 18(33).

Lee C-H, Zhu C, Malysz J, Campbell T, Shaughnessy T, Honore P, … Gopalakrishnan M (2011). α4β2 neuronal nicotinic receptor positive allosteric modulation: An approach for improving the therapeutic index of α4β2 nAChR agonists in pain. *Biochemical Pharmacology*, 82(8): 959–966.

Lee WY and Sine SM (2005). Principal pathway coupling agonist bindingto channel gating in nicotinic receptors. *Nature*, 438: 243–247.

Lee WY, Free C and Sine SM (2009). Binding to gating transduction in nicotinic receptors: Cys-loop energetically couples to pre-M1 and M2-M3 regions. *J Neurosci*, 29(10): 3189–3199.

Leiser SC, Bowlby MR, Comery TA and Dunlop J (2009). A cog in cognition: How the α7 nicotinic acetylcholine receptor is geared towards improving cognitive deficits. *Pharmacology & Therapeutics*, 122(3): 302–311.

Lester HA and Dougherty DA (2019). Nicotine Bound to Its Receptors: New Structures for a Vexing Pathopharmacological Problem. *Neuron*, 104(3): 431–432.

Levin ED (2013). Complex relationships of nicotinic receptor actions and cognitive functions. *Biochemical pharmacology*, 86: 1145–1152.

Li S-X, Huang S, Bren N, Noridomi K, Dellisanti CD, Sine SM and Chen L (2011). Ligand-binding domain of an α7-nicotinic receptor chimera and its complex with agonist. *Nature Neuroscience*, 14(10): 1253–1259.

Lips KS, Pfeil U and Kummer W (2002). Coexpression ofα9and α10 nicotinic acetylcholine receptors in rat dorsal root ganglion neurons. *Neuroscience*, 115(1): 1–5.

Liu L, Zhao-Shea R, McIntosh JM, Gardner PD and Tapper AR. (2012) Nicotine persistently activates ventral tegmental area dopaminergic neurons via nicotinic acetylcholine receptors containing α4 and α6 subunits. *Mol Pharmacol*, 81: 541–548.

Liu Q, Huang Y, Xue F, Simard A, DeChon J, Li G, Zhang J, Lucero L, Wang M, Sierks M, Hu G, Chang Y, Lukas RJ, Wu J (2009). A novel nicotinic acetylcholine receptor subtype in basal forebrain cholinergic neurons with high sensitivity to amyloid peptides. *J Neurosci*, 29:918–929.

Liu Q, Huang Y, Shen J, Steffensen S and Wu J (2012). Functional α7β2 nicotinic acetylcholine receptors expressed in hippocampal interneurons exhibit high sensitivity to pathological level of amyloid β peptides. *BMCNeurosci*, 13(1): 155.

Lohmann T, Torrao A, Britto L, Lindstrom J and Hamassaki-britto DE (2000). A comparative non-radioactive in situ hybridization and immunohistochemical study of the distribution of a7 and a8 subunits of the nicotinic acetylcholine receptors in visual areas of the chick brain. *Brain Res,* 852: 463-469.

Lombardo S and Maskos U (2015). Role of the nicotinic acetylcholine receptor in Alzheimer's disease pathology and treatment. *Neuropharmacology*, 96: 255–262.

Lucero LM, Weltzin MM, Eaton JB, Cooper JF, Lindstrom JM, Lukas RJ, Whiteaker P (2016). Differential α4(+)/(-)β2 Agonist-binding Site Contributions to α4β2 Nicotinic Acetylcholine Receptor Function within and between Isoforms. J Biol Chem, 291(5): 2444–2459.

Lummis SCR, Thompson AJ, Bencherif M and Lester HA (2011). Varenicline Is a Potent Agonist of the Human 5-Hydroxytryptamine3 Receptor. *J Pharmacol Exp Therap*, 339(1): 125–131.

Lynagh T, Komnatnyy VV and Pless SA (2017). Unique Contributions of an Arginine Side Chain to Ligand Recognition in a Glutamate-gated Chloride Channel. *J Biol Chem*, 292(9): 3940–3946.

Maldifassi MC, Martín-Sánchez C, Atienza G, Cedillo JL, Arnalich F, Bordas A, … Montiel C (2018). Interaction of the α7-nicotinic subunit with its human-specific duplicated dupα7 isoform in mammalian cells: Relevance in human inflammatory responses. *J Biol Chem,* jbc.RA118.003443.

Mantione E, Micheloni S, Alcaino C, New K, Mazzaferro S and Berrnudez Isabel (2012) Allosteric modulators of a4p2 nicotinic acetylcholine receptors: A new direction for antidepressant drug discovery. *Future Medicinal Chemistry*, 4: 2217-2230.

Marcovich I, Moglie M, Carpaneto Freixas, Trigila AP, Franchini LF, Plazas PV, Lipovsek M, Elgoyhen AB (2019). Distinct evolutionary trajectories of neuronal and hair 3 cell nicotinic acetylcholine receptors. Molecular Biology and Evolution, msz290.

Marotta CB, Rreza I, Lester HA and Dougherty DA (2014). Selective Ligand Behaviors Provide New Insights into Agonist Activation of Nicotinic Acetylcholine Receptors. *ACS Chemical Biology*, 9(5): 1153–1159.

Marotta CB, Lester HA and Dougherty DA (2015). An Unaltered Orthosteric Site and a Network of Long-Range Allosteric Interactions for PNU-120596 in α7 Nicotinic Acetylcholine Receptors. *Chemistry & Biology*, 22(8): 1063–1073.

Martinowich K, Schloesser RJ, Lu Y, Jimenez DV, Paredes D, Greene JS, … Lu B (2012). Roles of p75NTR, Long-Term Depression, and Cholinergic Transmission in Anxiety and Acute Stress Coping. *Biological Psychiatry*, 71(1): 75–83.

Maskos U, Molles BE, Pons S, Besson M, Guiard BP, Guilloux JP, Evrard A, Cazala P, Cormier A, Mameli-Engval M, Dufour N, Cloez-Tayarani I, Bemelmans A-P, Mallet J, Gardier AM, David V, Faure P, Granon S and Changeux JP (2005). Nicotine reinforcement and cognition restored by targeted expression of nicotinic receptors. *Nature*, 436: 103-107.

Mazzaferro S, Benallegue N, Carbone AL, Gasparri F, Vijayan R, Biggin PC, Moroni M and Bermudez I (2011). Additional acetylcholine (ACh) binding site at alpha4/alpha4 interface of (α4β2)2α4 nicotinic receptor influences agonist sensitivity. *J Biol Chem*, 286: 31043–31054.

Mazzaferro S, Gasparri F, New K, Alcaino C, Faundez M, Iturriaga Vasquez P, Vijayan R, Biggin PC and Bermudez I (2014). Non-equivalent Ligand Selectivity of Agonist Sites in $(\alpha4\beta2)_2\alpha4$ Nicotinic Acetylcholine Receptors. A key determinant of agonist efficacy. *J Biol Chem*, 289: 21795-21806.

Mazzaferro S, Bermudez I and Sine SN (2017). α4β2 nicotinic acetylcholine receptors: relationships between subunit stoichiometry and function at the single channel level. *J Biol Chem*, 292: 2729-40

McCallum SE, Cowe MA, Lewis SW and Glick SD (2012). a3b4 nicotinic acetylcholine receptors in the medial habenula modulate the mesolimbic dopaminergic response to acute nicotine in vivo. *Neuropharmacology,* 63: 434–440.

McClure JB, Swan GE, Jack L, Catz SL, Zbikowski SM, McAfee TA, Deprey M, Richards J, and Javitz H (2009) Mood, side-effects and smoking outcomes among persons with and without probable lifetime depression taking varenicline. *J Gen Intern Med*, 24: 563–569.

McCormack TJ, Melis C, Colon J, Gay EA, Mike A, Karoly R, Lamb PW, Molteni C and Yakel J (2010). Rapid desensitization of the rat α7 nAChR is facilitated by the presence of a proline residue in the outer β-sheet. *J Physiol*, 588: 4415-4429.

McLaughlin JT, Fu J, Sproul AD and Rosenberg RL (2006). Role of the outer beta-sheet in divalent cation modulation of α7 nicotinic receptors. *Mol Pharmacol*, 70: 16–22.

McLaughlin KA (2011). The Public Health Impact of Major Depression: A Call for Interdisciplinary Prevention Efforts. Prev Sci, 12(4), 361–371.

McWilliam H, Li WZ, Uludag M, Squizzato S, Park YM, Buso N, Cowley AP and Lopez R (2013). Analysis Tool Web Services from the EMBL-EBI. *Nucleic Acids Res*: 41-597.

Mehta D, Jackson R, Paul G, Shi J and Sabbagh M (2017). Why do trials for Alzheimer's disease drugs keep failing? A discontinued drug perspective for 2010-2015. *Expert Opinion on Investigational Drugs*, 26(6): 735–739.

Mexal S, Berger R, Logel J, Ross RG, Freedman R and Leonard S (2010). Differential regulation of alpha7 nicotinic receptor gene (CHRNA7) expression in schizophrenic smokers. *J Mol Neurosci*, 40(1–2): 185–195.

Medicines and Healthcare products Regulatory Agency (MHRA) (2007). Varenicline: possible effects on driving; psychiatric illness. *Drug Safety Update*, 1:12.

Meltzer RH, Thompson E, Soman KV, Song X-Z, Ebalunode JO, Wensel TG, … Pedersen SE (2006). Electrostatic Steering at Acetylcholine Binding Sites. Biophysical *Journal.* 91(4): 1302–1314.

Mihalak KB, Carroll FI and Luetje CW (2006). Varenicline is a partial agonist at alpha 4 beta 2 and a full agonist at alpha 7 neuronal nicotinic receptors. *Mol Pharmacol*, 70: 801-805.

Millar NS and Gotti C (2009). Diversity of vertebrate nicotinic acetylcholine receptors. *Neuropharmacology* 56(1): 237-46.

Miller PS and Aricescu AR (2014). Crystal structure of a human GABAA receptor. *Nature,* 512: 270–275.

Mineur YS, Mose TN, Blakeman S and Picciotto MR (2018). Hippocampal α7 nicotinic ACh receptors contribute to modulation of depression-like behaviour in C57BL/6J mice. *Br J Pharmacol,* 175(11): 1903–1914.

Mishina M, Tobimatsu T, Imoto K, Tanaka K, Fujita Y, Fakuda K, … Numa S (1985). Location of functional regions of acetylcholine receptor α-subunit by site directed mutagenesis. *Nature*, 313: 364–369.

Miura W, Hirano K and Miura M (2017). Iridium-Catalyzed Site-Selective C-H Borylation of 2-Pyridones. *Synthesis*, 49: 4745-4752.

Miwa JM, Freedman R and Lester HA (2011). Neural Systems Governed by Nicotinic Acetylcholine Receptors: Emerging Hypotheses. *Neuron*, 70: 20-33.

Miyajima T, Kumada T, Saito K and Fujii T (2013). Autism in siblings with autosomal dominant nocturnal frontal lobe epilepsy. *Brain & development*, 35: 155-157.

Miyazawa A, Fujiyoshi Y and Unwin N (2003). Structure and gating mechanism of the acetylcholine receptor pore. *Nature*, 423(6943): 949–955.

Mohamed TS, Jayakar SS and Hamouda AK (2015). Orthosteric and Allosteric Ligands of Nicotinic Acetylcholine Receptors for Smoking Cessation. Frontiers in Molecular *Neuroscience*, 8: 71.

Monod J, Wyman J and Changeux JP (1965). On the Nature of Allosteric Transitions: A Plausible Model. *J Mol Biol*, 12: 88–118.

Moore TJ, Furberg CD, Glenmullen J, Maltsberger JT and Singh S (2011) Suicidal behavior and depression in smoking cessation treatments. *PLoS ONE*, 6(11): e27016.

Morales-Perez CL, Noviello CM and Hibbs RE (2016). X-ray structure of the human alpha 4 beta 2 nicotinic receptor. *Nature*, 538: 411-415.

Morens DM, Grandinetti A, Reed D, White LR and Ross GW (1995). Cigarette smoking and protection from Parkinson's disease: false association or etiologic clue? *Neurology*, 45: 1041–1051.

Moretti M, Zoli M, George AA, Lukas RJ, Pistillo F, Maskos U, Whiteaker P and Gotti C (2014). The Novel α7β2-nicotinic Acetylcholine Receptor Subtype is expressed in Mouse and Human Basal Forebrain: Biochemical and Pharmacological Characterisation. *Mol Pharmacol*, 86; 306–317.

Moretti M, Fasoli F, Gotti C and Marks MJ (2018). Reduced α4 subunit expression in α4+− and α4+− /β2+− nicotinic acetylcholine receptors alters α4β2 subtype up-regulation following chronic nicotine treatment. *Br J Pharmacol*, 175(11), 1944–1956.

Moroni M, Zwart R, Sher E, Cassels BK and Bermudez I (2006). α4β2 nicotinic receptors with high and low acetylcholine sensitivity: pharmacology, stoichiometry, and sensitivity to long-term exposure to nicotine. *Mol Pharmacol*, 70(2): 755-768.

Moroni M, Vijayan R, Carbone A, Zwart R, Biggin P and Bermudez I (2008). Non-agonist-Binding Subunit Interfaces Confer Distinct Functional Signatures to the Alternate Stoichiometries of the α4β2 nicotinic receptor: An α4-α4 interface is required for Zinc potentiation. *J Neurosci*, 28(27): 6884-6894

Morris GM, Huey R, Lindstrom W, Sanner MF, Belew RK, Goodsell DS and Olson AJ (2009). Autodock4 and AutoDockTools4: automated docking with selective receptor flexiblity. *J Computational Chemistry*, 16: 2785-91.

Mukhtasimova N, Free C and Sine SM (2005). Initial coupling of binding to gating mediated by conserved residues in the muscle nicotinic receptor. *J Gen Physiol*, 126: 23- 39.

Mukhtasimova N, Lee WY, Wang HL and Sine SM (2009). Detection and trapping of intermediate states priming nicotinic receptor channel opening. *Nature*, 459: 451–454.

Mukhtasimova N and Sine SM (2013). Nicotinic receptor transduction zone: invariant arginine couples to multiple electron-rich residues. *Biophys J*, 104: 355–367.

Nayak TK and Auerbach A (2017). Cyclic activation of endplate acetylcholine receptors. *PNAS*, 114(45): 11914–11919.

Nelson ME, Kuryatov A, Choi CH, Zhou Y and Lindstrom J (2003). Alternate stoichiometries of α4β2 nicotinic acetylcholine receptors. *Mol Pharmacol*, 63: 332-341.

Nemecz A, Prevost MS, Menny A and Corringer PJ (2016). Emerging molecular mechanisms of signal transduction in pentameric ligand-gated ion channels. *Neuron*, 90: 452–470.

Oliveira ASF, Shoemark DK, Campello HR, Gallagher T, Sessions RB and Mulholland AJ (2019). Identification of the initial steps in signal transduction in the α4β2 nicotinic receptor: insights from equilibrium and nonequilibrium simulations. *Structure*, 27: 1171-1183.

Pandya A and Yakel JL (2013). Effects of neuronal nicotinic acetylcholine receptor allosteric modulators in animal behavior studies. *Biochem Pharmacol*, 86(8): 1054–1062.

Papke RL, Bagdas D, Kulkarni AR, Gould T, AlSharari SD, Thakur GA and Damaj MI (2015). The analgesic-like properties of the alpha7 nAChR silent agonist NS6740 is associated with non-conducting conformations of the receptor. *Neuropharmacology*, 91: 34-42.

Pettit DL, Shao Z and Yakel JL (2001). beta-Amyloid(1-42) peptide directly modulates nicotinic receptors in the rat hippocampal slice. *J Neurosci*, 1; 21(1): RC120.

Philip NS, Carpenter LL, Tyrka AR and Price LH (2012). The Nicotinic Acetylcholine Receptor as a Target for Antidepressant Drug Development. The *Scientific World Journal*, 2012: 104105.

Picciotto MR, Zoli M, Rimondini R, Lena C, Marubio LM, Pich EM, Fuxe K and Changeux JP (1998). Acetylcholine receptors containing the beta2 subunit are involved in the reinforcing properties of nicotine. *Nature*, 391: 173–177.

Picciotto MR, Brunzell DH and Caldarone BJ (2002). *Effect of nicotine and nicotinic receptors on anxiety and depression. Neuroreport,* 13(9): 1097–1106.

Picciotto MR and Kenny PJ (2020). Mechanisms of Nicotine Addiction. *Cold Spring Harbor Perspectives in Medicine*, a039610.

Pless SA and Ahern CA (2013). Unnatural Amino Acids as Probes of Ligand-Receptor Interactions and Their Conformational Consequences. *Annual Review of Pharmacology and Toxicology*, 53(1): 211–229.

Pless SA and Lynagh T (2014). Principles of agonist recognition in Cys-loop receptors. *Frontiers in Physiology*, 5: 160.

Pless SA and Lynch JW (2009). Ligand-specific conformational changes in the alpha1 glycine receptor ligand-binding domain. *J Biol Chem*, 284: 15847–15856.

Plested AJR (2014). Don’t Flip Out: AChRs are Primed to Catch and Hold Your Attention. *Biophysical Journal*, 107(1), 8–9.

Pons S, Fattore L, Cossu G, Tolu S, Porcu E, McIntosh JM, … Fratta W (2008). Crucial Role of α4 and α6 Nicotinic Acetylcholine Receptor Subunits from Ventral Tegmental Area in Systemic Nicotine Self-Administration. *Journal of Neuroscience*, 28(47): 12318–12327.

Prevost MS, Sauguet L, Nury H, Van Renterghem C, Huon C, Poitevin F, Baaden M, Delarue M and Corringer PJ (2012). A locally closed conformation of a bacterial pentameric proton-gated ion channel. *Nat Struct Mol Biol*, 19: 642–649.

Provini F, Plazzi G, Montagna P and Lugaresi E (2000). The wide clinical spectrum of nocturnal frontal lobe epilepsy. *Sleep Med Rev*, 4: 375-386.

Purohit P, Bruhova I, Gupta S and Auerbach A (2014). Catch-and-Hold Activation of Muscle Acetylcholine Receptors Having Transmitter Binding Site Mutations. *Biophysical Journal*, 107(1): 88–99.

Puskar NL, Xiu X, Lester HA and Dougherty DA (2011). Two neuronal nicotinic acetylcholine receptors, alpha4beta4 and alpha7, show differential agonist binding modes. *J Biol Chem*, 286: 14618–14627.

Puskar NL, Lester HA and Dougherty DA (2012). Probing the effects of residues located outside the agonist binding site on drug-receptor selectivity in the nicotinic receptor. *ACS Chem Biol*, 7(5): 841–846.

Qian C, Li T, Shen TY, Libertine-Garahan L, Eckman J, Biftu T and Ip S (1993). Epibatidine is a nicotinic analgesic. *European Journal of Pharmacology*, 250(3): R13–R14.

Quik M, O'Leary K and Tanner CM (2008). Nicotine and Parkinson's disease: implications for therapy. *Mov Disord*, 23(12): 1641–1652.

Quik M and Wonnacott S (2011). α6β2* and α4β2* nicotinic acetylcholine receptors as drug targets for parkinson’s disease. *Pharmacol Rev*, 63(4): 938–966.

Rayes D, De Rosa MJ, Sine SM and Bouzat C (2009). Number and locations of agonist binding sites required to activate homomeric cys-loop receptors. *J Neurosci*, 29(18): 6022–6032.

Rego-Campello H, Del Villar S, Honraedt A, Minguez T, Oliveira ASF, Ranaghan KE, Gallagher T (2018). Unlocking Nicotinic Selectivity via Direct C–H Functionalization of (−)-Cytisine. *Chem*, 4(7): 1710–1725.

Revah F, Bertrand D, Galzi JL, Devillers-Thiéry A, Mulle C, Hussy N, Bertrand S, Ballivet M and Changeux JP (1991). Mutations in the channel domain alter desensitization of a neuronal nicotinic receptor. *Nature*, 31; 353(6347): 846-9.

Ritz B and Rhodes SL (2010). After half a century of research on smoking and PD, where do we go now? *Neurology*, 74(11): 870–871.

Rowbotham MC, Duan RW, Thomas J, Nothaft W and Backonja MM (2009). A randomized, double-blind, placebo-controlled trial evaluating the efficacy and safety of ABT-594 in patients with diabetic peripheral neuropathic pain. *Pain*, 146(3): 245–252.

Rollema H, Chambers LK, Coe JW, Glowa J, Hurst RS, Lebel LA, Lu Y, Mansbach RS, Mather RJ, Rovetti CC, Sands SB, Schaeffer E, Schulz DW, Tingley FD and Williams KE (2007a). Pharmacological profile of the alpha(4)beta(2) nicotinic acetylcholine receptor partial agonist varenicline, an effective smoking cessation aid. *Neuropharmacology*, 52: 985-994.

Rollema H, Coe JW, Chambers LK, Hurst RS, Stahl SM and Williams KE (2007b). Rationale, pharmacology and clinical efficacy of partial agonists of alpha(4)beta(2) nACh receptors for smoking cessation. *Trends Pharmacol Sci*, 28: 316-325.

Rollema H, Guanowsky V, Mineur YS, Shrikhande A, Coe JW, Seymour PA and Picciotto MR (2009a). Varenicline has antidepressant-like activity in the forced swim test and augments sertraline's effect. *Eur J Pharmacol*, 605: 114–116.

Rollema H, Shrikhande A, Ward KM, Coe JW, Tseng E, Wang EQ, Mather RJ, Hurst RS, Williams KE, Vries M, Cremers T, Bertrand S and Bertrand D (2009b). Preclinical properties of the alpha 4 beta 2 nAChR partial agonists varenicline, cytisine and dianicline translate to clinical efficacy for nicotine dependence. *Biochem Pharmacol*, 78: 918-919.

Romero HK, Christensen SB, Di Cesare Mannelli L, Gajewiak J, Ramachandra R, Elmslie K. S, … McIntosh JM (2017). Inhibition of α9α10 nicotinic acetylcholine receptors prevents chemotherapy-induced neuropathic pain. *PNAS*, 114(10): E1825–E1832.

Rose GD, Geselowitz AR, Lesser GJ, Lee RH and Zehfus MH (1985). Hydrophobicity of amino-acid residues in globular proteins. Science, 229: 834-838.

Rucktooa P, Haseler CA, van Elk R, Smit AB, Gallagher T and Sixma TK (2012). Structural Characterization of Binding Mode of Smoking Cessation Drugs to Nicotinic Acetylcholine Receptors through Study of Ligand Complexes with Acetylcholine-binding Protein. *J Biol Chem*, 287: 23283-23293.

Sambrook J and Gething MJ (1989). Protein structure. Chaperones, paperones. *Nature*, 16; 342(6247): 224-5.

Sancar F and Czajkowski C (2004). A GABA$_A$ Receptor Mutation Linked to Human Epilepsy (2R43Q) Impairs Cell Surface Expression of Receptors. *JBC*, 279: 47034 –47039.

Saricicek A, Esterlis I, Maloney KH, Mineur YS, Ruf BM, Muralidharan A, … Bhagwagar Z (2012). Persistent β2*-Nicotinic Acetylcholinergic Receptor Dysfunction in Major Depressive Disorder. *American Journal of Psychiatry*, 169(8): 851–859.

Sarter M and Lustig C (2020). Forebrain Cholinergic Signaling: Wired and Phasic, not Tonic, and Causing Behavior. *J Neurosci*, 40(4): 712-719.

Satkunanathan N, Livett B, Gayler K, Sandall D, Down J and Khalil Z (2005). Alpha-conotoxin Vc1.1 alleviates neuropathic pain and accelerates functional recovery of injured neurones. Brain Res, 1059: 149–158.

Sauguet L, Shahsavar A, Poitevin F, Huon C, Menny A, Nemecz A, Haouz A, Changeux J-P, Corringer P-J and Delarue M (2014). Crystal structures of a pentameric ligand-gated ion channel provide a mechanism for activation. *PNAS*, 111: 966–971.

Schofield PR, Darlison MG, Fujita N, Burt DR, Stephenson FA, Rodrigues H, Rhee LM, Ramachandran J, Reale V, Glencorse TA, Seeburg PH and Barnard EA (1987). Sequence and functional expression of the GABA A receptor shows a ligand-gated receptor super-family. *Nature*, 16-22; 328(6127): 221-7.

Seo S, Henry JT, Lewis AH, Wang, N and Levandoski MM (2009). The Positive Allosteric Modulator Morantel Binds at Non-canonical Subunit Interfaces of Neuronal Nicotinic Acetylcholine Receptors. *J Neurosci*, 29(27): 8734–8742.

Sharples CGV, Kaiser S, Soliakov L, Marks MJ, Collins AC, Washburn M, Wright E, Spencer JA, Gallagher T, Whiteaker P and Wonnacott S (2000). UB-165: A novel nicotinic agonist with subtype selectivity implicates the alpha 4 beta 2*subtype in the modulation of dopamine release from rat striatal synaptosomes. *J Neurosci*, 20: 2783-2791.

Shim JC, Jung DU, Jung SS, Seo YS, Cho DM, Lee JH, … Kelly DL (2012). Adjunctive varenicline treatment with antipsychotic medications for cognitive impairments in people with schizophrenia: a randomized double-blind placebo-controlled trial. *Neuropsychopharmacology*, 37(3): 660–668.

Shytle RD, Silver AA, Lukas RJ, Newman MB, Sheehan DV and Sanberg PR (2002). Nicotinic acetylcholine receptors as targets for antidepressants. *Molecular Psychiatry*, 7(6): 525–535.

Sine SM, Quiram P, Papanikolaou F, Kreienkamp HJ and Taylor P (1994). Conserved tyrosines in the alpha subunit of the nicotinic acetylcholine receptor stabilize quaternary ammonium groups of agonists and curariform antagonists. *J Biol Chem*, 269: 8808–8816.

Slemmer JE, Martin BR and Damaj MI (2000). Bupropion is a Nicotinic Antagonist. *J Pharmacol Exp Ther*, 295(1): 321-327.

Sokalingam S, Raghunathan G, Soundrarajan N and Lee S-G (2012). A Study on the Effect of Surface Lysine to Arginine Mutagenesis on Protein Stability and Structure Using Green Fluorescent Protein. *PLoS ONE*, 7(7): e40410.

Son CD, Moss FJ, Cohen BN and Lester HA (2009). Nicotine Normalizes Intracellular Subunit Stoichiometry of Nicotinic Receptors Carrying Mutations Linked to Autosomal Dominant Nocturnal Frontal Lobe Epilepsy. *Molecular Pharmacology*, 75(5): 1137–1148.

St John PA (2009). Cellular trafficking of nicotinic acetylcholine receptors. *Acta Pharmacol Sin*, 30; 656–662.

Stefansson H, Rujescu D, Cichon S, Pietiläinen OPH, Ingason A, Steinberg S, … Buizer-Voskamp JE (2008). Large recurrent microdeletions associated with schizophrenia. *Nature*, 455(7210): 232–236.

Steinlein OK and Bertrand D (2008). Neuronal nicotinic acetylcholine receptors: from the genetic analysis to neurological diseases. *BiochemPharmacol*, 76: 1175-83.

Stephens SH, Logel J, Barton A, Franks A, Schultz J, Short M, … Leonard S (2009). Association of the 5′-upstream regulatory region of the α7 nicotinic acetylcholine receptor subunit gene (CHRNA7) with schizophrenia. *Schizophrenia Research*, 109(1-3): 102–112.

Stoker AK and Markou A (2013). Unraveling the neurobiology of nicotine dependence using genetically engineered mice. *Curr Opin Neurobiol*, 23(4): 493–499.

Taly A, Corringer PJ, Guedin D, Lestage P and Changeux JP (2009). Nicotinic receptors: allosteric transitions and therapeutic targets in the nervous system. *Nature Reviews Drug Discovery*, 8: 733-750.

Taly A, Hénin J, Changeux JP and Cecchini M (2014). Allosteric regulation of pentameric ligand-gated ion channels: an emerging mechanistic perspective. *Channels (Austin)*, 8: 350–360.

Tapia L, Kuryatov A and Lindstrom J (2007). Ca2+ permeability of the $(alpha4)_3(beta2)_2$ stoichiometry greatly exceeds that of $(alpha4)_2(beta2)_3$ human acetylcholine receptors. *Mol Pharmacol*, 71: 769–776.

Tapper AR, McKinney SL, Marks MJ and Lester HA (2007). Nicotine responses in hypersensitive and knockout alpha 4 mice account for tolerance to both hypothermia and locomotor suppression in wild-type mice. *Physiol Genomics*, 31: 422–428.

Tavares XDS, Blum AP, Nakamura DT, Puskar NL, Shanata JAP, Lester HA and Dougherty DA (2012). Variations in Binding Among Several Agonists at Two Stoichiometries of the Neuronal, alpha 4 beta 2 Nicotinic Receptor. *J Am Chem Soc*, 134: 11474-11480.

Thomas KH, Martin RM, Knipe DW, Higgins JPT and Gunnell D (2015). Risk of neuropsychiatric adverse events associated with varenicline: systematic review and meta-analysis. *BMJ*, 350(8): h1109–h1109.

Thompson AJ, Padgett CL and Lummis SC (2006). Mutagenesis and molecular modelling reveal the importance of the 5-HT3 receptor F-loop. *J Biol Chem*, 281: 16576–16582.

Thompson AJ, Lester HA and Lummis SC (2010). The structural basis of function in Cys-loop receptors. *Q Rev Biophys*, 43(4): 449-499.

Thomsen MS, Zwart R, Ursu D, Jensen MM, Pinborg LH, Gilmour G, Wu J, Sher E and Mikkelsen D (2015). α7 and β2 Nicotinic Acetylcholine Receptor Subunits Form Heteromeric Receptor Complexes that Are Expressed in the Human Cortex and Display Distinct Pharmacological Properties. *PLoS ONE*, 10(6): e0130572.

Timmermann D, Sandager-Nielsen K, Dyhring T, Smith M, Jacobsen AM, Nielsen EO, Grunnet M, Christensen JK, Peters D, Kohlhaas K, Olsen GM and Ahring P (2012). Augmentation of cognitive function by NS9283, a stoichiometry-dependent positive allosteric modulator of α2- and α4-containing nicotinic acetylcholine receptors. *Br J Pharmacol*, 167(1): 164–182

Tomaselli GF, McLaughlin JT, Jurman ME, Hawrot E and Yellen G (1991). Mutations affecting agonist sensitivity of the nicotinic acetylcholine receptor. *Biophys J*, 60: 721–727.

Tozaki H, Matsumoto A, Kanno T, Nagai K, Nagata T, Yamamoto S and Nishizaki T (2002). The inhibitory and facilitatory actions of amyloid-β peptides on nicotinic ACh receptors and AMPA receptors. *Biochemical and Biophysical Research Communications*, 294(1): 42–45.

Trott O and Olson AJ (2010). AutoDock Vina: improving the speed and accuracy of docking with a new scoring function, efficient optimization and multithreading. *J Computational Chemistry*, 31(1): 455-461.

Tuan EW, Horti AG, Olson TT, Gao Y, Stockmeier CA, Al-Muhtasib N, … Kellar KJ (2015). AT-1001 Is a Partial Agonist with High Affinity and Selectivity at Human and Rat α3β4 Nicotinic Cholinergic Receptors. *Molecular Pharmacology*, 88(4): 640–649.

Turrini P, Casu MA, Wong TP, De Koninck Y, Ribeiro-da-Silva A and Cuello AC (2001). Cholinergic nerve terminals establish classical synapses in the rat cerebral cortex: synaptic pattern and age-related atrophy. *Neuroscience*, 105(2): 277–285.

Tushingham S, Snyder CM, Brownstein KJ, Damitio WJ and Gang DR (2018). Biomolecular archaeology reveals ancient origins of indigenous tobacco smoking in North American Plateau. *PNAS*, 115(46): 11742-11747.

Unwin N (2005). Refined structure of the nicotinic acetylcholine receptor at 4Å resolution. *J Mol Biol,* 346(4): 967-89.

Van Arnam EB, Blythe EE, Lester HA and Dougherty DA (2013). An Unusual Pattern of Ligand-Receptor Interactions for the α7 Nicotinic Acetylcholine Receptor, with Implications for the Binding of Varenicline. *Molecular Pharmacology*, 84(2): 201–207.

Van Arnam EB and Dougherty DA (2014). Functional Probes of Drug Receptor Interactions Implicated by Structural Studies: Cys-Loop Receptors Provide a Fertile Testing Ground. *J Med Chem*, 57: 6289-6300.

Van der Spoel D, Lindahl E, Hess B, Groenhof G, Mark AE and Berendsen HJC (2005). GROMACS: Fast, Flexible and Free. *J Comp Chem*, 26: 1701-1719.

Venkatachalan SP and Czajkowski C (2008). A conserved salt bridge critical for $GABA_A$ receptor function and loop C dynamics. *PNAS*, 105(36), 13604–13609.

Verbitsky M, Rothlin CV, Katz E and Elgoyhen AB (2000). Mixed nicotinic–muscarinic properties of the α9 nicotinic cholinergic receptor. *Neuropharm*, 39: 2515-2524.

Vieta E, Thase ME, Naber D, D'Souza B, Rancans E, Lepola U, … Eriksson H (2014). Efficacy and tolerability offlexibly-dosed adjunct TC-5214 (dexmecamylamine) in patients with major depressive disorder and inadequate response to prior antidepressant. *Eur Neuropsychopharmacol*, 24(4): 564–574.

Walsh RM, Roh SH, Gharpure A, Morales-Perez CL, Teng J and Hibbs RE (2018). Structural principles of distinct assemblies of the human α4β2 nicotinic receptor. *Nature*, 557(7704): 261–265.

Wang HY, Lee DHS, D'Andrea MR, Peterson PA, Shank RP and Reitz AB (2000). β-Amyloid$_{1-42}$ Binds to α7 Nicotinic Acetylcholine Receptor with High Affinity. Journal *of Biological Chemistry*, 275(8): 5626–5632.

Wang J, Kuryatov A, Sriram A, Jin Z, Kamenecka TM, Kenny PJ and Lindstrom J (2015). An Accessory Agonist Binding Site Promotes Activation of α4β2* Nicotinic Acetylcholine Receptors. *J Biol Chem*, 290: 13907-13918.

Wang Y, Su DM, Wang RH, Liu Y and Wang H (2005). Antinociceptive effects of choline against acute and inflammatory pain. *Neuroscience*, 132(1): 49–56.

Wang Y, Xiao C, Indersmitten T, Freedman R, Leonard S and Lester HA (2014). The Duplicated α7 Subunits Assemble and Form Functional Nicotinic Receptors with the Full-length α7. *Journal of Biological Chemistry*, 289(38): 26451–26463.

Ware JH, Vetrovec GW, Miller AB, Van Tosh A, Gaffney M, Yunis C, Arteaga C and Borer JS (2013) Cardiovascular safety of varenicline: patient-level metaanalysis of randomized, blinded, placebo-controlled trials. *Am J Ther*, 20: 235–246.

Webb B and Sali A (2014). *Methods Mol Biol*, 1137: 1.

Weinberger AH, Kashan RS, Shpigel DM, Esan H, Taha F, Lee CJ, … Goodwin RD (2016). Depression and cigarette smoking behavior: A critical review of population-based studies. *The American Journal of Drug and Alcohol Abuse*, 43(4): 416–431.

Wessler I and Kirkpatrick CJ (2008). Acetylcholine beyond neurons: the non-neuronal cholinergic system in humans. *Br J Pharmacol,* 154: 1558–1571.

Williams DK, Stokes C, Horenstein NA and Papke RL (2009). Differential Regulation of Receptor Activation and Agonist Selectivity by Highly Conserved Tryptophans in the Nicotinic Acetylcholine Receptor Binding Site. *J Pharmacol Exp Therap*, 330(1): 40–53.

Wonnacott S (2015). Nicotinic ACh Receptors. *Tocris Bioscience Scientific Review series*.

World Health Organization (2017).WHO report on the global tobacco epidemic: Monitoring tobacco use and prevention policies. https://www.who.int/tobacco/global_report/2017/en/

Xiao Y & Kellar KJ (2004). The comparative pharmacology and up-regulation of rat neuronal nicotinic receptor subtype binding sites stably expressed in transfected mammalian cells. *J Pharmacol Exp Ther*, 310: 98–107.

Xiao Y, Fan H, Musachio JL, Wei ZL, Chellappan SK, Kozikowski AP and Kellar KJ (2006). Sazetidine-A, A Novel Ligand That Desensitizes α4β2 Nicotinic Acetylcholine Receptors without Activating Them. *Molecular Pharmacology*, 70(4): 1454–1460.

Xiu X, Hanek AP, Wang J, Lester HA and Dougherty DA (2005). A Unified View of the Role of Electrostatic Interactions in Modulating the Gating of Cys Loop Receptors. *J Biol Chem,* 280(50): 41655–41666.

Xiu X, Puskar NL, Shanata JA, Lester HA and Dougherty DA (2009). Nicotine binding to brain receptors requires a strong cation-π interaction. *Nature,* 458: 534–537.

Yang K, Hu J, Lucero L, Liu Q, Zheng C, Zhen X, Jin G, Lukas RJ and Wu J (2009). Distinctive nicotinic acetylcholine receptor functional phenotypes of rat ventral tegmental area dopaminergic neurons. *J Physiol*, 587(2): 345–361.

Yang T, Xiao T, Sun Q and Wang K (2017). The current agonists and positive allosteric modulators of α 7 nAChR for CNS indications in clinical trials. *Acta Pharmaceutica Sinica B*, 7(6): 611–622.

Zhang J, Xue F and Chang Y (2009). Agonist- and antagonist-induced conformational changes of loop F and their contributions to the rho1 GABA receptor function. *J Physiol*, 587: 139–153.

Zoli M, Léna C, Picciotto MR and Changeux JP (1998): Identification of four classes of brain nicotinic receptors using β2-subunit mutant mice. *J Neurosci*, 18: 4461–4472.

Zoli M, Pistillo F and Gotti C (2015). Diversity of native nicotinic receptor subtypes in mammalian brain. *Neuropharmacology*, 96(B): 302–311.

Zouridakis M, Giastas P, Zarkadas E, Chroni-Tzartou D, Bregestovski P and Tzartos SJ (2014). Crystal structures of free and antagonist-bound states of human α9 nicotinic receptor extracellular domain. *Nature Structural & Molecular Biology*, 21(11): 976–980.